Stoner Criteria in Transition Metal Oxides and Heavy Fermions

M.I. Brammall
Supervisor: M.W. Long

Submitted in conformity with the requirements
for the degree of Doctor of Philosophy
School of Physics and Astronomy
University of Birmingham

Declaration

The material contained within this thesis has not previously been submitted for a degree at the University of Birmingham or any other university. The research reported within this thesis has been conducted by the author unless indicated otherwise.

Signed .....

Abstract

Stoner Criteria in Transition Metal Oxides and Heavy Fermions

M.I. Brammall

This thesis is an examination of the uses of mean-field theory in problems of the theory of strongly-correlated electronic systems, particularly to the problem of orbital ordering in transition metal oxides. We will apply mean-field theory to various models for orbital ordering of transition metal oxides, and also show that mean-field theory is not as bad an approximation as it might initially seem.

We are also interested modelling superconductivity in heavy fermion systems. We conclude from our modelling on transition metal oxides that the mean-field theory we use based on the Stoner criterion will not be adequate to model such complicated phenomena. We propose an alternate mean-field theory based on non-linear fermionic transformations which we introduce. We suggest further improvements in the form of a non-orthogonal transformation, which we also introduce.

As a diversion, we model frustrated antiferromagnetism on a pyrochlore lattice. The particular material is $Gd_2Ti_2O_7$. We show that there are many effects in competition with each other. We conclude with a proposed magnetic structure which appears to be a better fit to experimental data than previous suggestions.

Dedication

To my parents, and also to my wife and son for severely delaying this thesis...

Acknowledgments

Firstly I would like to acknowledge the help of my supervisor Martin Long, or the big MW as we call him around the office (not really). Without him I would not have worked in strongly correlated systems, and probably would have gone into algebraic geometry instead. Also, I would have floundered rather more hopelessly in the field of strongly correlated systems than I did without his help. Incidentally, algebraic geometry still remains an attractive prospect. Ho hum indeed!

I would like to thank Dom for his random interjections and strange noises, and Steve for being understanding when I throw objects at him for a cheap laugh. Thanks to Amy for diverting Martin's attention from me at a time when I seemed to be hearing of some material I never heard of on a daily basis. I would thank Andy for providing some interesting problems, but he's not on Facebook. Also thanks to the current theory students, and some past ones too for doing unspecified things, but it seems the norm to thank lots of people.

Thanks go to my family; my wife, child and parents, for doing family stuff like driving me to drink and insanity. Also to Liam for inhabiting the attic, it was beginning to get a little lonely.

Lastly, I would like to acknowledge financial support from EPSRC, who paid me to occasionally do some physics, but mostly to read more mathematics than I should. In the least, it is still an EPSRC supported subject. They can take solace that now they are funding me in a subject appropriate manner.

Contents

List of Tables

List of Figures

Part I

Introductory Material

Chapter 1

Introduction

1.1 Introduction

There are two major themes discussed in this thesis. The first both in order and magnitude of discussion is the concept of orbital ordering. The second is that of superconductivity in strongly correlated electronic systems, namely heavy-fermion materials. In between these two sections, we will also present some work performed on a magnetic pyrochlore system which is unrelated to both sections, but perhaps illustrates nicely the simplicity that can be achieved with sensible interpretations of experimental data.

We will use a particular tool to analyse models and predict the behaviour of materials, and that is a generalisation of the Stoner criterion from Stoner's theory of ferromagnetism[37]. This will be used almost exclusively in our modelling, for better or worse. In part three, we show how to improve on the simple model of Stoner to incorporate correlations to some degree while still working in a single-particle framework.

The main problem with mean-field theory is that it is a weak-coupling theory, and in f-electron systems, we are no longer in a weak-coupling regime due to the f-electrons being so localised. Also, for $3d$ systems, mean-field theory is not as good an approximation as one might hope it is. Mean-field theory has a tendency to over-emphasise any ordering that may be present. Further, any ordering suggested by mean-field theory is perhaps even

non-existent in the model being approximated.

The goal of this thesis is to show that mean-field theory can be a good method of studying strongly correlated electronic systems, and more importantly, is a non-perturbative method. This makes it useful for describing phase transitions. Most of all, we wish to develop an improvement to mean-field theory which works in the limit of infinite local repulsion. To this end, we use the concept of a non-linear fermionic transformation. This takes into account the assumed infinite repulsion between strongly correlated electrons, while still allowing a single-particle mean-field picture of the system.

1.1.1 Orbital Ordering

The concept of an orbital ought to be familiar from studies of the Schrodinger equation for the hydrogen atom. Indeed, it is these same orbitals that we will use, even though there are no materials containing hydrogen modelled in this thesis. We will use them as reference points, and when we speak of a $3d$ orbital, for example, we will be taking the $3d$ orbital of hydrogen as a reference. We can draw the orbitals by considering surfaces of equiprobability, just as we can draw an orbit of a particle around a massive body as a surface of equal energy.

Orbitals have angular momenta associated with them, and hence moments. We are familiar with moments ordering in spin-systems, and we call this magnetism. We have no such succinct word for orbital ordering, and so we use can only use the term orbital ordering. Magnetism and orbital ordering are linked, and it is common to find one coexisting with the other. Usually, ferromagnetism is accompanied by an alternating orbital arrangement, sometimes called an antiferro-orbital arrangement to draw an analogy with antiferromagnetism. Conversely, antiferromagnetism is accompanied by an orbital arrangement with the same orbitals on each atom. Again, to draw the analogy with ferromagnetism, this is often called a ferro-orbital arrangement.

A model that is well-used, but perhaps not applicible to our work, is the Kugel-Khomskii

model (KK) [23]. The starting Hamiltonian is the Hubbard model. The Hamiltonian is then expanded to second order in perturbtion theory. A key component that the KK model accounts for that we do not is the spin-orbit coupling. We assume the spins to be fixed, and so do not describe this aspect of the problem at all. Indeed, accounting for the spin degrees of freedom would make our line of modelling prohibitively difficult. It has been suggested that the KK Hamiltonian gives rise to an ordered isotropic spin phase, and that an energy gap in the spin excitations can be caused by spin-orbit interactions. Since we assume a static background of spins throughout, we are focusing on a slightly different problem.

The style of orbital ordering in the KK model is perhaps a little inflexible for when we use non-standard orbitals. It is, however, perhaps widely more applicible than our modelling, which is really at the level of individual materials, and cannot really be translated verbatim between materials. Furthermore, the KK model is best applied to a material with a Mott insulating state. It relies on magnetic superexchange, and does the perturbation in terms of superexchange processes. This renders it inapplicible, since our materials are metallic, and the exchange mechanism is double exchange. It is precisely double exchange that allows us to avoid describing the magnetism in problems of orbital ordering. None of the materials we consider are Mott insulators.

1.2 Scope and Aims of the Thesis

The principle aim of the thesis is to show that the Stoner criterion can be used to effectively model theoretical systems, and coupled with a good amount of common sense and a critical mind, much progress can be made. However, we also acknowledge that sometimes we can get nowhere using the Stoner criterion alone, and so we make transformations on the model we are working with to make the mean-field approximations used more reliable.

1.3 Outlook

The remainder of this part is a discussion of the experimental systems that we will model, and some results from well-known models that are relevant to us. There are three main examples of strongly correlated electronic system of interest to us. The first that we will come across are the colossal magnetoresistors. The second main class of materials are the heavy fermion materials. Related to these are the high-temperature superconductors. Finally, we will have cause to discuss frustration in magnets. We have a long treacherous road to walk before we can begin to model these systems, but the scenery is pleasant, and will be detailed below.

In chapter two, we examine some ideas from physical chemistry, and motivate their application to our modelling. The first idea we consider is the Hund's rules [41] from atomic physics. Since we are dealing with materials often containing localised electrons, the concept of atomic orbitals survives to quite a large extent. We can then apply Hund's rules to calculate the likely configuration of electronic levels. This, however, is in competition with the electrostatic field of the crystalline environment, which can lead to splitting of the energy levels. This is the subject of crystal field theory.

Since we will focus on problems of orbital ordering, we can expect distortions to take place since orbitals are anisotropic for all but the zero angular momentum orbitals. Jahn and Teller explained this in their seminal work, which we discuss in section 2.4. Orbital ordering is the basic mechanism to achieve the distortion observed in degenerate non-linear molecules, and so this is the relevance of the Jahn-Teller effect for us.

Chapter three sees us move into discussions of experimental systems. These are the systems we outlined in the beginning of this introduction. As we will see, strongly correlated electronic systems offer a wealth of phenomena. Unfortunately, this makes their modelling difficult, and we will have to resort to approximations and focusing on the most salient features of the materials.

We will be unable to progress very far without models, and in chapter four we outline important properties of the two most important models for this thesis. The first is the Hubbard model, and is notorious for its difficulty. Later in this chapter, things get even more complicated as we introduce the Anderson lattice which is thought to contain the essential physics of heavy fermion materials.

The models we will employ are usually impossible to solve exactly. We are thus forced to use some method of approximation to gain insight into their solution. This is the subject of chapter five, and is mean-field theory. This allows us to develop effective single-particle pictures for interacting many-particle systems. It has well documented problems, however, and we will try to improve on these problems in the later chapters of this thesis.

In chapter six, we finally move away from introductory material, and begin to discuss applications of the models to physical systems. We will be modelling the ordering of electrons in the t_{2g} representation of the cubic group.

Chapter seven continues in a similar vein to chapter six, but for a different material, and so we have to take different things into account in our modelling. We will model the orbital ordering for electrons in the e_g sector of the representation of the cubic group in d-orbital space. Our intention is to model a certain region of the phase diagram of the colossal magnetoresistive manganites.

We find some weaknesses of mean-field theory when we come to discuss impurities and fluctuations in problems involving orbital ordering in the e_g representation. The concept of an orbital Nagaoka problem is introduced in this chapter. Solving this, we find an improvement on the mean-field solution. While the improved solution corresponds to a situation which is perhaps not physical, the solution is mathematically a better one than the mean-field theory, and so we should be wary of mean-field theory.

We will deviate from using the Stoner criterion in chapter nine to illustrate and expand on some work undertaken outside of the scope of the Stoner Criterion, which is intended for

publication. In chapter 9 we analyse the experimental literature of $Gd_2Ti_2O_7$, and resolve some inconsistencies in both the experimental and theoretical literature by predicting some states of our own.

In the latter part of the thesis, we will begin modelling superconductivity in heavy fermion materials, where we find competition between the RKKY and Kondo effects introduced in this chapter. This leads to very complicated and surprising behaviour, and we will find our modelling is not sophisticated enough to capture anything that could correspond to a real heavy-fermion material. However, we will develop a toy-model with some ideas on how to embellish the model into a more sophisticated theory that will capture some real features of heavy fermion materials. Chapter ten begins the task of improving mean-field theory. We do this by introducing the concept of a non-linear fermionic transformation. In practise, this means constructing creation and annihilation operators where $d^\dagger_\uparrow d^\dagger_\downarrow$ is not the same as creating a $d^\dagger_\downarrow$. Then we apply the transformation developed to the Anderson lattice.

This generates an effective Hubbard model description of the Anderson lattice. We develop a mean-field theory based on the transformation. We suggest further improvements to the non-linear transformations developed in chapter eleven by introducing the concept of a non-linear, non-orthogonal transformation. We feel that this will provide a more physically realistic setting for the calculation. Unfortunately, it is quite difficult to perform mean-field theory in the manner we have used in this thesis, and so we can only outline what we will do in the future.

Chapter 2

Physics and Chemistry of Solids

2.1 Introduction

Before we can hope to construct models of materials, we need to be able to understand their chemistry. This chapter is intended to outline the three most pertinent examples of phenomena in physical chemistry that will be relevant to our modelling of material systems. The first is a set of laws from atomic physics, called Hund's rules which determine the electronic configuration of the ground state of atoms.

Since we will be working with crystalline materials, it is unreasonable to expect these laws to survive. Surprisingly, most of them do, but the crystalline environment has its own set of energy scales which compete with Hund's rules. The energy of the crystal field interaction is enough to beat some of the energy scales set by Hund's rules. These are the crystal field levels, and divide our space of orbitals into a set of irreducible representations of the symmetry group of the crystal. In most of the examples we look at, the crystallographic point group will be the cubic group, usually written as O_h.

Since we will discuss mostly problems of orbital ordering in this thesis, we will have occasion to refer to the Jahn-Teller effect. This is an effect that lifts the degeneracy of electronic levels by causing an orbital ordering to distort the crystal. Jahn and Teller demonstrated that a non-linear molecule with degeneracy would distort to remove the degeneracy. Orbital

ordering is the typical mechanism for this lifting of degeneracy, and so the Jahn-Teller effect is relevant to us.

Some of the materials that we model are metallic magnets, and the exchange processes that take place in these materials are important for our modelling. The double exchange of Zener shows us that in the materials we model, we can often ignore the spin-degree of freedom when combining double exchange ideas with the crystal field splitting of ions. Finally, in the heavy fermion materials that we will model, there is a competition between the RKKY and Kondo effects, and so we must also elaborate on these effects a little.

2.2 Hund's Rules

Hund's rules are derived purely from phenomenological considerations[41]. They are rules for determining the configuration of the spin and orbital angular momentum of electrons in an atom possessing an incomplete degenerate outer shell. Some of the rules survive when we consider molecules in a crystalline environment, and a discussion of this will follow this section.

Hund's rules form a hierarchy for determining the spin and orbital ground-state configurations of the atoms. We list the rules in order here:

1. The total spin S should be maximal.

2. The orbital angular momentum L should be maximal, with constraints provided by the first rule and Pauli exclusion.

3. The total angular momentum J should be $|L - S|$ for less than half-filled shells, and $L + S$ for more than half-filled shells.

We may be concerned about applying Hund's rule to a solid where there is a lower degree of symmetry than that of an atom in free space. However, some of Hund's rules can survive

and be relevant in solids. This is due to the relatively high-energy scale for the first rule, and the slightly lower energy scale for the second rule.

Even though the rules are empirical in nature, there is some justification on a theoretical level for their existence, which we discuss here, along with some implications.

2.2.1 The First Rule

The largest relevant atomic physics energy arises from exchange. Due to the Pauli principle, when two electrons have parallel spins they must have an antisymmetric spatial wavefunction, whereas when the electrons have an antisymmetric spin wavefunction then they must have a symmetric spatial wavefunction. We express this by

$$\Psi(r_1, r_2, ..., r_n) = \Psi(r_{\sigma(1)}, r_{\sigma(2)}, ..., r_{\sigma(n)}) \tag{2.1}$$

for the symmetric case and

$$\Psi(r_1, r_2, ..., r_n) = \mathrm{sgn}(\sigma)\Psi(\mathrm{r}_{\sigma(1)}, \mathrm{r}_{\sigma(2)}, ..., \mathrm{r}_{\sigma(\mathrm{n})}) \tag{2.2}$$

where $\sigma(i)$ is a permutation of the ith-coordinate, and $\mathrm{sgn}(\sigma)$ is the sign of the permutation, with $+1$ corresponding to even permutations and -1 to odd permutations.

Since the electron-electron interaction takes the form

$$\int d^3r_1 \int d^3r_2 |\psi(r_1, r_2)|^2 \frac{e^2}{|r_1 - r_2|} \tag{2.3}$$

the wavefunction for parallel spins has a lower energy as it vanishes where the interaction is maximal. This interaction leads to Hund's first rule which is that the total spin of an open shell is maximal.

2.2.2 The Second Rule

The next most important energy scale controls the choice of orbitals and competes directly with the crystal-field energy scale in transition metals. The physical source of the energy is again electrostatic. A classical explanation is that electrons orbiting an atom are less likely to meet if the electrons orbit the atom in the same sense. Hund's second rule is thus that the orbital angular momentum is maximised, subject to the restriction of Fermi statistics.

The second Hund's rule aligning the orbital angular momentum is on a similar energy scale to the spin energy but is a fraction of it. Subject to crystal-field splitting interferring with Hund's second rule, the orbital angular momentum is quenched in transition metals. The rare earth elements, on the other hand, have such localised f-electrons that often the third Hund's rule is also observed.

2.2.3 The Third Rule

The third Hund's rule originates from relativistic effects and is usually small. The effect is to induce a coupling between an electron's spin and its orbital angular momentum, also called spin-orbit coupling. The result is that for the first half of the shell the total spin and total angular momentum are anti-parallel, whereas for the second half they are parallel.

$$\begin{aligned} j &= |l - s|, n < M \\ j &= l + s, n > M \end{aligned} \tag{2.4}$$

For Ce the spin-orbit coupling energy is around 0.25 eV and for Yb the spin-orbit energy is of the order of 1 eV. In comparison transition metals typically have spin-orbit couplings of around 0.1 eV.

It is important to realise that the role of the crystal field in the rare-earths is not to stabilise the cubic harmonics, but is more subtle. The spin-orbit effects win and so we

cannot separate the spin from the orbital angular momentum. It is the different rather more complicated j_z states which are split by the crystal field.

2.3 Crystal Field Theory

In a spherically symmetric atom, the orbitals within a given shell are energetically degenerate, as discussed above. In a crystalline environment, we cannot expect this degeneracy to be present. The breaking of this symmetry is the subject of crystal field theory. It was developed in 1929 by Hans Bethe [5]. The basic idea is that electrons in a crystalline environment are effected by the electrostatic field of the surrounding ions. This electrostatic field is called the crystal field. The origin of the splitting originates from the anisotropic charge distribution of the orbitals, and hence of the charge distribution.

For a simple example, consider a transition metal oxide with a perovskite crystal structure. We restrict attention to the active $L = 2$ d-shell. In the $\hat{x}^2 - \hat{y}^2$ and $3\hat{z}^2 - \hat{r}^2$ orbitals, the orbitals will point directly at the oxygen anions, and therefore will experience a strong coulombic repulsion. The $\hat{x}\hat{y}$, $\hat{y}\hat{z}$, and $\hat{z}\hat{x}$ orbitals, however, point in between the oxygen anions, and so will experience less coulomb repulsion. There is therefore an energetic difference between these sets of orbitals, and we have lost the 5-fold orbital degeneracy. We now have a set of three degenerate orbitals and a set of two degenerate orbitals with a splitting between the two.

In this section, we will develop these ideas more concretely. The splitting of the levels is determined by the representations of the group of symmetries of the crystal. The levels are grouped according to irreducible representations of the point group of the crystal. Group theory can only tell us the splittings of the orbitals, and not the energetics so we are unable to determine the sequence of the levels. An alternative is to look at inelastic neutron scattering data, and this is often used when using group theoretic methods become complicated. This happens quickly for f-electron systems.

There is a systematic nomenclature for labelling point groups which is used throughout the literature, and that is Mulliken symbols. There is an account of the nomenclature in the book by [25] for the reader who is curious of the meaning of these symbols. For our purposes, there are only two irreducible representations of groups of interest. That is the t_{2g} and e_g irreducible representations of the cubic group. The $L = 2$ d-orbitals form a five dimensional vector space, while the order of the cubic group is 48. Since the dimension of an irreducible representation of a finite group must divide the order of the group, we find that the five dimensional d-orbital vector space decomposes into an irreducible doublet representation and an irreducible triplet representation.

Take as an example $LaMnO_3$. The crystal structure is perovskite. There is a octahedron of oxygen atoms surrounding every manganese atom. The platonic dual to an octahedron is a cube, and so the octahedral group is isomorphic to the cubic group, and hence their irreducible representations will be isomorphic. The t_{2g} and e_g representations of these groups are thus identical, and we can talk of the same orbitals in the representations.

The story does not end here. There are also weak and strong crystal field splittings. In the weak case, the high-spin state is realised where, taking the case of cubic splittings for d-orbitals, the t_{2g} sector is half-filled first, then the e_g sector is half-filled. This is repeated for the next half.

For the strong-field case, the low-spin state is realised. Following the last example, the t_{2g} sector is completely filled, and *then* the e_g sector is filled. For the 3d elements, the former situation is realised up to cobalt, and the latter for the elements past cobalt. Cobalt containing compounds are interesting, since both situations can be realised.

2.4 The Jahn-Teller Effect

If we consider a set of orbitals lying in a shell, say the d-orbitals, then we expect the orbitals to be split by a crystal field, which depends on the symmetry of the crystalline environment.

In the case of d-orbitals in a cubic environment, we have splittings into the t_{2g} and e_g representations.

If we consider the motion of a hole in an otherwise filled d-shell in a cubic environment, say Cu^{2+}, then there will be a degeneracy in the orbital ground state between the $\hat{x}^2 - \hat{y}^2$ orbital and the $3\hat{z}^2 - \hat{r}^2$ orbital, providing there is no further lifting of the degeneracy. However, Jahn and Teller ([19], [38]) formulated and proved a theorem which describes when a further lifting of the degeneracy is energetically favourable.

The problem of the lifting of the orbital degeneracy was first tackled by Landau with phenomenological arguments. He argued that the ordering of orbitals will induce a distortion of the crystal, and this distortion of the crystal will cost an energy $E_1 \propto \alpha(\delta z)^2$, for some energy scale α and distortion δd. This will induce a splitting between the $3\hat{z}^2 - \hat{r}^2$ and the $\hat{x}^2 - \hat{y}^2$ orbital. It is then energetically favourable for two electrons to lie in the $3\hat{z}^2 - \hat{r}^2$ orbital than the $\hat{x}^2 - \hat{y}^2$ orbital which gains an energy $E_2 \propto -\beta\delta d$ with some seperate energy scale β. The total energy associated with distorting the crystal and repopulating the electronic levels is $E_1 + E_2 = \alpha(\delta d)^2 - \beta\delta d$ and this energy is minimised for a distortion of the order $\delta d = \frac{\beta}{2\alpha}$.

Things were not as simple as this, however. The situation was complicated by molecules with linear geometries and orbitally degenerate ground states, such as CO_2, not showing Jahn-Teller distortions. The splitting between the orbital levels in CO_2 is $\propto (\delta d)^2$, and therefore no Jahn-Teller distortion will occur.

The doubts thrown over the simple physical arguments provided by Landau were rigourously resolved by Jahn and Teller, who used group and representation theoretic methods to prove that the only molecules with an orbitally degenerate ground state that do not distort to lift the degeneracy are those with a linear geometry. However, as with most group theoretic methods employed in physics, it can only tell us the nature of the splittings leading to the crystalline distortion. It cannot tell us the magnitude of such effects.

2.5 Double Exchange

Double-exchange was first proposed by Zener [43]. We take as an example to illustrate the double exchange mechanism, and one that will be especially important to us later, the exchange between an Mn^{4+} and an Mn^{3+} ion mediated by an intermediate oxygen atom. The situation is illustrated in (2.1).

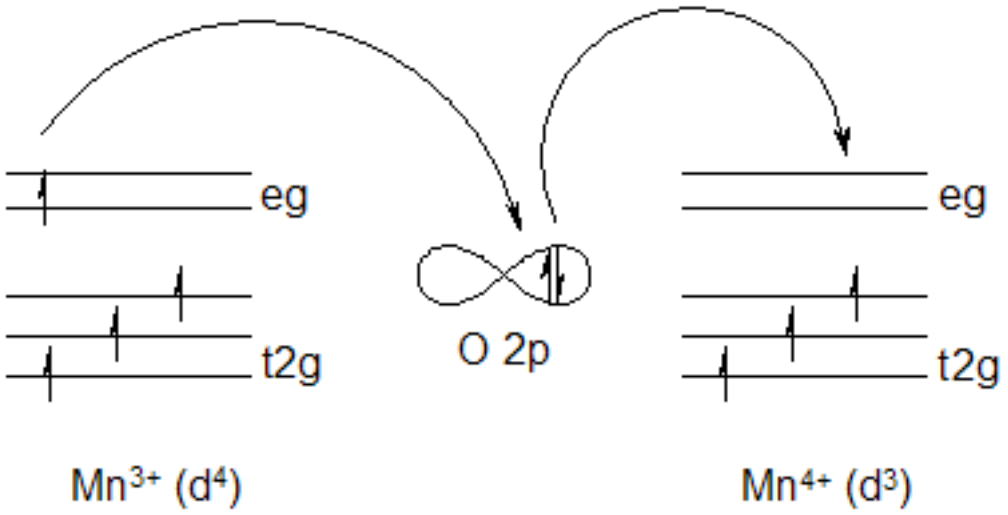

Figure 2.1: Double Exchange in an Mn-O-Mn chain.

Double-exchange tells us that electrons move most easily if electrons do not have to reorient spins when moving between ions in order to avoid paying Hund's rule energies. Delocalisation reduces the energy, and so this leads to ferromagnetic correlations between neighbouring ions. For us, it will be one of the most used exchange mechanisms, notably when we discuss exchange in saturated ferromagnets.

In the case of a saturated ferromagnet, double exchange enables us to avoid describing the spin degree of freedom in itinerant magnets. The spin is guaranteed to be of one species only, and though the assignment of up or down to the z component of a spin is arbitrary, it will be fixed and it will be polarised due to the large Hund's rule penalty for hopping, as an example, an electron in the e_g sector on Mn^{3+} to the empty e_g sector on Mn^{4+}. The only

degree of freedom left for the electron is which e_g orbital to hop into.

2.6 Summary

We have discussed some of the more pertinent examples of phenomena in physical chemistry relevant to our modelling. There are three such phenomena, the Hund's rules and crystal field theory being intimately related. The third, the Jahn-Teller effect occurs in problems of orbital ordering, and will be one of the major concerns of this thesis. We have also discussed an important exchange mechanism for modelling that we will perform, and this is the double exchange mechanism. Double exchange will allow us to avoid describing spin-degrees of freedom in certain problems of orbital ordering that we will consider.

Now that we have presented some ideas in physical chemistry, we can employ these to describe real materials, and this is the subject of the next chapter.

Chapter 3

Materials

3.1 Introduction

Now that we have the required aspects of physical chemistry, we are able to discuss some of the materials that we will be interested in. We will discuss some examples of the strongly correlated materials that we will consider in this thesis. These materials are the heavy fermion materials and the colossal magnetoresistors. We will focus on a few representative compounds in each case, and discuss their crystal structures, phases, and electronic phenomena in each compound. While not directly relevant to the work in this thesis, the high-temperature superconductors are the one of the main sources of interest in strongly correlated materials, and do bear more than a passing resemblance to the heavy fermion materials, and so an honorary short discussion of them is made. While the high-temperature superconductors and colossal magnetoresistive manganites are fairly generic in their phases diagrams, the heavy-fermion compounds have a wide range of phase diagrams. We focus on a single representative element, UPt_3.

3.2 Colossal Magnetoresistors

We will proceed with investigations into colossal magnetoresistive (CMR) materials. We will begin with an overview of the magnetoresistive effect. Following this will be a discussion of

the manganites, which are perhaps the best understood of all the colossal magnetoresistive materials. There are other materials displaying the CMR effect, such as Sr_2FeMoO_6, but we will postpone discussion of these materials to a later chapter.

3.2.1 The Magnetoresistive Effect

The magnetoresistive effect was discovered by Lord Kelvin in 1856[39]. Experiments were performed on samples of iron placed in a magnetic field. It was found that the resistivity increased when the magnetic field was parallel to the direction of the current. However, when the field was applied perpendicular to the direction of the current, it was found that the resistivity decreased. Kelvin was able to lower the resistivity by around 5%.

Until the late 1980s, it was thought impossible to lower the resistivity of a material by application of a magnetic field any more than Lord Kelvin was able to. However, in 1988, two research groups independently made vast progress in increasing the magnetoresistive ratio. The materials exhibiting this effect were trilayer Fe/Cr/Fe, and multilayer Fe/Cr discovered independently by the groups led by Grunberg[12] and Fert[10] respectively. Both were awarded the 2007 Nobel Prize in Physics for their efforts.

This was further improved by the discovery of CMR materials, such as the LCMO and LSMO manganites that we will discuss extensively in this section. Here, the magnetoresistive ratio is increased by several orders of magnitude. In contrast to the technological applicability of the GMR materials, the CMR effect is typically displayed at low temperatures only. A possible exception is Sr_2FeMoO_6, but this material is difficult to make reliably, and oxygen leeching seems to take place in the material.

3.2.2 The CMR Manganites

The manganites are a class of materials displaying the colossal magnetoresistive effect. The parent compound, $LaMnO_3$ has a perovskite crystal structure, which will be one of the most

common crystal structures we use in this thesis (figure 3.1). Since the structure is locally octahedral, which is the platonic dual of a cube, we have a local cubic symmetry.

Manganites have a fairly long history in condensed matter physics, although certainly not as long as magnetite, a compound we will discuss later. The first paper containing results for manganites was presented in 1950 by Van Santen [40]. In this paper, La was replaced either by Ca, Sr, or Ba, and results for polycrystalline samples of (La, Ca)MnO_3, (La, Sr)MnO_3 and (La, Ba)MnO_3 were reported. The main result was the appearance of ferromagnetism in these compounds.

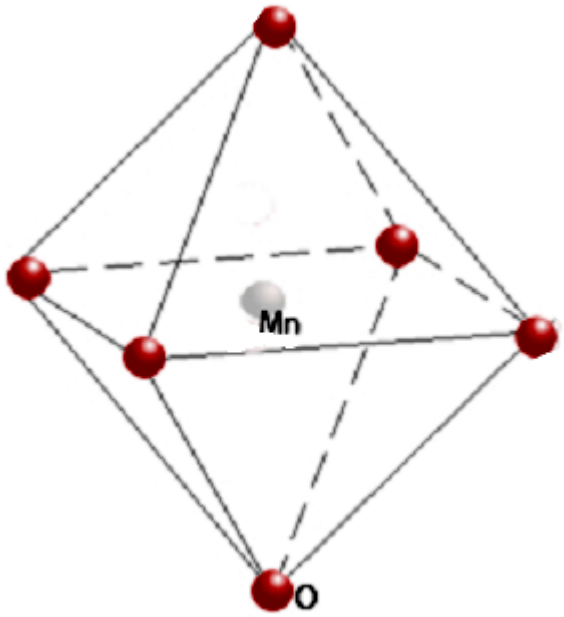

Figure 3.1: Crystal Structure of the $La_{1-x}Ca_xMnO_3$ Manganites

Since we have a crystal with cubic symmetry, the d-orbitals will split as cubic crystal fields, the t_{2g} and e_g representations. The electronic configuration is illustrated in (3.2).

As is typical for strongly correlated electronic materials, such as the high-temperature superconductors and heavy-fermion materials, the manganites have a varied and rich phase diagram. The phase diagram for a variety of manganites share a lot of generic features.

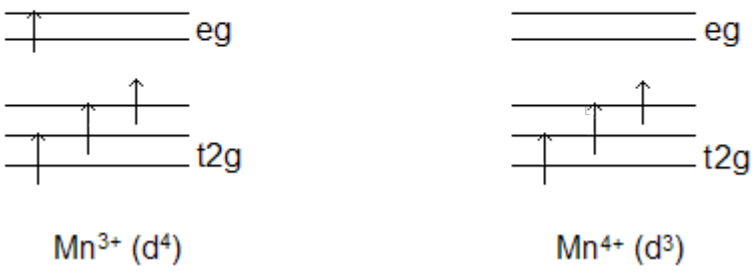

Figure 3.2: Crystal Field Scheme for the $La_{1-x}A_xMnO_3$ Manganites

The phase diagram for hole-doped $La_{1-x}Sr_xMnO_3$ is shown in figure 3.3. Certainly, there is no agreement on the nature of all the phases observed, as would be expected for such a complicated material. There are a variety of spin, orbital and charge orderings that occur at various points on the phase diagram. Various discussions can be found in [7, 31]

We now move on to a discussion of the phases in the phase diagram for $La_{1-x}Sr_xMnO_3$. At $x = 0$, we have the parent compound $LaMnO_3$. Here, we have a Jahn-Teller phase which exists at very high temperature. The orbital ordering causing the Jahn-Teller distortion is unclear, but numerous proposals have been put forward. One proposal states the orbital ordering is alternating $3\hat{x}^2 - \hat{r}^2$ and $3\hat{y}^2 - \hat{r}^2$ in a staggered pattern. Whatever the nature of the ordering, it is a tough Mott insulator.

As we dope from $x = 0$, double exchange mechanisms will begin to take operation, and we have seen in the previous chapter, this leads the system towards being a ferromagnet. For a while, the canted antiferromagnetism survives, but eventually gives way to a ferromagnetic insulating phase, with the emergence of charge ordering at low temperatures, peaking at $x = 1/8$. Further doping melts the insulating phase and the material tends towards metallic behaviour. This region is a ferromagnetic metal, and is the region of most interest to the CMR community. At $x = 3/8$, the Curie temperature for the ferromagnetism reaches its peak.

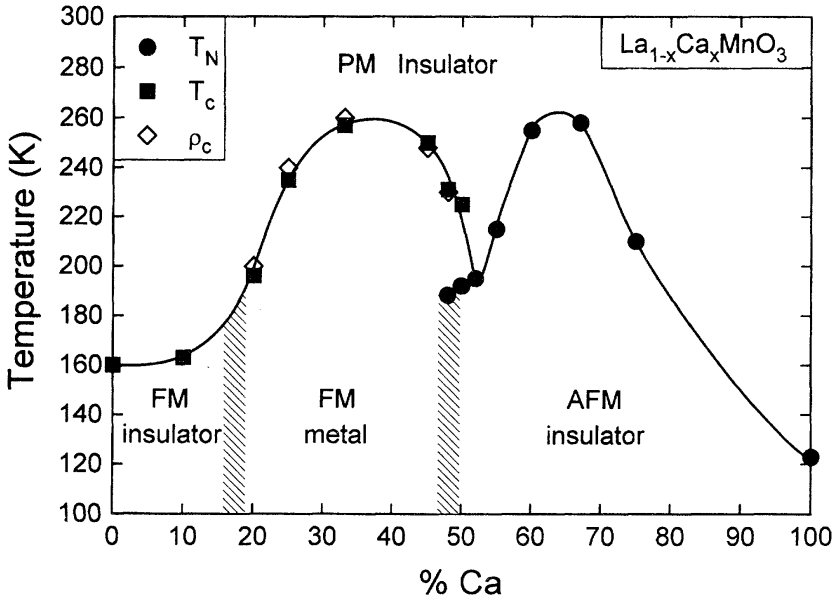

Figure 3.3: Generic phase diagram of the hole-doped manganites (From [28])

At $x = 0.5$ we find the so-called CE phase. Experiments suggest that charge is stacked along the z-axis.

When $x > 0.5$, the ferromagnetic region disappears quickly, and is replaced by an anti-ferromagnetic phase competing with a charge ordered phase. It also illustrates the strong asymmetry in particles and holes. This in particular implies any Hubbard model approach will only work for one of the regions in the phase diagram, since we can switch between holes and particles in the Hubbard model at half-filling.

There is controversy over the $x = 2/3$ region of the phase diagram. Radaelli et. al. [30] suggest a Wigner crystal-like arrangement, with charge spread over the material. Other authors suggest a stripe-like phenomena is present, and charge is concentrated. There is strong theoretical evidence that these two states are very close in energy, and hopefully the mystery can be resolved with experiments in the near future.

3.3 Magnetism in Pyrochlore Systems

Magnetism is pyrochlore systems is a subject of intense current interest, with most interest in the materials exhibiting the spin-ice phenomenon. We will not have occasion to discuss spin-ice[6] in the work that we have done, but we will discuss some aspects of the phenomena for completeness, and to illustrate why the pyrochlore material we consider later on does not display spin-ice behaviour, which is possibly the first phenomena that is brought to mind by most when discussing magnetism in pyrochlore systems.

3.3.1 The Pyrochlore Crystal Structure

The pyrochlore crystal structure is slightly intimidating at first sight. It is a network of tetrahedra and octahedra. The space group for the material is Fd-3m. The pyrochlore materials typically have formula $A_2B_2O_7$, with A and B typically rare earths or transition metals. For our purposes, we regard it as a network of tetrahedra. The structure of pyrochlore is shown in figure 3.4.

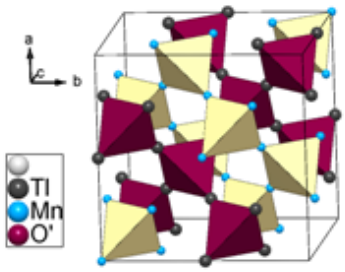

Figure 3.4: The Pyrochlore Structure

The tetrahedral network in pyrochlore lends itself well to materials exhibiting geometric frustration and novel forms of magnetism. Frustration occurs when even after breaking the symmetry, there is still some degeneracy that prevents us from singling out a ground state. The ferromagnetic materials include the materials displaying the spin-ice phenomenom, which we will only discuss briefly since spin-ice is tangent to our interests. On the antifer-

romagnetic side, we have the material of interest to us, $Gd_2Ti_2O_7$. Both of these materials have interesting magnetism originating from geometric frustration.

3.3.2 Spin-Ice

Spin-ice is a material of a high degree of current interest. It is a system with spin-degrees of freedom on a pyrochlore system. Ordinary water ice is a system exhibiting surprisingly complex behaviour. The hydrogen bonds satisfy a 'two in, two out' rules. In other words, two hydrogen atoms lie close to each oxygen atom, and two hydrogen atoms should lie away from each oxygen atom. This arrangement leads to a large residual entropy, and is the motivation for the moniker "spin ice". This situation is illustrated in figure 3.5.

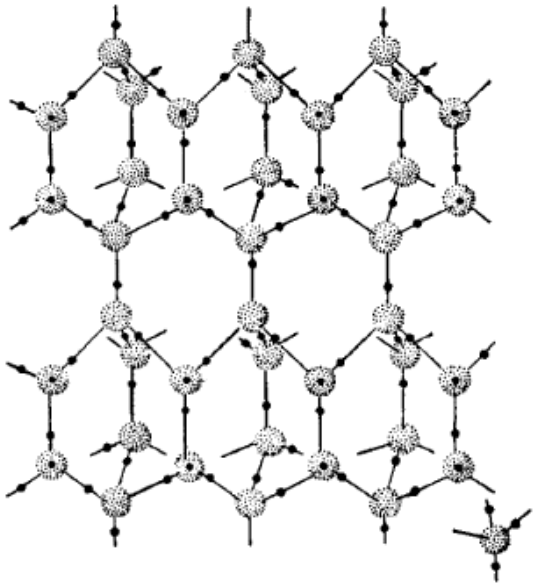

Figure 3.5: Ice structure. Oxygen atoms are the large vertices, and hydrogen atoms are the small black circles. As we can see, each oxygen atom has two hydrogen atoms close by, and two neighbours which have hydrogen atoms close by.

In spin-ice, we have the situation where two of the magnetic moments point towards the centre of the tetrahedron, and two of the moments point away from the centre of the tetrahedron. This situation is illustrated in figure 3.6, and the analogy between water-ice and spin-ice is clear.

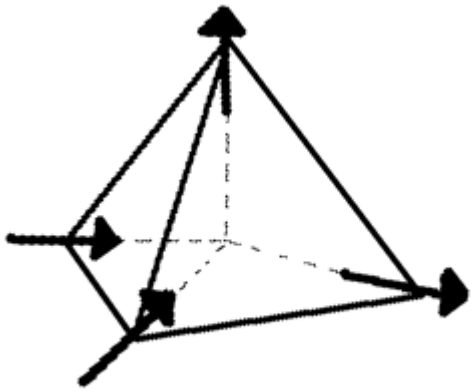

Figure 3.6: Spin-ice

Spin-ice is an example of a frustrated ferromagnetic, in contrast to the rather more elementary frustration found in triangular antiferromagnets, which incidentally we have cause to discuss in section 3.3.3. Locally strong crystal field effects cause the spins to point in or out of the local tetrahedra. Coupled with long-range dipolar interactions, this creates quasiparticles resembling magnetic monopoles.

3.3.3 Antiferromagnets on a Pyrochlore Lattice

More relevant to the work we will undertake is an antiferromagnet on a pyrochlore lattice. This is a highly frustrated geometry. Consider the antiferromagnetic Heisenberg model on a triangular lattice. This is the prototypical example of geometric frustration. Since a tetrahedron is a polyhedron formed from triangles, we can expect a large degree of frustration in tetrahedral antiferromagnets. Further, the pyrochlore structure is a network of tetrahedra, and so pyrochlore systems are often synonymous with frustration and novel effects can arise from this, such as the spin-ice phenomena discussed above.

3.4 Heavy-Fermion Materials

One of the class of strongly correlated electronic compounds that has received a lot of attention is the heavy fermion compounds. They are typically U, Ce, or Yb based intermetallics, although Np, Pu compounds have been reported to display heavy-fermion behaviour. As such, heavy-fermion compounds are almost invariably f-electron systems, although LiV_2O_4 arguably displays heavy-fermion behaviour, despite containing no elements beyond the transition series. A detailed review of heavy fermion systems can be found in the review article by Stewart [34].

The adjective heavy stems from the large effective masses of the conduction electrons, which can be probed directly by de Haas-van Alphen measurements. The cyclotron masses m_c of the quasiparticles in magnetic resonance measurements of the magnetisation is measured in this experiment, and are found to be in the range $10^2 - 10^3 m_e$. The cyclotron mass is obtained from the cyclotron frequency ν in a magnetic field of strength B from the relation

$$m_c = \frac{eB}{2\pi\nu} \tag{3.1}$$

Electrons in an interacting system have an effective mass $m*$, and the effective mass is usually different from the bare electron mass, m_e. The effective mass is said to have been renormalised by the interactions. Heavy fermions are materials characterised by a large effective mass of the conduction electrons.

The path to the discovery of heavy fermion materials began in the 70s with the observation of mixed-valance materials. The first heavy fermion material discovered was $CeAl_3$. The discovery of the enormous enhancement of the effective mass caused a certain amount of interest. The interest in heavy fermion materials, however, really began with the discovery of superconductivity in $CeCu_2Si_2$. by Steglich et. al. [33]

There are certain experimental signatures of heavy fermion behaviour. The first is a very

large linear coefficient γ of the specific heat capacity C, which in temperature ranges much smaller than the Debye and Fermi temperatures looks like

$$C = \gamma T + \beta T^3$$

where γ is at least 400 mJ/f-Atom Mol K, which is perhaps a little arbitrary. By contrast, an ordinary metal would have $\gamma \approx 1$ mJ/f-Atom Mol K. The relation between γ and the effective mass $m*$ is

$$\gamma \propto m* \tag{3.2}$$

and so it is suggestive that a large γ would correspond to a large effective mass.

3.4.1 UPt_3

UPt_3 is a heavy fermion superconductor. UPt_3 is interesting because of an antiferromagnetic ordering between spins coexisting with superconductivity. The antiferromagnetism sets in at $T_N = 5$ K. The bulk superconductivity was discovered in UPt_3 at $T_c = 0.54$ K by Stewart *et al.* [35] in 1984. The superconductivity of UPt_3 is complicated, and is thought to have multiple phases of superconductivity. A detailed review can be found in the review article [20]

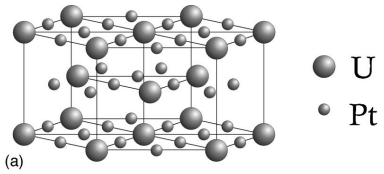

Figure 3.7: Crystal Structure of UPt_3

In addition to the discovery of superconductivity, Stewart et al. presented evidence which indicated that UPt_3 is a superconductor with superconductivity propagated by spin-fluctuations. Since then, there has been a large amount of work on superconductivity of UPt_3

because of its unique nature. The dispersion of bands of UPt_3 is due to the hybridization of the U 5f shell with the Pt 5d shell. Direct overlap of the U atoms is negligible since the minimum U-U distance is 4.13 A, which is well below the Hill limit of 3.4 A. At distances greater than this, 5f orbitals cease to overlap and become localised moments in the absence of hybrdisation with a conduction band.

3.5 High-Temperature Cuprate Superconductors

The high-temperature superconducting cuprates are one of the biggest reasons for the intense interest that has been generated in strongly correlated electronic systems, and though they are not directly relevant to the work performed in this thesis, not mentioning them at all in a work on strongly correlated electrons would be a huge omission. The first high-temperature superconductor was discovered by Bednorz and Muller in 1986 [4]. This material was $La_{2-x}Ba_xCuO_4$, and displayed a superconducting transition around 30 K. This was thought to be the upper-limit for phonon mediated superconductors. The critical temperature of cuprate superconductors has increased dramatically since 1986.

Although there are different families of high-temperature superconductors, there is at least one thing common to all and that is the existence of a plane of CuO_2 (figure 3.8) where the superconductivity takes place. The phase diagram for the cuprates is fairly generic 3.9.

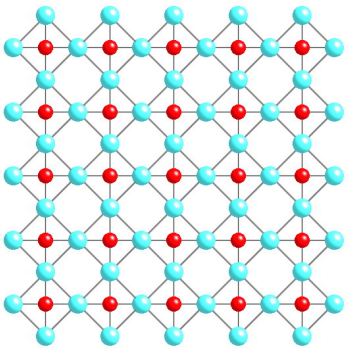

Figure 3.8: Copper-Oxygen Planes

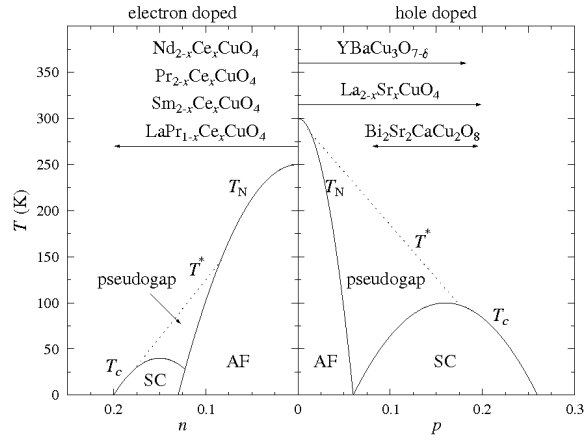

Figure 3.9: Generic phase diagram of the Cuprates

Another reason for this short section on the superconducting cuprates is that they bear resemblance to heavy fermion systems. Indeed, the models that are thought to describe these two systems can be mapped onto each other, at least if one takes the Anderson lattice model and *d-p* model to be the models that describe the heavy-fermion materials and high-T_C superconductors respectively.

3.6 Summary

Strongly correlated materials are wide in range, and we have only discussed a few examples here. All the materials discussed here are strongly correlated due to the Coulomb interaction between electrons with wave-functions of short spatial extent. Strong correlations can also exist due to reduced dimensionality, such as in organic magnets, and carbon nanotubes, but we will not have occasion to discuss them here.

We discussed examples of the strongly correlated materials that we will attempt to model in this thesis. We will model them with various degrees of success. The CMR manganites and the frustrated pyrchlore antiferromagnets are modelled reasonably well, we feel. The heavy-fermion superconductors, however, are a completely different matter, and are far more complex and have a wide range of phase diagrams. Our modelling is thus done at the level

of a toy-model for the heavy fermion materials.

Chapter 4

Models

4.1 Introduction

The Hubbard model is the first of the models that we will use in this thesis to be discussed. It was introduced by Hubbard in 1963 in a series of six papers[13, 14, 15, 16, 17, 18]. It is perhaps the simplest models of interacting electrons that one could construct. Unfortunately, its solution is still intractable. We must resort to approximations if we are to make any progress in solving the model. These methods of approximation will be discussed in chapter four.

There are rigorous results on ferromagnetism in the Hubbard model. One of the most important for us in the Nagaoka ferromagnetism[26]. In chapter seven, we will generalise this to a ferro-orbital arrangement, and find that the exact solvability of the problem disappears, and we are again forced to approximation.

We then discuss an even more complicated model than the Hubbard model, the Anderson lattice. This would seem an unreasonable thing to do, since we cannot solve even the simpler model. However, the Hubbard model is missing an essential physical process for modelling heavy fermion materials, and that is hybridisation. The interplay between local moments and conduction electrons is critical for modelling heavy fermion behaviour, and also we believe this to be the case for modelling the high-temperature superconductors.

4.2 The Hubbard Model

The Hubbard model takes the form

$$\mathcal{H} = -t \sum_{<jj'>\sigma} c^{\dagger}_{j'\sigma} c_{j\sigma} + U \sum_{j} c^{\dagger}_{j\uparrow} c_{j\uparrow} c^{\dagger}_{j\downarrow} c_{j\downarrow}. \tag{4.1}$$

$c_{j\sigma}$ is an operator that creates a valence electron on site j with spin σ. While the model apparently is simplistic, and indeed it is simple to understand the physics behind the model. We have electrons that are itinerant on some lattice. The electrons gain an energy t for moving to a nearest-neighbour site, and pay an energy U if there was already an electron of opposite spin on the site the electron hopped to. Of course, Pauli exclusion applies and so it is not possible to hop to a site where an electron with the same spin is located. Despite the simplicity with which one can describe the model, it is notoriously difficult to solve even on a geometry as simple as the square lattice.

4.2.1 The Nagaoka Problem: An Exactly Solvable Limit

It is desirable to have exactly solvable limits of models, even if they do not correspond to physically realisable situations. This is the case with the Nagaoka problem[26], which considers the half-filled Hubbard model in the infinite U limit, with the removal of a single particle creating a hole. It is one of the few rigourous results in magnetism, and shows the stability of ferromagnetism in the Hubbard model.

Nagaoka studied the limit where the antiferromagnetic kinetic exchange is suppressed. At exact half-filling, the charge degrees of freedom are completely frozen. Removing a single electron creates a hole, and this hole delocalises on a background on spins. It turns out that under very general conditions, the homogeneity of a completely spin-polarized background is optimal for the propagation of the hole, thus kinetic energy favours ferromagnetism. This is stated in the celebrated Nagaoka theorem.

Let the number of electrons be N. If the lattice satisfies a certain connectivity condition, then the ground state has the maximal total spin, and it is unique, apart from the trivial $(N-1)$-fold spin degeneracy. The connectivity conditions require the existence of interconnecting loops, where the loops should pass through no more than four sites. The lattice is also required to be bipartite. This excludes the triangular lattice, which is a frustrated geometry, and we will have cause to discuss frustrated systems further in chapter nine.

The formulation of the Nagaoka theorem makes it clear that the number of lattice sites has to be finite. Thus when speaking of the Nagaoka theorem for say the square lattice we mean arbitrarily large but finite pieces of the square lattice. When taking the thermodynamic limit, we are unsure if the Nagaoka state has an extent beyond that of a point in the phase diagram of the Hubbard model. Numerical simulations have been performed, but the situation remains unclear. The only certainty is that more than one hole is analytically intractable for now.

4.3 The Anderson Impurity Model

The Anderson lattice is a generalisation the model employed by Anderson[3] to describe a magnetic impurity in a host metal. The Anderson impurity model takes the form

$$\mathcal{H} = -t \sum_{j\sigma} c^{\dagger}_{j\sigma} c_{j'\sigma} + V \sum_{\sigma} \left(f^{\dagger}_{\sigma} c_{0\sigma} + c^{\dagger}_{0\sigma} f_{\sigma} \right) + \epsilon f^{\dagger}_{\sigma} f_{\sigma} + U f^{\dagger}_{\uparrow} f_{\uparrow} f^{\dagger}_{\downarrow} f_{\downarrow} \tag{4.2}$$

where f_σ is the annihilation operator for the magnetic impurity, chosen to sit somewhere on the lattice, $c_{j\sigma}$ is a conduction electron annihilation operator at the site indexed by j, with spin σ. The f operator is a fermion, and hence has fermionic commutation relations.

This model is similar in form to the Hubbard model, but the physical situation is completely different. Firstly, the itinerant electrons are not the strongly correlated electrons. In the Hubbard model, there is only one species of electron, and these electrons play both roles.

In the Anderson lattice, the strongly correlated electrons are localised, and are only able to participate in the physics of the problem by hybridisation with the conduction electrons governed by the term in V. The term in U is the usual on-site repulsion between strongly correlated electrons, which in this case would be electrons on the magnetic impurity. The term in t is the tight-binding model type transport of the conduction electrons.

4.3.1 The Kondo Effect and RKKY

In order to gain some insight it is worth studying an isolated impurity in the sea of conduction electrons The experimental input is that of low concentrations of magnetic impurities in a paramagnetic host. For examples, doping Mn into Cu, we do not find any magnetic ordering at low temperatures. First we will tackle a limit of the Anderson model that of $V \to 0$ when the systems decouple.

There is a canonical transformation called the Schrieffer-Wolff[32] transformation that takes us from the Anderson impurity model to the Kondo model[22]. The idea is that we perform a Unitary transformation which is chosen to diagonalise H to order V. If the states transform as $|\psi' >= \exp(-S)|\psi >$, then the Hamiltonian transforms as $H \to \exp(-S)H\exp(S)$. Here, S is skew-Hermitian. We write the Hamiltonian as a Taylor series

$$\exp(\lambda S)H\exp(-\lambda S) = H + \sum_{n=1}^{\infty} \frac{\lambda}{n!}[S,[S,[\ldots H] \tag{4.3}$$

where there are n commutators in the last term on the right-hand side.

To see this, consider

$$\frac{d}{d\lambda}\exp(\lambda S)O\exp(-\lambda S) = \exp(\lambda S)[S,O]\exp(-\lambda S) \tag{4.4}$$

As $\lambda \to 0$, we can see

$$\frac{d}{d\lambda}O = [S,O] \tag{4.5}$$

and so the derivative acts as commutation, and continuing the series, we have

$$\exp(\lambda S) H \exp(-\lambda S) = H + [S, H] + \frac{1}{2}[S, [S, H]] + \dots . \tag{4.6}$$

Let $H_1 = [S, H]$, $H_2 = [S, [S, H]]$, and so forth.

Let H_1 and S be small. Grouping terms of similar orders, we obtain

$$H' = H_0 + (H_1 + [S, H_0]) + \left([S, H_1] + \frac{1}{2}[S, [S, H_1]] \right). \tag{4.7}$$

The trick is now to find an S such that

$$H_1 + [S, H_0] = 0 \tag{4.8}$$

and then

$$H' = H_0 + \frac{1}{2}\,[S, H_1] + O(\delta^3) \tag{4.9}$$

where the second term is $O(\delta^2)$.

The initial problem is then mapped onto a new problem which is second order in δ. There are several important considerations. The first is that if there is a contribution at order δ, then no such S exists. We cannot find an analogue in the Hubbard model, for example, due to the lack of hybridisation. This will be of no concern to us, however. Further, the presence of degeneracy can make the technique fail.The transformation modifies the *states* and the new meaning of the operators must be carefully interpreted. We must also be able to find S, rather than demonstrate its existence, to be able to perform the transformation.

The small parameter is assumed to be V, the hybridisation between the two systems

$$H_0 = \sum_{\mathbf{k}\sigma} \epsilon_{\mathbf{k}} c^\dagger_{\mathbf{k}\sigma} c_{\mathbf{k}\sigma} + \Delta \sum_\sigma f^\dagger_\sigma f_\sigma + U \hat{n}^f_\uparrow \hat{n}^f_\downarrow$$

$$H_1 = \frac{V}{\sqrt{N}} \sum_{\mathbf{k}\sigma} \left(f_\sigma^\dagger c_{\mathbf{k}\sigma} + c_{\mathbf{k}\sigma}^\dagger f_\sigma \right)$$

Now let us find S, let us look at:

$$S_0 = \sum_{\mathbf{k}\sigma} A_{\mathbf{k}\sigma} f_\sigma^\dagger c_{\mathbf{k}\sigma}$$

$$[H_0, S_0] = \sum_{\mathbf{k}\sigma} \left(\Delta + U\hat{n}_{\bar{\sigma}}^f - \epsilon_{\mathbf{k}} \right) A_{\mathbf{k}\sigma} f_\sigma^\dagger c_{\mathbf{k}\sigma} \sim H_1 = \frac{V}{\sqrt{N}} \sum_{\mathbf{k}\sigma} \left(f_\sigma^\dagger c_{\mathbf{k}\sigma} + c_{\mathbf{k}\sigma}^\dagger f_\sigma \right)$$

which is similar to the first part of H_1, but there is a second contribution so we now include:

$$S_1 = \sum_{\mathbf{k}\sigma} B_{\mathbf{k}\sigma} \hat{n}_{\bar{\sigma}}^f f_\sigma^\dagger c_{\mathbf{k}\sigma}$$

$$[H_0, S_1] = \sum_{\mathbf{k}\sigma} \left(\Delta + U - \epsilon_{\mathbf{k}} \right) B_{\mathbf{k}\sigma} \hat{n}_{\bar{\sigma}}^f f_\sigma^\dagger c_{\mathbf{k}\sigma}$$

Use $S_0 + S_1$ with carefully chosen coefficients which both cancel the term in $\hat{n}_{\bar{\sigma}}^f$ and reproduce the correct coefficient in H_1:

$$B_{\mathbf{k}\sigma} \left(\Delta + U - \epsilon_{\mathbf{k}} \right) + A_{\mathbf{k}\sigma} U = 0$$

$$\left(\Delta - \epsilon_{\mathbf{k}} \right) A_{\mathbf{k}\sigma} = \frac{V}{\sqrt{N}}$$

and hence

$$A_{\mathbf{k}\sigma} = \frac{V}{\sqrt{N}} \frac{1}{\Delta - \epsilon_{\mathbf{k}}}$$

$$B_{\mathbf{k}\sigma} = \frac{V}{\sqrt{N}} \frac{-U}{(\Delta - \epsilon_{\mathbf{k}})(\Delta + U - \epsilon_{\mathbf{k}})}$$

and then remembering that the commutator is anti-symmetric

$$S = \frac{V}{\sqrt{N}} \sum_{\mathbf{k}\sigma} \frac{1}{\Delta - \epsilon_{\mathbf{k}}} \left(f_\sigma^\dagger c_{\mathbf{k}\sigma} - c_{\mathbf{k}\sigma}^\dagger f_\sigma \right) \left[1 - \frac{\hat{n}_{\bar{\sigma}}^f U}{\Delta + U - \epsilon_{\mathbf{k}}} \right]$$

which can be written as

$$S = \frac{V}{\sqrt{N}} \sum_{\mathbf{k}\sigma} \left(f_\sigma^\dagger c_{\mathbf{k}\sigma} - c_{\mathbf{k}\sigma}^\dagger f_\sigma \right) \left[\frac{1 - \hat{n}_{\bar{\sigma}}^f}{\Delta - \epsilon_{\mathbf{k}}} + \frac{\hat{n}_{\bar{\sigma}}^f}{\Delta + U - \epsilon_{\mathbf{k}}} \right] \tag{4.10}$$

The effective Hamiltonian is

$$\frac{1}{2}\left[S, H_1\right] = \frac{V^2}{2N} \sum_{\mathbf{k}\sigma} \sum_{\mathbf{q}\tau} \left[\left(f_\sigma^\dagger c_{\mathbf{k}\sigma} - c_{\mathbf{k}\sigma}^\dagger f_\sigma \right) \left[\frac{1 - \hat{n}_{\bar{\sigma}}^f}{\Delta - \epsilon_{\mathbf{k}}} + \frac{\hat{n}_{\bar{\sigma}}^f}{\Delta + U - \epsilon_{\mathbf{k}}} \right], \left(f_\tau^\dagger c_{\mathbf{q}\tau} + c_{\mathbf{q}\tau}^\dagger f_\tau \right) \right]$$

$$= \frac{V^2}{2N} \sum_{\mathbf{k}\mathbf{q}\sigma} \frac{U}{(\epsilon_{\mathbf{k}} - \Delta)(\Delta + U - \epsilon_{\mathbf{k}})} \left(f_\sigma^\dagger c_{\mathbf{k}\sigma} f_{\bar{\sigma}}^\dagger c_{\mathbf{q}\bar{\sigma}} + c_{\mathbf{k}\sigma}^\dagger c_{\mathbf{q}\bar{\sigma}} f_{\bar{\sigma}}^\dagger f_\sigma + c_{\mathbf{k}\sigma}^\dagger f_\sigma c_{\mathbf{q}\bar{\sigma}}^\dagger f_{\bar{\sigma}} + c_{\mathbf{q}\bar{\sigma}}^\dagger c_{\mathbf{k}\sigma} f_\sigma^\dagger f_{\bar{\sigma}} \right)$$

$$+ \frac{V^2}{2N} \sum_{\mathbf{k}\mathbf{q}\sigma} \left[\frac{1 - \hat{n}_{\bar{\sigma}}^f}{\Delta - \epsilon_{\mathbf{k}}} + \frac{\hat{n}_{\bar{\sigma}}^f}{\Delta + U - \epsilon_{\mathbf{k}}} \right] \left(f_\sigma^\dagger f_\sigma \delta_{\mathbf{k}\mathbf{q}} - f_\sigma f_\sigma^\dagger \delta_{\mathbf{k}\mathbf{q}} + c_{\mathbf{k}\sigma} c_{\mathbf{q}\sigma}^\dagger - c_{\mathbf{k}\sigma}^\dagger c_{\mathbf{q}\sigma} \right)$$

We can isolate three contributions

$$\frac{V^2}{N} \sum_{\mathbf{k}\mathbf{q}\sigma} \frac{1}{\Delta - \epsilon_{\mathbf{k}}} \left[f_\sigma^\dagger f_\sigma - c_{\mathbf{k}\sigma}^\dagger c_{\mathbf{q}\sigma} \right] + \frac{U}{(\epsilon_{\mathbf{k}} - \Delta)(\Delta + U - \epsilon_{\mathbf{k}})} \hat{n}_\sigma^f \hat{n}_{\bar{\sigma}}^f$$

A 'non-interacting' bit which renormalises the energies and allows the conduction electrons to 'scatter' off the origin.

$$\frac{V^2}{2N} \sum_{\mathbf{k}\mathbf{q}\sigma} \frac{U}{(\epsilon_{\mathbf{k}} - \Delta)(\Delta + U - \epsilon_{\mathbf{k}})} \left[f_\sigma^\dagger f_{\bar{\sigma}}^\dagger c_{\mathbf{q}\bar{\sigma}} c_{\mathbf{k}\sigma} + c_{\mathbf{k}\sigma}^\dagger c_{\mathbf{q}\bar{\sigma}}^\dagger f_{\bar{\sigma}} f_\sigma \right]$$

A term which connects to either vacant or doubly occupied f-atoms.

$$\frac{V^2}{2N} \sum_{\mathbf{k}\mathbf{q}\sigma} \frac{U}{(\epsilon_{\mathbf{k}} - \Delta)(\Delta + U - \epsilon_{\mathbf{k}})} \left[c_{\mathbf{k}\sigma}^\dagger c_{\mathbf{q}\bar{\sigma}} f_{\bar{\sigma}}^\dagger f_\sigma + c_{\mathbf{q}\bar{\sigma}}^\dagger c_{\mathbf{k}\sigma} f_\sigma^\dagger f_{\bar{\sigma}} - c_{\mathbf{k}\sigma}^\dagger c_{\mathbf{q}\sigma} f_{\bar{\sigma}}^\dagger f_{\bar{\sigma}} - c_{\mathbf{q}\sigma}^\dagger c_{\mathbf{k}\sigma} f_{\bar{\sigma}}^\dagger f_{\bar{\sigma}} \right]$$

which can be rewritten as:

$$\frac{V^2}{N}\sum_{\mathbf{kq}}\frac{U}{(\epsilon_{\mathbf{k}}-\Delta)(\Delta+U-\epsilon_{\mathbf{k}})}\left[-\hat{n}_{\mathbf{kq}}\hat{n}^f+\hat{\mathbf{s}}_{\mathbf{kq}}.\hat{\mathbf{S}}^f\right]$$

where:

$$\hat{n}_{\mathbf{kq}}=\frac{1}{2}\sum_{\sigma}c^{\dagger}_{\mathbf{k}\sigma}c_{\mathbf{q}\sigma} \qquad \hat{n}^f=\frac{1}{2}\sum_{\sigma}f^{\dagger}_{\sigma}f_{\sigma}$$

$$\hat{\mathbf{s}}_{\mathbf{kq}}=\frac{1}{2}\sum_{\sigma\tau}c^{\dagger}_{\mathbf{k}\sigma}\sum_{\sigma\tau}c_{\mathbf{q}\tau} \qquad \hat{\mathbf{S}}^f=\frac{1}{2}\sum_{\sigma\tau}f^{\dagger}_{\sigma}\sum_{\sigma\tau}f_{\tau}$$

are average electron numbers and spins.

This final term is the residual interaction between the f-electron spin and the conduction electrons. This final term is the interesting one for the magnetic impurity doped into a paramagnetic host, and makes a connection to the Kondo Hamiltonian

$$H=\sum_{\mathbf{k}\sigma}\epsilon_{\mathbf{k}}c^{\dagger}_{\mathbf{k}\sigma}c_{\mathbf{k}\sigma}+J\hat{\mathbf{s}}_0.\hat{\mathbf{S}}^f$$

where $\hat{\mathbf{s}}_0$ is the spin operator for the conduction electrons on site zero.

$$J=\frac{V^2U}{(\mu-\Delta)(\Delta+U-\mu)}$$

The resolution of the Kondo Hamiltonian is that a *Kondo singlet* forms. The simplest calculation which suggests this result is variational, and is due to Varma and Yafet[42].

$$\mid\psi\rangle=\left[a+\sum_{\mathbf{k}\sigma}A_{\mathbf{k}\sigma}f^{\dagger}_{\sigma}c_{\mathbf{k}\sigma}\right]\prod_{\epsilon_{\mathbf{k}}<\mu}\left(c^{\dagger}_{\mathbf{k}\uparrow}c^{\dagger}_{\mathbf{k}\downarrow}\right)\mid 0\rangle$$

The Fermi sea is allowed to populate the f-level. It is crucial that the chosen state has the symmetry of the unique Fermi sea and that the f-electron is *not* present in the reference

state.

$$\langle\psi \mid \psi\rangle = \mid a \mid^2 + \sum_{\mathbf{k}\sigma} \mid A_{\mathbf{k}\sigma} \mid^2$$

$$\langle\psi \mid H \mid \psi\rangle = \mid a \mid^2 E_0 + \sum_{\mathbf{k}\sigma} \mid A_{\mathbf{k}\sigma} \mid^2 (E_0 + \Delta - \epsilon_{\mathbf{k}})$$

$$+\frac{V}{\sqrt{N}} \sum_{\mathbf{k}\sigma} \sum_{\epsilon_{\mathbf{k}}<\mu} a^* A_{\mathbf{k}\sigma} + \frac{V}{\sqrt{N}} \sum_{\mathbf{k}\sigma} \sum_{\epsilon_{\mathbf{k}}<\mu} a A^*_{\mathbf{k}\sigma}$$

Minimisation over the parameters provides:

$$\frac{\partial}{\partial a^*} \quad \mapsto \quad E_0 a + \frac{V}{\sqrt{N}} \sum_{\mathbf{k}\sigma} \sum_{\epsilon_{\mathbf{k}}<\mu} A_{\mathbf{k}\sigma} = \epsilon a$$

$$\frac{\partial}{\partial A^*_{\mathbf{k}\sigma}} \quad \mapsto \quad (E_0 + \Delta - \epsilon_{\mathbf{k}}) A_{\mathbf{k}\sigma} + \frac{V}{\sqrt{N}} a = \epsilon A_{\mathbf{k}\sigma}$$

We need to consider the cases of both a singlet and a triplet for comparison.

For the triplet case we have

$$\sum_{\sigma} A_{\mathbf{k}\sigma\sigma} = T_{\mathbf{k}} \left(f^\dagger_\uparrow c^\dagger_{\mathbf{k}\downarrow} + f^\dagger_\downarrow c^\dagger_{\mathbf{k}\uparrow} \right)$$

$$\epsilon = E_0 + \Delta - \epsilon_{\mathbf{k}} \geq E_0 + \Delta - \mu = \epsilon_T$$

while the singlet gives

$$\sum_{\sigma} A_{\mathbf{k}\sigma} = S_{\mathbf{k}} \left(f^\dagger_\uparrow c^\dagger_{\mathbf{k}\downarrow} - f^\dagger_\downarrow c^\dagger_{\mathbf{k}\uparrow} \right)$$

$$S_{\mathbf{k}} = \frac{V}{\sqrt{N}} \frac{a}{\epsilon + \epsilon_{\mathbf{k}} - \Delta - E_0}$$

$$\epsilon = E_0 + \frac{V^2}{N} \sum_{\mathbf{k}} \sum_{\epsilon_{\mathbf{k}}<\mu} \frac{2}{\epsilon + \epsilon_{\mathbf{k}} - \Delta - E_0}$$

If we set $\epsilon \equiv \epsilon_S = \epsilon_T - \delta$ then:

$$\Delta - \mu - \delta = 2V^2 \frac{1}{N} \sum_{\mathbf{k}} \frac{1}{\epsilon_{\mathbf{k}} - \mu - \delta} \mapsto V^2 \int_{-\infty}^{\mu} d\epsilon \rho(\epsilon) \frac{1}{\epsilon - \mu - \delta}$$

as $\delta \mapsto 0$ there is a logarithmic divergence caused by the states near μ:

$$\Delta - \mu - \delta \doteq V^2 \rho(\mu) \ln \left[\frac{\delta}{W + \mu} \right]$$

where W is the band-width:

$$\delta \sim W \exp \left(-\frac{\mu - \Delta}{V^2 \rho(\mu)} \right)$$

so:

$$\epsilon_S = \epsilon_T - W \exp \left(-\frac{\mu - \Delta}{V^2 \rho(\mu)} \right)$$

There is always a *small* energy gain from the situation when the local moment forms a singlet with a conduction electron close to the Fermi surface. This is the *Kondo singlet*, and is the cause of a resistance minimum in metals containing magnetic impurities.

The energy gain is *non-perturbative*. To all orders in perturbation theory in V, the contribution to the energy is zero. This tendency to form a local singlet ensures that the local moment fluctuates in direction and therefore does not lead to ordering of spins at low temperatures.

Now we move on to the RKKY effect. If we consider the limit $V \to 0$ in the Anderson hamiltonian, there will be no hybridisation between the conduction electrons and the local moments. In the absence of hybridisation, the conduction electrons form a non-degenerate Fermi sea, while the local moments form a degenerate sea of spins. There is a method of lifting the spin-degeneracy of the local moments by performing perturbation theory to fourth order.

A local moment changes orientation by creating particle and hole excitations with dif-

ferent spin orientations. These excitations then travel across to a second local moment and annihilate by changing its orientation in a complementary way. In the intermediate state both local moments are occupied:

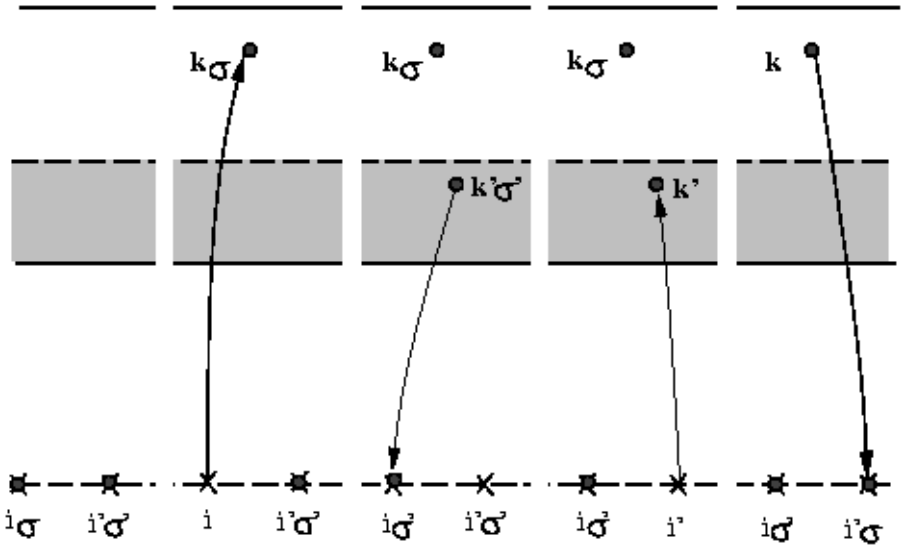

From the diagram shown in figure 4.3.1, we can see that this contributes an energy

$$(-1)\frac{V^4}{N^2}\sum_{\mathbf{k}\mathbf{k}'}\theta(\epsilon_{\mathbf{k}}-\mu)\theta(\mu-\epsilon_{\mathbf{k}'})e^{i(\mathbf{k}-\mathbf{k}').(\mathbf{R}_i-\mathbf{R}_{i'})}(-1)\delta_{\tau\sigma'}\delta_{\tau'\sigma}\frac{1}{\epsilon_{\mathbf{k}}-\Delta}\frac{1}{\epsilon_{\mathbf{k}'}-\epsilon_{\mathbf{k}}}\frac{1}{\epsilon_{\mathbf{k}}-\Delta}$$

$$J_{ij}\sim\frac{V^4}{N^2}\sum_{\mathbf{k}\mathbf{k}'}\frac{\theta(\epsilon_{\mathbf{k}}-\mu)\theta(\mu-\epsilon_{\mathbf{k}'})}{(\epsilon_{\mathbf{k}'}-\epsilon_{\mathbf{k}})(\Delta-\epsilon_{\mathbf{k}})^2}4e^{i(\mathbf{k}-\mathbf{k}').(\mathbf{R}_i-\mathbf{R}_{i'})}\sim\frac{V^4}{(\Delta-\mu)^2}\chi_{ij}$$

where χ_{ij} is the paramagnetic susceptibility of the conduction electrons.

This interaction is called the RKKY interactions and dominates in metals. Magnetism is the natural result:

$$H\sim\frac{V^4}{(\Delta-\mu)^2}\frac{1}{N}\sum_{\mathbf{k}}\hat{\mathbf{S}}_{-\mathbf{k}}.\hat{\mathbf{S}}_{\mathbf{k}}\chi_{\mathbf{k}}$$

In the Anderson lattice, the magnetism is perturbative while the Kondo effect is non-perturbative. In the limit $V \mapsto 0$ magnetism is expected to win.

4.4 The Anderson Lattice

The Anderson Lattice model is a generalisation of the impurity model to that of a lattice of f-sites. The model is easily done by adding a sum over sites on the f operators

$$\mathcal{H} = -t \sum_{j\sigma} c^{\dagger}_{j\sigma} c_{j'\sigma} + V \sum_{j\sigma} \left(f^{\dagger}_{j\sigma} c_{j\sigma} + c^{j\dagger}_{j\sigma} f_{j\sigma} \right) + \epsilon \sum_{j\sigma} f^{\dagger}_{j\sigma} f_{j\sigma} + U \sum_{j} f^{\dagger}_{j\uparrow} f_{j\uparrow} f^{\dagger}_{j\downarrow} f_{j\downarrow} \qquad (4.11)$$

There are two natural limits of the Anderson lattice. The first is the atomic limit, where $V \to 0$, and we have an array of local moments decoupled from the conduction electrons. The second is the case that the penalty for double occupation vanishes, $U \to 0$. Here, the strongly correlated electrons decouple, and the local moments can hybridise with the conduction electrons freely.

4.4.1 Schrieffer-Wolff and the Kondo Lattice

Schrieffer and Wolff, as we saw above, showed that the Anderson impurity model is equivalent to the Kondo model in a certain parameter regime. This is where single impurity occupancy is heavily favoured and double occupancy of the impurity level is prohibitively energetically costly. The Schrieffer-Wolff transformation was introduced for deriving the Kondo impurity model from the impurity Anderson model. The derivation of the Kondo lattice from the Anderson lattice proceeds through the same steps, and gives essentially the same results, except for additional f-f hopping terms. We will not outline the calculation since it is lengthy, we have basically outlined the steps required in the impurity case, and we will not be using the Kondo lattice model. This is due to the Kondo lattice being written in terms of spin operators. As is well known, there is no Wick's theorem for spin operators, and so the

methods we will use in later chapters will not apply. For this reason, even though we will consider the Anderson lattice in the Kondo lattice regime of infinite repulsion and at least one f-electron present, we will work with the Anderson lattice only.

4.5 Summary

We have introduced the two models that will feature the most heavily in this thesis. The first by order of presentation and weight is the Hubbard model. The second is the Anderson lattice model. They are both examples of Hamiltonians which can be used to describe strongly correlated electronic materials.

We are now at the stage where we have some insight into materials, and some standard models to aid us in building models for individual materials. What we do not have is some method of solving them. The models we have introduced here are usually too difficult to solve without approximation, even though the models themselves are only approximations to physical systems.We will introduce a method for solving models in a single particle picture that we will use througout this thesis, and that is mean-field theory.

Chapter 5

Mean-Field Theory

5.1 Introduction

Strongly correlated electronic systems typically require non-perturbative methods to solve their assoicated models. Perturbative methods typically fail to describe the many-body ground state of the system. Perturbation theory is built upon the notion that the kinetic portion of the many-electron Schrodinger equation is the dominant part of the Hamiltonian, and weak correlations are typically added in the form of a finite set of Feynman diagrams. This approach does not capture even the very basic properties of strongly correlated systems such as the generation of robust energy gaps in the spectra, of an origin different than the well-known band gaps that lead to insulating behavior when the chemical potential lies in those gaps.

Unfortunately, non-perturbative methods are notorious for their complexity, and lack of coherent framework for their study. One method we can use to understand strongly correlated materials is mean-field theory.

Mean-field theory is a tool for studying many-body physics in a single-particle picture. It will be used quite extensively throughout this thesis, and so it is worth introducing in some detail. In the context of the lattice models we will use exclusively, mean-field theory takes its name from considering a particle on a given site to feel an averaged contribution from all

particles on other lattice sites.

We consider first the Hubbard model. As discussed, the Hubbard model is

$$H = -t \sum_{<jj'>\sigma} c^{\dagger}_{j\sigma} c_{j'\sigma} + U \sum_{j} n_{j\uparrow} n_{j\downarrow}. \tag{5.1}$$

In the limit $U \to 0$ this model is solvable, since it reduces to the tight-binding model. In the regime $U \neq 0$, however, the model is in general impossible to solve in dimensions other than one. This is unfortunate, since it is possibly the most basic model of interacting electrons one could construct. We are then forced to resort to methods of approximation. Mean-field theory is one such method of approximation.

To illustrate the basic ideas of mean-field theory, let us consider the term in U in (5.6). To solve the tight-binding model, we diagonalise the Hamiltonian by a Bloch-transformation[11], which takes us into reciprocal-space. Applying a Bloch transformation to $U \sum_j n_{j\uparrow} n_{j\downarrow}$ leaves us with a mess in the interaction term, although the kinetic part of the Hamiltonian will be diagonalised. The momentum conservation in the interaction term in reciprocal space makes the Hamiltonian far more difficult to solve than it was in real space, where the interaction term was diagonal.

We cannot diagonalise the Hubbard Hamiltonian in general. To proceed, we shall employ mean-field theory to approximate the many-body effects in a single-particle picture. We consider the interaction term to consist of averaged fields. That is, we consider the interction term to take the form

$$\begin{aligned} U \sum_{j} n_{j\uparrow} n_{j\downarrow} &\approx U \sum_{j} (n_{j\uparrow} < n_{j\downarrow} > + n_{j\downarrow} < n_{j\uparrow} > \\ &- c^{\dagger}_{j\uparrow} c_{j\downarrow} < c^{\dagger}_{j\downarrow} c_{j\uparrow} > - c^{\dagger}_{j\downarrow} c_{j\uparrow} < c^{\dagger}_{j\uparrow} c_{j\downarrow} > \\ &+ c^{\dagger}_{j\uparrow} c^{\dagger}_{j\downarrow} < c_{j\uparrow} c_{j\downarrow} > + < c^{\dagger}_{j\uparrow} c^{\dagger}_{j\downarrow} > c_{j\uparrow} c_{j\downarrow} \end{aligned} \tag{5.2}$$

The first line corresponds to $\hat{z}$-axis magnetism, the second to $\hat{x} - \hat{y}$ magnetism, and the third to superconductivity. This replaces the correlated multi-particle Hamiltonian with a single-particle effective Hamiltonian with rescaled physical quantities. We can see that the term

$$n_{j\uparrow} < n_{j\downarrow} > + n_{j\downarrow} < n_{j\uparrow} \tag{5.3}$$

corresponds to z-axis magnetism by noticing an imbalance in either the spin-up or spin-down population will lead to the formation of a moment, and hence magnetism. The term

$$c^{\dagger}_{j\uparrow} c^{\dagger}_{j\downarrow} < c_{j\uparrow} c_{j\downarrow} > + < c^{\dagger}_{j\uparrow} c^{\dagger}_{j\downarrow} > c_{j\uparrow} c_{j\downarrow} \tag{5.4}$$

can be seen to lead to superconductivity because a non-zero $< c_{j\sigma} c_{j\bar{\sigma}} >$ will that Cooper pairs have started forming. For the term

$$c^{\dagger}_{j\uparrow} c_{j\downarrow} < c^{\dagger}_{j\downarrow} c_{j\uparrow} > - c^{\dagger}_{j\downarrow} c_{j\uparrow} < c^{\dagger}_{j\uparrow} c_{j\downarrow} > \tag{5.5}$$

we note that $< c^{\dagger}_{j\uparrow} c_{j\downarrow} >< c^{\dagger}_{j\downarrow} c_{j\uparrow} >$ can be written as $(m^x + im^y)(m^x - im^y)$.

We can now diagonalise this mean-field Hamiltonian by employing the assumption that the averages do not change with respect to site position, and thus the reciprocal space mean-field Hamiltonian takes the form

$$H = -t \sum_{\mathbf{k}\sigma} (\gamma(\mathbf{k}) + U < n_{\bar{\sigma}} >) c^{\dagger}_{\mathbf{k}\sigma} c_{\mathbf{k}\sigma}. \tag{5.6}$$

Here, $\gamma_(\mathbf{k})$ is the structure factor. We have diagonalised the Hamitonian in a mean-field approximation and can easily read off the spectrum.

5.2 Landau Mean-Field Theory

We will now move on to describe the Landau theory of phase transitions. This was introduced by Landau to provide a framework to describe phase transitions at a classical level. This is achieved through the concept of an order parameter. Landau theory describes the behaviour of the free energy, G, and a function of the order parameter Θ. The choice of the order parameter must respect the symmetry present in the description of the problem.

The idea is that the free-energy should be analytic in the order parameter, and so the free-energy should admit a Taylor expansion in terms of the order parameter

$$G = G_0 + G_1\Theta + G_2\Theta^2 + G_3\Theta^3 + G_4\Theta^4 + \dots. \tag{5.7}$$

We can show $G_1 = 0$ from the condition that the free-energy is minimised in thermodynamic equilibrium, which we assume. G_3 is often equal to 0 as well. Landau theory is typically applied to second-order phase transition, and G_3 being non-zero guarantees a first-order transition. In this thesis, we are no longer guaranteed that $G_3 = 0$ since we will have cubic invariants present in our system and so we must include it. However, this forces any phase transition to be first-order, and so all the results of criticality and universality do not apply here. The vanishing of the coefficient G_2 is of particular interest to us, since this gives us the Stoner criterion, which we now move on to discuss.

5.3 The Stoner Criterion and its Stability

We now describe one of the most used concepts in this thesis. That is the Stoner criterion and its stability. It is used to predict where phase transitions occur as a function of the order parameter in the Landau expansion of the free-energy. This concept comes from the Stoner model of ferromagnetism, which we outline briefly here.

Stoner considered a simple model of ferromagnetism[37]. The observation that in a

paramagnetic metal, the density of states is equal for both spin species is the starting point. Applying a field will tend to order the electrons ferromagnetically. When the electrons develop a ferromagnetic ordering, there will be a bias to one species or the other. This will alter the density of states for both species, and there will be a gap in the energy spectrum.

When transitioning to a ferromagnet, the system will develop a spin polarisation towards one species, which we will label as $\uparrow$ and the population that electrons will be depleted from will be labelled $\downarrow$. The energy gain from depopulating one spin species is $\delta\epsilon\delta n$, and we have to pay an energy $U(n/2+\delta n)(n/2-\delta n)$, and so the system will transit to a ferromagnetic state if

$$-\delta\epsilon\delta n + U\delta n\delta n > 0 \tag{5.8}$$

which is achieved when

$$U\frac{\delta n}{\delta\epsilon} > 1 \tag{5.9}$$

or in other words

$$U\rho(\epsilon) > 1 \tag{5.10}$$

where $\rho(\epsilon)$ is the density of states.

We call the above result the *Stoner Criterion* for the free Fermi Gas to display ferromagnetism in an applied field. It is important to note that the state is *itinerant*. As we will see, this Stoner criterion is the same as the expression for the Stoner criterion of the Hubbard model to display itinerant ferromagnetism. Note that if a cubic invariant G_3 term was present, if we have no moment then $G_2 = 0$. However, differentiating G with respect to Θ twice, we have

$$\Theta^2 = \frac{-G_2 - 3G_3\Theta}{6G_4} \tag{5.11}$$

and so even if G_2 is zero, G_3 may not be and ordering could have developed in the system already. This is the first-order nature of the transition described by a non-zero G_3 in the

Landau free-energy.

5.4 Mean-Field Theory of the Hubbard Model

We now relate the Stoner model to Landau theory, and this idea will be used throughout the thesis from the other direction. We can generalise the notion of the Stoner criterion to other models where the order parameter is not that of a simple ferromagnet, but an order parameter for orbital ordering. We will see that the vanishing of G_2 leads to the same result predicted by the elementary argument presented above.

The dispersion of the Hubbard model at the mean-field level takes the form

$$E_\sigma = -t\gamma_k Z + U(n + \sigma m) \tag{5.12}$$

where γ_k is the structure factor, $\sigma = \pm 1$ in the sum, and σ as an index represents the spin. This leads to a Gibbs free-energy of

$$G = \frac{1}{2N}\sum_\sigma \int d\gamma \rho(\gamma)(E_\sigma - \mu) f_\sigma - TS - U(\frac{n^2}{4} - m^2) \tag{5.13}$$

where S is the entropy. The free-energy formally depends on n, m and μ. However, it should be clear that n depends on μ, and so we do not need to worry about n in an expansion of the free-energy. Expanding in the order parameter, we have

$$G = G_0 + \frac{1}{2}G_{mm}m^2 + \left(\frac{1}{24}G_{mmmm} + \frac{1}{2}\delta\mu^2 G_{\mu\mu} + \frac{1}{2}m^2\delta\mu G_{\mu mm}\right)m^4. \tag{5.14}$$

This is minimised when $\delta\mu = 0$, from which we have

$$\delta\mu G_{\mu\mu} + G_{\mu mm} = 0 \tag{5.15}$$

$$\rightarrow \quad \delta\mu = -\frac{G_{\mu mm}}{G_{\mu\mu}} \tag{5.16}$$

which leads to the result

$$G = G_0 + \frac{1}{2}G_{mm}m^2 + \left(\frac{1}{24}G_{mmmm} - \frac{1}{8}\frac{G_{\mu mm}^2}{G_{\mu\mu}}\right)m^4 \tag{5.17}$$

The phase diagram of the mean-field Hubbard model on a bipartite lattice is show in figure 5.1. It is remarkable that ferromagnetism is completely eliminated from the low doping regime: below a lower critical density $n < n_{\mathrm{cr}}$, the ground state remains paramagnetic even at $U \to \infty$. It has to be emphasized that the theories we are referring to here are not exact, in the sense that we cannot be sure that the area in the phase diagram which bears the label FM, is indeed ferromagnetic. The claims about the absence of ferromagnetism, however, are far more dependable. In particular, Kanamori[21] brought a cogent argument to show that the Hubbard model cannot have low density ferromagnetism in three-dimensional systems.

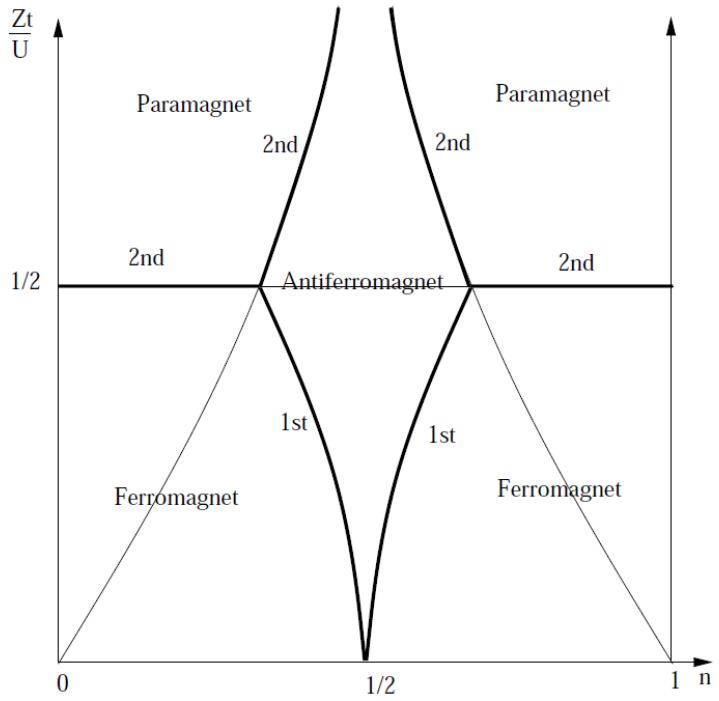

Figure 5.1: Phase Diagram of the Mean-Field Hubbard Model on a Cubic Lattice.

The Nagaoka state is at the centre-bottom of the phase diagram, where mean-field theory

suggests that ferromagnetism extends from this point. Whether this can believed is still an open question.

5.5 Mean-Field Analysis of the Anderson Lattice

We now proceed to use mean-field theory on the Anderson Lattice model (4.11), which is of a great deal of interest to us in the latter part of this thesis. This section presents somewhat a strawman argument, since mean-field theory is known to give a poor approximation to the real physics of the Anderson latticen due to its overemphasis on ordering.

For ease of analysis, we will assume ferromagnetic correlations and search for order in a square lattice. We will show that the model has ferromagnetic order in the mean-field approximation, contrary to the heavy-fermion systems we hope to model.

We will make a mean-field approximation for the quartic term in U. We will take as our mean-fields the number operators for the f electrons, and the magnetic contributions. Our mean-field Hamiltonian then is

$$\begin{aligned}\mathcal{H} &= -t\sum_{jj'\sigma} c^\dagger_{j\sigma}c_{j'\sigma} + V\sum_{j\sigma}\left(f^\dagger_{j\sigma}c_{j\sigma} + c^\dagger_{j\sigma}f_{j\sigma}\right) + \epsilon\sum_{j\sigma} f^\dagger_{j\sigma}f_{j\sigma} \\ &\quad + U\sum_{j\sigma}\left(< f^\dagger_{j\sigma}f_{j\sigma} > f^\dagger_{j\bar{\sigma}}f_{j\bar{\sigma}} - < f^\dagger_{j\bar{\sigma}}f_{j\sigma} > f^\dagger_{j\sigma}f_{j\bar{\sigma}}\right) \qquad (5.18)\end{aligned}$$

where

$$< f^\dagger_{j\sigma}f_{j\sigma} > = \frac{1}{2}n_\sigma + \sigma m^z \qquad (5.19)$$

$$< f^\dagger_{j\sigma}f_{j\bar{\sigma}} > = S^x + i\sigma S^y \qquad (5.20)$$

We can ignore the magnetic terms in the x and y directions by quantising in the z direction,

and writing $m^z = m$, we have

$$\mathcal{H} = -t\sum_{jj'\sigma} c^\dagger_{j\sigma}c_{j'\sigma} + V\sum_{j\sigma}\left(f^\dagger_{j\sigma}c_{j\sigma} + c^\dagger_{j\sigma}f_{j\sigma}\right) + \sum_{j\sigma}\left(\epsilon + U(n+\sigma n)f^\dagger_{j\sigma}f_{j\sigma}\right) \quad (5.21)$$

$$(5.22)$$

We can now Bloch transform this mean-field Hamiltonian to obtain

$$\mathcal{H} = -tZ\sum_{k\sigma}\gamma_k c^\dagger_{k\sigma}c_{k\sigma} + V\sum_{k\sigma}\left(f^\dagger_{k\sigma}c_{k\sigma} + c^\dagger_{j\sigma}f_{j\sigma}\right) + \sum_{k\sigma}\left(\epsilon + U(n+\sigma n)f^\dagger_{k\sigma}f_{k\sigma}\right) \quad (5.23)$$

$$(5.24)$$

which is diagonal in k-space.

We can rewrite our k-space mean-field Hamiltonian as

$$\mathcal{H} = \sum_{k\sigma}\begin{bmatrix} f^\dagger_{k\sigma}, c^\dagger_{k\sigma} \end{bmatrix}\mathcal{H}_{\mathcal{MF}}\begin{bmatrix} f_{k\sigma} \\ c_{k\sigma} \end{bmatrix} \quad (5.25)$$

where

$$\mathcal{H}_{\mathcal{MF}} = \begin{bmatrix} \epsilon + U\left(n+\sigma m\right) & V \\ V & -tZ\gamma_k \end{bmatrix} \quad (5.26)$$

Again, γ_k is the structure factor, and Z is the coordination number.

The eigenvalues for H_{MF} give us the mean-field dispersion for the Anderson lattice, and are

$$E(K)^\pm_\sigma = \frac{-t\gamma_k Z + \epsilon + U\left(n+\sigma m\right)}{2} \pm \sqrt{\left(\frac{\epsilon + t\gamma_k Z + U\left(n+\sigma m\right)}{2}\right)^2 + V^2} \quad (5.27)$$

The next step is to find the single-particle correlations, for which we employ the method

of Green's functions. The correlations are given by the formula

$$< c_i^\dagger c_{i'} >= \int_C \frac{dz}{2\pi i} f(z-\mu) G(z)_{ii'} \tag{5.28}$$

where f is the Fermi function, and G is the Green's function for the mean-field Hamiltonian $\mathcal{H}_{MF}$, defined by

$$G(z) = \left[z - \mathcal{H}_{MF}\right]^{-1} \tag{5.29}$$

and in our case is equal to

$$G(z) = \frac{1}{(z-(a_\sigma - \chi_\sigma))(z-(a_\sigma+\chi_\sigma))} \begin{bmatrix} z-(a_\sigma+d_\sigma) & -V \\ -V & z-(a\sigma+d\sigma) \end{bmatrix} \tag{5.30}$$

where

$$a_\sigma = \frac{1}{2}\left(-t\gamma_k Z + \epsilon + U(n+\sigma m)\right) \tag{5.31}$$

$$d_\sigma = \frac{1}{2}\left(-t\gamma_k Z - \epsilon - U(n+\sigma m)\right) \tag{5.32}$$

$$\chi_\sigma = \sqrt{d_\sigma^2 + V^2} \tag{5.33}$$

The poles of this Green's function reside at

$$z_\sigma = a_\sigma + \sigma\chi_\sigma \tag{5.34}$$

We can now obtain the self-consistent equations for the number of f-electrons ,n_f, and the

magnetic moment, m. These are given by

$$n = \frac{1}{N}\sum_k (\langle f^\dagger_{k\uparrow} f_{k\uparrow}\rangle + \langle f^\dagger_{k\downarrow} fk\downarrow\rangle) \tag{5.35}$$

$$m = \frac{1}{N}\sum_k (\langle f^\dagger_{k\uparrow} f_{k\uparrow}\rangle - \langle f^\dagger_{k\downarrow} fk\downarrow\rangle) \tag{5.36}$$

We can find the expectation values from the Green's functions defined above, and we find

$$< f^\dagger_{k\sigma} f_{k\sigma} >= \frac{1}{4}\left(\left(1+\frac{\chi_\sigma}{d_\sigma}\right) f(a_\sigma + d_\sigma) + \left(1-\frac{\chi_\sigma}{d_\sigma}\right) f(a_\sigma - d_\sigma)\right) \tag{5.37}$$

Inserting these into the self-consistent equations, we find

$$\begin{aligned} n &= \frac{1}{4}\left(\left(1+\frac{\chi_\sigma}{d_\sigma}\right) f(a_\sigma + d_\sigma) + \left(1-\frac{\chi_\sigma}{d_\sigma}\right) f(a_\sigma - d_\sigma)\right) \\ &+ \frac{1}{4}\left(\left(1+\frac{\chi_\sigma}{d_\sigma}\right) f(a_\sigma + d_\sigma) + \left(1-\frac{\chi_\sigma}{d_\sigma}\right) f(a_\sigma - d_\sigma)\right) \qquad (5.38) \\ m &= \frac{1}{4}\left(\left(1+\frac{\chi_\sigma}{d_\sigma}\right) f(a_\sigma + d_\sigma) + \left(1-\frac{\chi_\sigma}{d_\sigma}\right) f(a_\sigma - d_\sigma)\right) \\ &+ \frac{1}{4}\left(\left(1+\frac{\chi_\sigma}{d_\sigma}\right) f(a_\sigma + d_\sigma) + \left(1-\frac{\chi_\sigma}{d_\sigma}\right) f(a_\sigma - d_\sigma)\right). \qquad (5.39) \end{aligned}$$

We can solve these self-consistent equations numerically, and some results are discussed in the appendix. In particular, we find for almost all ranges of parameters, we have some form of magnetism, which is disastrous for modelling heavy fermion materials.

We can also perform a Stoner analysis on the Anderson lattice, but it is a great deal more complicated than the case for the Hubbard model, and does not offer much of interest, and so we omit such an analysis.

5.6 Limitations of Mean-Field Theory

We have seen that mean-field theory predicts the Anderson lattice to exhibit ferromagnetism. Since it is hoped that this model captures the essential physics of heavy-fermions materials, we must find some alternative method of solving the Anderson lattice.

We note that we have effectively introduced two new species of fermion into the problem, which are represented by a change of basis

$$\begin{aligned} d_k^\dagger &= \cos\theta_k f_k^\dagger + \sin\theta_k c_k^\dagger \\ g_k^\dagger &= -\sin\theta_k f_k^\dagger + \cos\theta_k c_k^\dagger \end{aligned} \tag{5.40}$$

Transforming this relationship into real space, we obtain

$$\begin{aligned} d_j^\dagger &= \frac{1}{\sqrt{N}}\sum_k \exp(-ikR_j)(\cos\theta_k f_k^\dagger + \sin\theta_k c_k^\dagger) \\ g_j^\dagger &= \frac{1}{\sqrt{N}}\sum_k \exp(-ikR_j)(-\sin\theta_k f_k^\dagger + \cos\theta_k c_k^\dagger) \end{aligned} \tag{5.41}$$

and placing two f electrons on the same lattice site will happen eventually in the mean-field Anderson lattice due to the oscillatory term in R_j. We have decorrelated the strongly correlated f-electrons, and we would like to avoid double occupancy at all costs. This is controlled by the term in U in both the Hubbard and Anderson lattice models. If we take the limit $U \to \infty$, then double occupation of a state with strongly correlated electrons becomes infinitely expensive, and will be prohibited. Virtual processes such as superexchange will still be permitted at certain special fillings. In general, however, double occupation of a strongly correlated state will be projected out of the description of our theories.

There are various methods for achieving this. Most commonly known is the Gutzwiller variational method. We will present a method of our own based on the Gutzwiller method later in this thesis.

5.7 Summary

We have introduced some basic concepts of mean-field theory, and analysed in some detail one of the methods of performing mean-field approximations, that of the Landau theory of phase transitions. We presented a review of Stoner's criterion for ferromagnetism, and we showed how this can be linked to the Landau theory of phase transitions.

We applied the Stoner criterion to the Hubbard model, and discussed the mean-field phase diagram of the Hubbard model. The Nagaoka state is truly special, since it is a point we can solve exactly, but moving into non-infinitesimal dopings, we are unable to say whether the ferromagnetism extends beyond this point, even though mean-field theory predicts that it should.

We also considered mean-field solutions of the Anderson lattice, and we can see that the predictions of mean-field theory are unsatisfactory. We will suggest improvements to the usual method of performing mean-field theory in chapter ten.

Part II

Orbital Ordering, Magnetism and Heavy Fermion Systems

Chapter 6

Saturated Ferromagnetism in t_{2g} Systems

6.1 Introduction

We now move on to develop a model for a saturated ferromagnet consisting of t_{2g} electrons. Since the ferromagnetism is saturated, we can avoid describing the spin degree of freedom. We are thus concerned only with the orbital degree of freedom, and we are interested in any order that this may show. We will develop a mean-field theory based on a generalised Hubbard model. We then find the Stoner criterion for orbital ordering.

There are various materials that we feel the theory describes at some level. The first of these is Sr_2FeMoO_6. This material is a colossal magnetoresistor. We will also discuss applying the theory we develop to the orbitally ordered state of magnetite. Also within the possible scope of the theory is $SrRuO_3$. This is an itinerant system, while the isoelectronic system $CaRuO_3$ is not. We will suggest some reasons for this, after a discussion of some inconsistencies in the literature.

6.2 Experimental Input

It was hoped that we would be able to describe a model for Jahn-Teller distortions in an itinerant system, Sr_2FeMoO_6. However, it was found that the state described by the orbital ordering was insulating. This suggests a mean-field approach is perhaps inappropriate to describe the phase transition to an orbitally ordered state. Unfortunately, with the Hubbard model developed, the suggested improvements to mean-field theory in chapter 10 are inappliciable.

Sr_2FeMoO_6 is an experimentally intriguing material and has generated a lot of interest. We will apply the predictions of the model developed in this chapter to it. Sr_2FeMoO_6 shows evidence of colossal magnetoresistive behaviour. This colossal magnetoresistive behaviour stems from tunneling between grains [44]. The material is half-metallic, where only one spin-species is active at the Fermi surface. It also shows a magnetic transition at $T_C = 400K$.

It has a double perovskite crystal structure, with Fe and Mo alternately being at the center of an octahedron of oxygen atoms. The electronic configuration of the material is $Sr_2^{2+}Fe^{3+}Mo^{5+}O_6^{2-}$. Since the material has a perovskite crystal structure, there is a cubic symmetry to the crystal structure and hence a crystal-field splitting into t_{2g} and e_g orbitals.

In this case, the t_{2g} orbitals are lower in energy than the e_g orbitals. The electronic configuration is such that Fe has a half-full d-shell of ferromagnetic spins, and Mo has a single d electron, which ought to be oppositely aligned to the Fe spins in order to gain energy from hopping (figure 6.2).

We thus have the problem of a t_{2g} electron moving in a background of oppositely aligned spins. The single electron lying on the molybdenum site is spin-down and is free to hybridise with the electrons on the oxygen atom. The electron can move to the nearest-neighbour molybdenum by hopping onto the iron atom, then hybridising with the oxygen and a nearest-neighbour molybdenum atom.

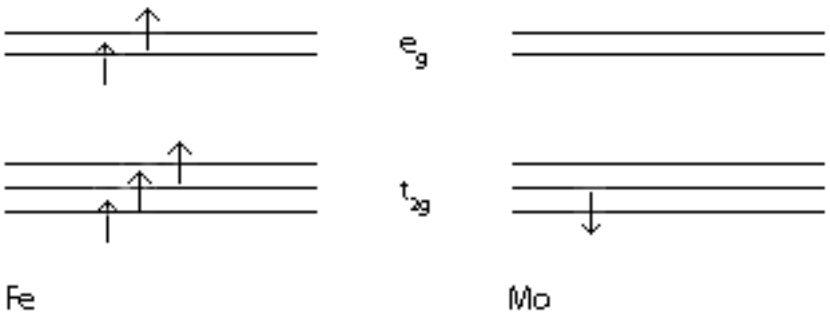

Figure 6.1: Crystal Field Scheme for Sr_2FeMoO_6

There is an experimentally detected distortion, which suggests the possibility of orbital ordering. This distortion, however, is quite small, and we will not seek to model it. This is likely to be due to the ordering in the t_{2g} sector, since this subset of orbitals experience less coulombic repulsion in a cubic environment than will an electron in the e_g sector.

Our argument rests on the gradient of the density of states. The material is essentially planar with the relevant hopping taking place on a square lattice of alternating Fe and Mo sites. Setting the energy at an Fe site to be zero, and the energy at an Mo site to be Δ, the hopping Hamiltonian is represented by the matrix $\begin{pmatrix} 0 & -tZ\gamma_k \\ -tZ\gamma_k & \Delta \end{pmatrix}$ and thus the dispersion is

$$\epsilon(k) = \frac{\Delta}{2} \pm \sqrt{(\Delta/2)^2 + (tZ\gamma_k)^2} \tag{6.1}$$

From this, we get a density of states that looks like the square lattice density of states for a Hubbard model, but with a gap of size Δ, and we plot this density of states in figure 6.2.

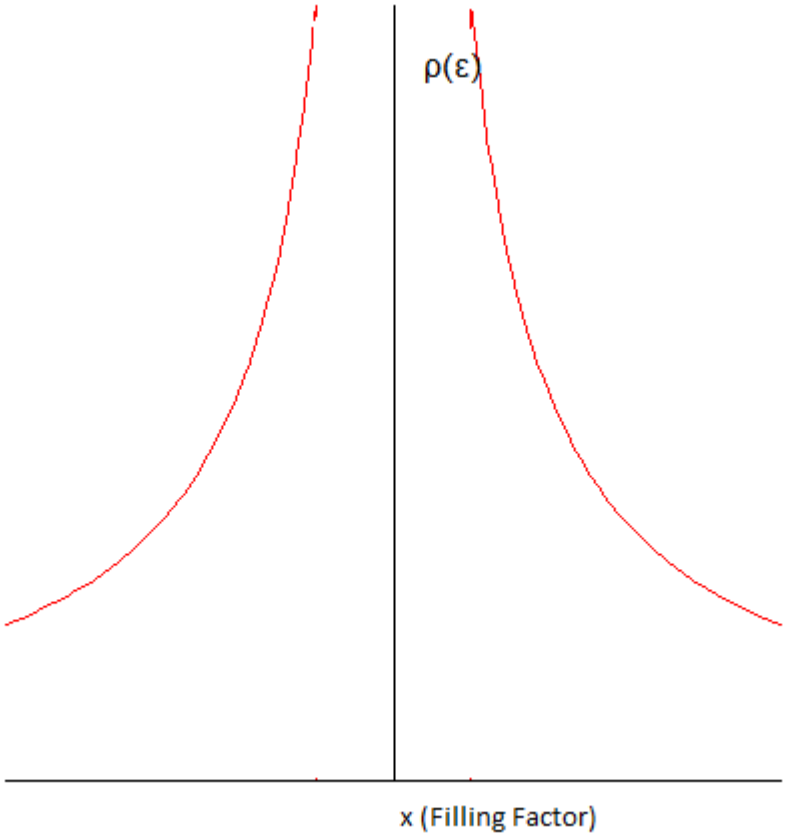

Figure 6.2: Density of States for Sr_2FeMoO_6 - a square lattice density of states with a gap for the Hubbard model. Plotted is the density of states versus the chemical potential.

6.3 Model for Itinerant Magnetism in Saturated t_{2g} Ferromagnets

We assume that the spin is saturated, and hence we discard the possibility of spin fluctuations in our modeling. In other words, we will ignore the spin degree of freedom. Spin-1/2 problems come with two states, and we have three states in the t_{2g} representation. This may suggest that a spin-1 problem may be more appropriate. However, the three states in a spin-1 problem are not related by symmetry, while the cubic d t_{2g} orbitals are related to each other by rotations. This makes a spin-1 representation of the t_{2g} sector inappropriate for our modelling.

We model the system as a generalised Hubbard model. The role of the spin, as mentioned before, is now played by the t_{2g} orbitals. We assume the electrons to be itinerant, and so we have to take care in describing the hopping. We will assume that the hopping only takes place beween like orbitals. By this, we mean that the $\hat{x}\hat{y}$ orbital only connects to the $\hat{x}\hat{y}$ orbital, and not the $\hat{x}\hat{z}$ orbital or $\hat{y}\hat{z}$ orbital. This enables us to only consider two-dimensional planes of the original three-dimensional problem.

The Hubbard model for this system takes the form

$$\mathcal{H} = -t \sum_{<jj'>\alpha} c^{\dagger}_{j\alpha} c_{j'\alpha} + \frac{U}{2} \sum_{j} n_j (n_j - 1) \tag{6.2}$$

c is an electron creation operator, and j is a site index centred on molybdenum, and α labels the orbitals. The index $< jj' >_\alpha$ represents a hopping between nearest neighbours mediated by the orbital labelled by α. We wish to perform a mean-field analysis on this Hamiltonian, and find the Stoner criterion for orbital ordering.

For fermions, $\hat{n}^2_{j\alpha} = \hat{n}_{j\alpha}$, and using this we can rewrite the above Hamiltonian as

$$\mathcal{H} = -t \sum_{<jj'>\alpha} c^{\dagger}_{j\alpha} c_{j'\alpha} + \frac{U}{2} \sum_{j,\alpha\neq\beta} n_{j\alpha} n_{j\beta}. \tag{6.3}$$

Suppressing the factor of a half by summing only $\beta > \alpha$, the Hamiltonian we will work with is

$$\mathcal{H} = -t \sum_{<jj'>\alpha} c^{\dagger}_{j\alpha} c_{j'\alpha} + U \sum_{j\alpha} n_{j\alpha} \sum_{\beta>\alpha} n_{j\beta}. \tag{6.4}$$

The mean-field Hamiltonian is given by

$$\mathcal{H} = -t \sum_{<jj'>\alpha} c^{\dagger}_{j\alpha} c_{j'\alpha} + U \sum_{j\alpha} n_{j\alpha} \sum_{\beta>\alpha} < n_{j\beta} > . \tag{6.5}$$

Since the correlation function is the same for all sites j, we can write $n_\alpha =< n_{j\alpha} >$, where

$$n_\alpha = \frac{1}{3}\left(n_0 + \omega^\alpha m + \omega^{-\alpha} m^*\right) \tag{6.6}$$

where ω is a cube-root of unity which is not equal to 1. Here m is a complex order parameter representing the occupancy of the orbitals.

The dispersion for this model is given by

$$\begin{aligned} E_{k\alpha} &= -t\gamma_{k\alpha} Z + U \sum_{\beta \neq \alpha} n_\beta \\ &= -t\gamma_{k\alpha} Z + U(\sum_{\beta} n_\beta - n_\alpha) \end{aligned} \tag{6.7}$$

which further simplifies to

$$E_{k\alpha} = -t\gamma_{k\alpha} Z + U(3n_0 - n_\alpha)$$

and finally, we have

$$E_{k\alpha} = -t\gamma_{k\alpha} Z + U(2n_0 - \omega^\alpha m - \omega^{-\alpha} m^*). \tag{6.8}$$

6.4 The Stoner Criterion

Now we have the dispersion, we move on to find the Stoner criterion for orbital ordering. The Gibbs free-energy takes the form

$$G = \sum_{k\alpha} (E_{k\alpha} - \mu) f(E_{k\alpha} - \mu) - TS - U(n^2 + \frac{1}{2}|m|^2). \tag{6.9}$$

Expanding G in terms of m and m^*, we obtain

$$G = G_0 + G_2|m|^2 + G_3(m^3 + m^{*3}) + G_4|m|^4 \tag{6.10}$$

The Stoner criterion is obtained from the coefficient of m^2 in the expansion above at $m = 0$. The Stoner criterion will tell us at which point the orbitals begin to order. This criterion is given by

$$G_{mm^*} = 0. \tag{6.11}$$

where

$$\begin{aligned} G_{mm^*} &= \sum_{\gamma_k \alpha} \left(\frac{\partial^2 E_\sigma}{\partial |m|^2} f(E_k) + \frac{\partial E_\sigma}{\partial m} \frac{\partial E_\sigma}{\partial m^*} \frac{\partial f(E_k)}{\partial E_k} - U \right) \\ &= U^2 \frac{\partial f(E_k)}{\partial E_k}. \end{aligned} \tag{6.12}$$

and so at $m = 0$, we have

$$U^2 \rho(0) = U \tag{6.13}$$

and so our Stoner criterion is

$$U\rho(0) = 1 \tag{6.14}$$

where $\rho(0)$ is the density of states at the Fermi energy.

The stability of the Stoner criterion is given by the next order term in the expansion. In this case, since we are expanding with third roots of unity, we have third order terms that contribute to the expansion, unlike in the case where we expand with second roots of unity and all odd order terms cancel.

To calculate the stability of the Stoner criterion in this Hubbard model, we need to calculate the coefficients of m^3 and m^{*3}. These coefficients turn out to be the same, and are given by the third derivative of the free-energy with respect to m or m^*. The stability of the transition is guaranteed by

$$\frac{\partial^3 G}{\partial m^3} = -3U^3 \int d\gamma \frac{d\rho(\gamma)}{d\epsilon} \frac{df}{d\gamma}. \tag{6.15}$$

We can see the stability depends on the gradient of the density of states. The above is the coefficient of m^3, and denoting the integral by A, we have

$$G = G_0 + G_2 m^2 - 6AU^3|m|^3 \cos(3\theta). \tag{6.16}$$

where we have written $m = |m| \exp(i\theta)$, and $m + m^* = 2|m| \cos\theta$. We need to minimise this over θ. We have

$$-6AU^3 \frac{d\cos(3\theta)}{d\theta} = 6AU^3 \frac{1}{3} \sin(3\theta) \tag{6.17}$$

and this is zero when $\theta = \frac{n\pi}{3}, n \in \mathbb{N}$. However, we are interested in the minima, so we have

$$-6AU^3 \frac{d^2\cos(3\theta)}{d\theta^2} = 6AU^3 \frac{1}{9} \cos(3\theta). \tag{6.18}$$

Whether we have a minimum or a maximum depends on the gradient of the density of states. If we assume the gradient is positive, then the minima occur at the odd values of n. If the gradient is negative, then the minima occur at odd even values of n.

6.5 Densities of States and Orbital Populations

We now move on to a more direct calculation of the occupations of the orbitals. We assume an arbitrary density of states, and we will show that the case where one orbital is biased in favour of two orbitals is the lower energy state. We will calculate the energy difference between the system biasing one orbital in favour of the other two, and the system biasing two orbitals in favour of the remaining orbital.

We consider first the case that one orbital is used in favour of two. The populations are

then given by

$$n_1 = n + 2m \tag{6.19}$$

$$n_2 = n - m \tag{6.20}$$

$$n_3 = n - m. \tag{6.21}$$

n_1 is given by

$$n + 2m = \int_{-\infty}^{\mu+\delta_+} d\epsilon \rho(\epsilon) \tag{6.22}$$

while n_2 and n_3 are given by

$$n - m = \int_{\infty}^{\mu-\delta_-} d\epsilon \rho(\epsilon). \tag{6.23}$$

$\delta_\pm$ is the change in chemical potential from raising one orbital and lowering the other two respectively. In the absence of this shift, we have

$$n = \int_{\infty}^{\mu} d\epsilon \rho(\epsilon)$$

and so, subtracting these from the orbitals, we have

$$2m = \int_{0}^{\delta_+} d\epsilon \rho(\epsilon + \mu) \tag{6.24}$$

$$m = \int_{-\delta_-}^{0} d\epsilon \rho(\mu + \epsilon) \tag{6.25}$$

We now consider the energies of these populations

$$E_1 = 2\int_{-\infty}^{\mu+\delta_+} d\epsilon\epsilon\rho(\epsilon) + 2\int_{\infty}^{\mu-\delta_-} d\epsilon\epsilon\rho(\epsilon) \tag{6.26}$$

and, noting that

$$E_0 = \int_{-\infty}^{\mu} d\epsilon(\mu + \epsilon)\rho(\epsilon + \mu)$$

we find

$$E_1 = E_0 + \int_0^{\delta_+} d\epsilon(\mu+\epsilon)\rho(\epsilon+\mu) - 2\int_{-\delta_-}^{0} d\epsilon(\mu+\epsilon)\rho(\mu+\epsilon) \quad (6.27)$$

$$= E_0 + \int_0^{\delta_+} d\epsilon\epsilon\rho(\epsilon+\mu) - 2\int_{-\delta_-}^{0} d\epsilon\epsilon\rho(\mu+\epsilon) \quad (6.28)$$

We now consider the case that the system will bias two orbitals in favour of a third. The populations in this case are given by

$$n_1 = n - 2m \quad (6.29)$$

$$n_2 = n + m \quad (6.30)$$

$$n_3 = n + m \quad (6.31)$$

Again, the populations are found to be

$$n + 2m = \int_{-\infty}^{\mu-\Delta_+} d\epsilon\rho(\epsilon) \quad (6.32)$$

$$n - m = \int_{-\infty}^{\mu+\Delta_-} d\epsilon\rho(\epsilon) \quad (6.33)$$

and since

$$n = \int_{-\infty}^{\mu} d\epsilon\rho(\epsilon)$$

we are left with, after subtracting this from the populations

$$2m = \int_{-\Delta_+}^{0} d\epsilon\rho(\epsilon+\mu) \quad (6.34)$$

$$m = \int_{0}^{\Delta_-} d\epsilon\rho(\mu+\epsilon) \quad (6.35)$$

The energies for these are given by

$$E_2 = \int_{-\infty}^{\mu-\Delta_+} d\epsilon\epsilon\rho(\epsilon) + 2\int_{-\infty}^{\mu+\Delta_-} \epsilon d\epsilon\rho(\epsilon). \tag{6.36}$$

Using

$$E_0 = \int_{-\infty}^{\mu} d\epsilon(\mu+\epsilon)\rho(\epsilon+\mu)$$

we have

$$\begin{aligned} E_1 &= E_0 - \int_{-\Delta_+}^{0} d\epsilon(\mu+\epsilon)\rho(\epsilon+\mu) + 2\int_{0}^{\Delta_-} d\epsilon(\mu+\epsilon)\rho(\mu+\epsilon) && (6.37)\\ &= E_0 - \int_{-\Delta_+}^{0} d\epsilon\epsilon\rho(\epsilon+\mu) + 2\int_{0}^{\Delta_-} d\epsilon\epsilon\rho(\mu+\epsilon) && (6.38)\\ &= E_0 - \int_{0}^{\Delta_+} d\epsilon\epsilon\rho(\epsilon+\mu) + 2\int_{-\Delta_-}^{0} d\epsilon\epsilon\rho(\mu+\epsilon) && (6.39) \end{aligned}$$

We now move on to calculate the difference in energy between these two possibilities. We need to make this consideration in order to determine whether the system would like to use one orbital or two orbitals. The system will of course adopt the configuration that is lower in energy. The energy difference is

$$\Delta E = E_1 - E_2 = \int_0^{\delta_+} d\epsilon\,\epsilon\rho(\epsilon+\mu) - 2\int_{-\delta_-}^{0} d\epsilon\,\epsilon + \int_0^{\Delta_+} d\epsilon\,\epsilon\rho(\epsilon+\mu) - 2\int_{-\Delta_-}^{0} d\epsilon\,\epsilon$$

$$2m = \int_0^{\delta_+} d\epsilon\rho(\mu+\epsilon) = \int_{-\Delta_+}^{0} d\epsilon\rho(\mu+\epsilon)$$

$$m = \int_{-\delta_-}^{0} d\epsilon\rho(\mu+\epsilon) = \int_0^{\Delta_-} d\epsilon\rho(\mu+\epsilon)$$

$$\int_0^{\alpha} d\epsilon\rho(\mu+\epsilon) = A.$$

and α is given by

$$\alpha = \frac{A}{\rho_0} - \frac{\rho_1 A^2}{2\rho^3} + \dots . \tag{6.40}$$

Expanding ρ, we have

$$\rho(\mu + \epsilon) = \rho_0 + \epsilon\rho_1 + \frac{\epsilon^2}{2}\rho_2 + \dots \tag{6.41}$$

where $\rho_1 = \frac{d\rho}{d\epsilon}$, $\rho_2 = \frac{d^2\rho}{d\epsilon^2}$

$$\delta_+ = \frac{2m}{\rho_0} - \frac{2m^2\rho_1}{\rho^3} + \dots \tag{6.42}$$

$$\Delta_+ = \frac{2m}{\rho_0} + \frac{2m^2\rho_1}{\rho^3} + \dots \tag{6.43}$$

$$\delta_- = \frac{m}{\rho_0} + \frac{m^2\rho_1}{2\rho^3} + \dots \tag{6.44}$$

$$\Delta_- = \frac{m}{\rho_0} - \frac{m^2\rho_1}{2\rho^3} + \dots \tag{6.45}$$

Finally, we have the difference in energy between the two choices of ordering is given by

$$\Delta E = \rho\left(\frac{\delta_+^2 - \Delta_+^2}{2} + \delta_-^2 - \Delta_-^2\right) + \rho_1\left(\frac{\delta_+^3 + \Delta_+^3}{3} - \frac{2}{3}(\delta_+^3 + \Delta_+^3)\right) \tag{6.46}$$

and this is equal to

$$= -2\frac{\rho_1}{\rho_0^3}m^3 \tag{6.47}$$

where ρ_1 is the gradient of the density of states.

The choice between an insulating orbitally ordered regime and a metallic orbitally ordered regime depends entirely on the gradient of the density of states. If the gradient is positive, the system will elect to use one orbital to order. If the gradient is negative, however, the system will use two orbitals to order, and we will find metallic behaviour.

6.6 Results and Comparison to Experimental Systems

6.6.1 Sr_2FeMoO_6

We are at one third filling, and hence the gradient of the density of states for the material is positive since we have the scaled square lattice density of states. The model implies that the material will use a single orbital to order, and so will display insulating behaviour. This is unfortunate, since we know the material to be metallic. The model as it stands is found not to be applicible to Sr_2FeMoO_6.

The material is difficult to make experimentally due to disorder being hard to eliminate. An interesting extension on the work done here would be to use a disordered approach via an Anderson disorder model[2] for random potentials. As we have not carried out this work, we are unsure whether the resulting model would display metallic behaviour.

6.6.2 Magnetite

Magnetite, (Fe_3O_4), is also a candidate for the application of the model developed in this chapter. It has an inverse spinel crystal structure. However, we will restrict our attention to a subset of the crystal. Magnetite undergoes a transition at 119 K, where hopping is frozen on the octahedral complex of the spinel structure, and takes place only on the tetrahedra of Fe^{3+} and Fe^{2+}. Magnetite, however, is a very complicated material, and it is unreasonable to expect such a simple approach to capture more than a rough overview of its properties.

We will assume that all the Fe^{3+} are saturated, and hence the problem is reduced to three interpenetrating one-dimensional chains of motion. Since the density of states has a negative gradient at this point, we would expect the material to use two bands rather than one, as in the case of Sr_2FeMoO_6.

Bearing in mind the complexity of the material, we cannot draw any reasonable conclusions for magnetite from such a brief examaniation for the model we have developed in this

chapter. However, things do look promising, more so than the material we original intended to model, and would be a great start for future work in applications of the model we have developed.

6.6.3 Ruthenates

The particular ruthenates that we consider here are $SrRuO_3$ and $CaRuO_3$. They are again locally perovskite materials, except with a great deal of distortion. This is important to our considerations. We assumed previously that only like orbitals were connected. In the event of distortion, it will be the case that, for example, an electron in the $\hat{x}\hat{y}$ orbital can hop into one of the $\hat{y}\hat{z}$ or $\hat{z}\hat{x}$ orbitals. We model this distortion first. As mentioned, the $SrRuO_3$ and $CaRuO_3$ compounds are at least locally perovskite, and each Ru atom sees an octahedron of O atoms surrounding it. The neighbouring octahedron is distorted relative to this.

We can model the distortion most effectively by rotating the x, y, z coordinate system 45 degrees to match the line along with the oxygen atoms make a zig-zag pattern. To describe the distortion, we rotate to face this line, perform a rotation on the new basis by an angle θ, which is the angle that the oxygen atoms are distorted by, and then we rotate back to the original basis. This is achieved by the matrix

$$C = \begin{bmatrix} \frac{1}{\sqrt{2}} & \frac{1}{\sqrt{2}} & 0 \\ -\frac{1}{\sqrt{2}} & \frac{1}{\sqrt{2}} & 0 \\ 0 & 0 & 1 \end{bmatrix} \begin{bmatrix} \cos\theta & 0 & -\sin\theta \\ 0 & 1 & 0 \\ \sin\theta & 0 & \cos\theta \end{bmatrix} \begin{bmatrix} \frac{1}{\sqrt{2}} & -\frac{1}{\sqrt{2}} & 0 \\ \frac{1}{\sqrt{2}} & \frac{1}{\sqrt{2}} & 0 \\ 0 & 0 & 1 \end{bmatrix} \tag{6.48}$$

The consequences of the distortion for our modelling is that while in the cases we have considered before, the hopping only took part between orbitals of the same type. That is, the $\hat{x}\hat{y}$ orbital only connects with the $\hat{x}\hat{y}$ orbital, and similarly with the other t_{2g} orbitals. With the distortion, we have the $\hat{x}\hat{y}$ orbital on one atom connecting not only to the $\hat{x}'\hat{y}'$ orbital on a neighbouring atom, but also to the $\hat{y}'\hat{z}'$ and $\hat{z}'\hat{x}'$ orbitals on the same neighbouring atom.

We will clearly need to model the hopping in $SrRuO_3$ and $CaSrRuO_3$ very carefully, but the model developed in this chapter quite conceivably form the basis of future work on this material.

We note that matching any prediction of the model to experiment will be a difficult task in itself due to the confusion in the experimental literature. For example, there are papers claiming $CaRuO_3$ is a paramagnet, and some claiming it is a ferromagnet. Clearly, we will have more to contend with than interpreting predictions of a theoretical model.

6.7 Summary

We have developed a model for orbital ordering in the t_{2g} sector for ferromagnetic itinerant systems. We find that the resulting behaviour depends on the sign of the gradient of the density of states. When it is positive, we will have an itinerant orbitally ordered system.

We originally thought the model would be able to describe an itinerant system displaying Jahn-Teller distortions. The material we had in mind for this was Sr_2FeMoO_6. As we see from our modelling, the Jahn-Teller phase of the material is insulating. Experimentally, the material is complicated, and is difficult to make pure samples of. The material is known to display colossal magnetoresistance, and this must be accompanied by an insulating phase. This is likely the phase we describe with our modelling, if any.

The modelling is such that any material with itinerant t_{2g} electrons could be described by it. Two materials that potentially could be modelled are magnetite, and $\{Sr,Ca\}RuO_3$. Work has not been undertaken on these materials, but they would be the immediate candidates for applications of the model.

Chapter 7

Cubic Symmetric Orbitals and Ordering

7.1 Introduction

We now construct a model for a transition metal oxide with a saturated spin and possessing only degrees of orbital freedom in the e_g sector. We had in mind the CMR manganites while developing this model. Since the spin is saturated, we will ignore the spin degrees of freedom, and concentrate on only the orbital degree of freedom and its ordering.

For the remainder of the investigation, we will assume that we have a saturated ferromagnet, and that the material is metallic. Working in the saturated ferromagnetic region allows us to ignore the spin degrees of freedom, and simplifies the description considerably. Unfortunately, it rules out any hope of describing the breakdown of the magnetism which is crucial for describing the magnetoresistive phenomenon.

We consider only two energy scales. These are energies that come from atomic physics. The Coulomb energy between electrons is dominant throughout the phase diagram, and restricts charge fluctuations greatly. The second large atomic energy is the Hund's coupling, and this forces the electrons into a high-spin state. This energy allows us to fix the spin on each atom, and thus assuming a ferromagnetic arrangement of spins, we can avoid describing the spin degree of freedom.

The next energy scale that is important is the hybridization between the atoms and the oxygen ions. This energy scale leads to delocalization of the electrons. The electrons delocalise through double exchange, which is a second order process, and consequently dominates the magnetic exchange which is a fourth-order process.

Finally, we have an energy scale associated with the local structural distortions.The energy from the hybridisation competes with the energy from the local distortion of the crystal structure throughout the phase diagram, and leads to a variety of phases. We assume that the hybridisation is dominant, and consequently we also have a metallic phase.

7.2 e_g Orbitals and Pseudospin

We begin with the consideration of the e_g orbitals, in the standard cubic basis of $3z^2 - 1$ and $x^2 - y^2$. We thus have two orbitals to work with. We consider linear combinations of these orbitals to get two new orbitals.

$$\begin{aligned} c_1 &= \frac{1}{\sqrt{3}}(\omega_3 \hat{x}^2 + \omega_3^2 \hat{y}^2 + \hat{z}^2) \\ c_2 &= \frac{1}{\sqrt{3}}(\omega_3^2 \hat{x}^2 + \omega_3 \hat{y}^2 + \hat{z}^2) \end{aligned}$$

where ω_3 is a cube-root of unity. These orbitals have now cubic symmetric charge distributions, and in fact are conjugates. The charge distribution of the new cubic symmetric orbitals are shown in figure 7.1.

We can map this problem on to that of a spin-1/2 problem, since both form a two-dimensional vector space, and hence there exists an isomorphism between the two vector spaces. We can do this by identifying

$$|\uparrow> = c_1 \tag{7.1}$$

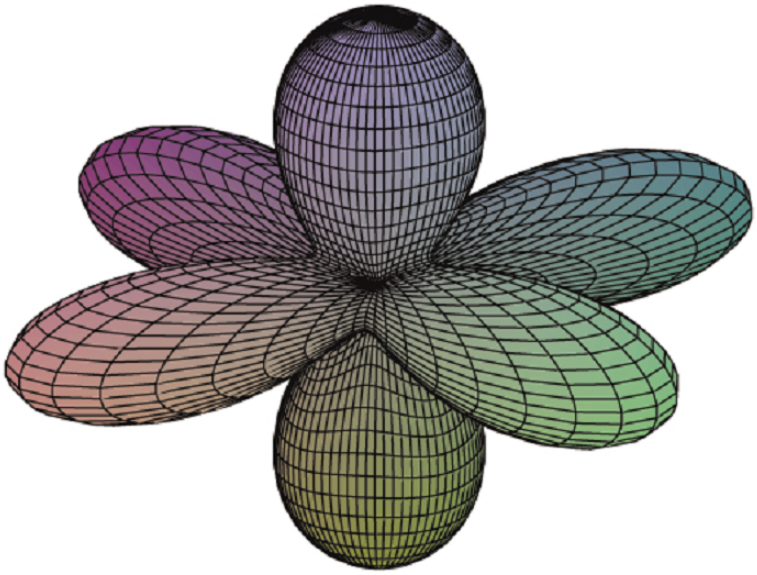

Figure 7.1: Charge distribution of the cubic symmetric orbitals

$$|\downarrow>= c_2 \tag{7.2}$$

We can get back to the standard e_g orbitals by

$$|\uparrow> +|\downarrow>= \frac{\hat{x}^2 - \hat{y}^2}{\sqrt{2}}$$

$$|\uparrow> -|\downarrow>= \frac{2\hat{z}^2 - \hat{x}^2 - \hat{y}^2}{\sqrt{6}}$$

For spin-half, we have the spin operators which satisfy the commutation relations

$$\left[\hat{S}^\alpha, \hat{S}^\beta\right] = i\epsilon^{\alpha\beta\gamma}\hat{S}^\gamma \tag{7.3}$$

and the anti-commutation relations

$$\left\{\hat{S}^\alpha, \hat{S}^\beta\right\} = \frac{1}{2}\delta^{\alpha\beta}. \tag{7.4}$$

The magnetism is described by choosing a particular component of spin and using its expec-

tation value as the order parameter

$$m = \langle \hat{S}^z \rangle \qquad \left(\hat{S}^z\right)^2 = \frac{1}{4} \tag{7.5}$$

In an isotropic model the component chosen is arbitrary and breaks rotational symmetry. In an anisotropic model the choice of component only lifts the residual point symmetry. The appearance of magnetism is the generation of a non-zero value for m. Note that the space of states can be described by quantising parallel to the direction of the magnetic moment and then the vector

$$\begin{bmatrix} \cos\frac{\theta}{2} e^{-i\frac{\phi}{2}} \\ \sin\frac{\theta}{2} e^{+i\frac{\phi}{2}} \end{bmatrix} \tag{7.6}$$

may be interpreted as the state with the spin oriented along the direction corresponding to $\{\theta, \phi\}$. We can interpret these coordinates as spherical polar coordinates for a fixed unit radius, and that as these angles are varied the entire space is mapped out.

The cubic symmetric orbitals correspond to $\theta = 0, \pi$, and these are analogous to Ising spins where we project on to the $\hat{z}$ component of the spin. For $\theta = \pm\frac{\pi}{2}$, we are on the equator of the sphere, and these correspond to the symmetry broken orbitals such as $3\hat{z}^2 - 1$ and $\hat{x}^2 - \hat{y}^2$. These orbitals are thus analogous to spins in the XY-model. For values inbetween these, we have a general Heisenberg-like spin.

Since we are dealing with an itinerant problem we need to generalise to

$$\hat{S}^\alpha = \frac{1}{2} \sum_{\sigma\sigma'} c^\dagger_\sigma \hat{\sigma}^\alpha_{\sigma\sigma'} c_{\sigma'} \tag{7.7}$$

where $\hat{\sigma}^\alpha$ are the Pauli matrices and

$$\hat{S}^\alpha \hat{S}^\alpha = \frac{1}{3} \sum_\beta \hat{S}^\beta \hat{S}^\beta = \frac{1}{4} \hat{N} \left(2 - \hat{N}\right) \tag{7.8}$$

where

$$\hat{N} = c_{\uparrow}^{\dagger} c_{\uparrow} + c_{\downarrow}^{\dagger} c_{\downarrow} \tag{7.9}$$

is the number operator. This provides the appropriate behaviour when $\hat{N}$=1 and guarantees the vanishing of the orbital moment when the site is either empty or doubly occupied. Note that $\hat{N}\left(2-\hat{N}\right)$ is a projection operator which projects onto average single occupancy.

For one d-electron with no spin label, the orbital angular momentum is described by an operator which also satisfies the commutation relations

$$\left[\hat{L}^{\alpha}, \hat{L}^{\beta}\right] = i\epsilon^{\alpha\beta\gamma}\hat{L}^{\gamma} \tag{7.10}$$

and is restricted by

$$\sum_{\alpha} \hat{L}^{\alpha}\hat{L}^{\alpha} = 6 \tag{7.11}$$

describing a space of five states. For perovskites there is a strong cubic symmetry term that lifts this degeneracy down to a triply degenerate t_{2g} subspace and the currently relevant doubly degenerate e_g subspace. This separation can be accomplished using a single central operator

$$\begin{aligned} \hat{e} \equiv \frac{\hat{L}^z\hat{L}^x\hat{L}^y + \hat{L}^y\hat{L}^x\hat{L}^z}{4\sqrt{3}} &= \frac{\hat{L}^x\hat{L}^y\hat{L}^z + \hat{L}^z\hat{L}^y\hat{L}^x}{4\sqrt{3}} \\ &= \frac{\hat{L}^y\hat{L}^z\hat{L}^x + \hat{L}^x\hat{L}^z\hat{L}^y}{4\sqrt{3}} \end{aligned} \tag{7.12}$$

which provides a projection operator

$$\hat{e}^2 = \frac{\hat{P}}{4} \qquad \hat{P}^2 = \hat{P} \tag{7.13}$$

which projects onto the e_g subspace. When in the e_g subspace the operator $\hat{e}$ provides an operator which can play the role of a spin-half component. The states which diagonalise the

operator are

$$|\uparrow\rangle \propto \frac{1}{\sqrt{3}}\left(\omega^2\hat{x}^2 + \omega\hat{y}^2 + \hat{z}^2\right) \tag{7.14}$$

$$|\downarrow\rangle \propto \frac{1}{\sqrt{3}}\left(\omega\hat{x}^2 + \omega^2\hat{y}^2 + \hat{z}^2\right) \tag{7.15}$$

where ω satisfies

$$\omega^3 = 1 \tag{7.16}$$

$$1 + \omega + \omega^2 = 0 \tag{7.17}$$

and is a non-trivial cube-root of unity. These two states are the *unique* e_g states that maintain the cubic charge symmetry and are *not* expected to distort the local octahedron if single occupied.

We may describe the full orbital space using

$$\begin{bmatrix} \cos\frac{\theta}{2}e^{-i\frac{\phi}{2}} \\ \sin\frac{\theta}{2}e^{+i\frac{\phi}{2}} \end{bmatrix} \tag{7.18}$$

in correspondence to the spin-half problem. However, the isotropy is lost and the orbitals are physically quite distinct in character. As well as the two complex cubic symmetric orbitals, the states associated with $\theta = \frac{\pi}{2}$ are also special and are both real and maximally symmetry broken

$$|\,\phi\rangle \propto \left(\frac{2}{3}\right)^{\frac{1}{2}}\left[\cos\left(\frac{\phi}{2} + \frac{2\pi}{3}\right)\hat{x}^2 + \cos\left(\frac{\phi}{2} - \frac{2\pi}{3}\right)\hat{y}^2 + \cos\left(\frac{\phi}{2}\right)\hat{z}^2\right] \tag{7.19}$$

with $|\,\phi\rangle$ and $|\,\phi + \pi\rangle$ forming an orthonormal basis for any value of ϕ. The case ϕ=0, π provides the orbital basis

$$\left\{\frac{2\hat{z}^2 - \hat{x}^2 - \hat{y}^2}{\sqrt{6}},\ \ \frac{\hat{x}^2 - \hat{y}^2}{\sqrt{2}}\right\} \tag{7.20}$$

and the cases $\phi{=}\frac{\pi}{3}$, $\frac{4\pi}{3}$ and $\phi{=}\frac{2\pi}{3}$, $\frac{5\pi}{3}$ yield the analogues with Cartesian axes interchanged. The other important case is $\phi{=}\frac{\pi}{2}$, $\frac{3\pi}{2}$ which yields the intriguing

$$\left\{\frac{(\sqrt{3}+1)\hat{x}^2-(\sqrt{3}-1)\hat{y}^2-2\hat{z}^2}{2\sqrt{3}},\right.$$
$$\left.\frac{-(\sqrt{3}-1)\hat{x}^2+(\sqrt{3}+1)\hat{y}^2-2\hat{z}^2}{2\sqrt{3}}\right\} \tag{7.21}$$

which are *equivalent, orthogonal* orbitals of value in static orbital ordering problems but not much use to the current investigation.

7.3 Theoretical Modelling

We work again with a Hubbard model to describe the system. The Hubbard model takes its standard form, with the roles of spins played by the cubic symmetric orbitals

$$\mathcal{H}=-t\sum_{<jj'>\sigma}d^{\dagger}_{j\sigma}d_{j'\sigma}+U\sum_{j}d^{\dagger}_{j\uparrow}d_{j\uparrow}d^{\dagger}_{j\downarrow}d_{j\downarrow}. \tag{7.22}$$

Here, σ represents the orbital degree of freedom rather than the spin degree of freedom. The creation and annihilation operators create electrons in one of the cubic symmetric orbitals, with fixed spin. .

As with the usual Hubbard model, the exact behaviour is intractable and a first pass at the phase diagram can be extracted from mean-field theory. Although this overemphasises order in general, in a full three-dimensional system it is not thought to be too unphysical since order is usually anticipated. Even the mean-field phase diagram has complications for our model, since the hopping energy depends on the orientation of the pseudo-spin and consequently we need to resolve the choice of orbital as well as uncovering the relevant phase boundaries.

In the mean-field approximation, the Hamiltonian takes the form

$$\begin{aligned}\mathcal{H} &= -2Zt\sum_{k\sigma}\begin{pmatrix} c^\dagger_{k\uparrow} & c^\dagger_{k\downarrow}\end{pmatrix}\beta_k\begin{pmatrix} c_{k\uparrow}\\ c_{k\downarrow}\end{pmatrix} \\ &+ U\sum_{k}\begin{pmatrix} c^\dagger_{k\uparrow} & c^\dagger_{k\downarrow}\end{pmatrix}\begin{pmatrix} n+m_3 & m_1+im_2\\ m_1-im_2 & n-m_3\end{pmatrix}\begin{pmatrix} c_{k\uparrow}\\ c_{k\downarrow}\end{pmatrix}\end{aligned} \tag{7.23}$$

where

$$\beta_k = \begin{pmatrix} \cos(k_x)+\cos(k_y)+\cos(k_z) & \omega\cos(k_x)+\omega^2\cos(k_y)+\cos(k_z)\\ \omega^2\cos(k_x)+\omega\cos(k_y)+\cos(k_z) & \cos(k_x)+\cos(k_y)+\cos(k_z)\end{pmatrix} \tag{7.24}$$

For convenience, we write

$$\gamma_k = \cos(k_x)+\cos(k_y)+\cos(k_z)$$

$$\Gamma_k = \omega\cos(k_x)+\omega^2\cos(k_y)+\cos(k_z)$$

so that we can write the Hamiltonian matrix as

$$\mathcal{H}_{MF} = \begin{bmatrix} -2Zt\gamma_k + U(n+|m|) & \Gamma_k + Um\\ \bar{\Gamma_k} + U\bar{m} & -2Zt\gamma_k + U(n-|m|)\end{bmatrix} \tag{7.25}$$

where m is a complex number.

We can find the eigenvalues of $\mathcal{H}_{MF}$ to get the band-structure

$$E_\sigma(k) = -2t\gamma_k + 2Un + \sigma\sqrt{|\gamma_k|^2 + U^2m^2 - 2Utm(\omega\Gamma_k\exp(i\phi) + c.c.)},$$

which we will write as

$$E_\sigma(k) = -2t\gamma_k + 2Un + \sigma\Delta(k), \tag{7.26}$$

As usual, we can form the Gibbs free-energy

$$G = \sum_{k\sigma} (E_{k\sigma} - \mu)\, f(E_{k\sigma}) - TS - U(n^2 - m^2). \tag{7.27}$$

where S is the entropy.

We will calculate again the Stoner criterion. As in previous cases, this is given by the vanishing of the quadratic coefficient in the Landau expansion. The first derivative of G is given by

$$\frac{\partial G}{\partial m} = \sum_{k\sigma} \frac{\partial E_{k\sigma}}{\partial m} f_{k\sigma} - \frac{\partial}{\partial m} U(n^2 - m^2).$$

Calculating these, we find

$$\frac{\partial E_{k\sigma}}{\partial m} = \sigma \frac{\partial \Delta(k)}{\partial m}$$

and we find this to be

$$\frac{\partial E_{k\sigma}}{\partial m} = \sigma \frac{U^2 m - tU \sin\theta\Gamma}{\Delta}.$$

and also,

$$\frac{\partial}{\partial m} U(n^2 - m^2) = -2Um.$$

For the Stoner criterion, we need to work with the second derivative of the Gibbs free energy, which is given by

$$\frac{\partial^2 G}{\partial m^2} = \sum_{k\sigma} \left[\left(\frac{\partial E_{k\sigma}}{\partial m} \right)^2 \frac{\partial f_{k\sigma}}{\partial E_{k\sigma}} + \frac{\partial^2 E_{k\sigma}}{\partial m^2} f_{k\sigma} \right] - \frac{\partial^2}{\partial m^2} U(n^2 - m^2).$$

Now, using

$$\frac{\partial}{\partial m} \Delta \frac{\partial \Delta_{k\sigma}}{\partial m} = \left(\frac{\partial \Delta}{\partial m} \right)^2 + \Delta \frac{\partial^2 \Delta}{\partial m^2} = U^2$$

we find

$$\frac{\partial^2 \Delta}{\partial m^2} = \frac{1}{\Delta}\left(U^2 - \left(\frac{\partial \Delta}{\partial m}\right)^2\right)$$

and thus the second derivative of G can be written as

$$\frac{\partial^2 G}{\partial m^2} = \sum_{k\sigma}\left[\left(\frac{U^2 m - tU\sin\theta\Gamma}{\Delta}\right)^2 \frac{\partial f_{k\sigma}}{\partial E_{k\sigma}} + \frac{1}{\Delta}\left(U^2 - \left(\frac{\partial \Delta}{\partial m}\right)^2\right) f_{k\sigma}\right] - 2U.$$

Taking the limit as $m \to 0$, and setting the second derivative to zero, we find the Stoner criterion to be

$$1 = \frac{U}{2}\sum_{k\sigma}\left[\left(\frac{\sin\theta\Gamma}{|\bar{\gamma}|}\right)^2 \frac{\partial f_{k\sigma}}{\partial E_{k\sigma}} + \frac{1}{t|\bar{\gamma}|}\left(1 - \left(\frac{\sin\theta\Gamma}{|\bar{\gamma}|}\right)^2\right) f_{k\sigma}\right]. \tag{7.28}$$

Using the cubic symmetry of the lattice, we find that the terms in $\bar{\gamma}^2$ and $\bar{\gamma}^{*2}$ vanish, and thus we are left with

$$\Gamma^2 = |\hat{\gamma}|^2$$

and the Stoner criterion for the model is simply

$$1 = \frac{U}{2}\sum_{k\sigma}\left[\sin^2\theta \frac{\partial f_{k\sigma}}{\partial E_{k\sigma}} + \frac{1}{t|\bar{\gamma}|}\cos^2\theta f_{k\sigma}\right]. \tag{7.29}$$

We define

$$B = \sin^2\theta \frac{\partial f_{k\sigma}}{\partial E_{k\sigma}} \tag{7.30}$$

and

$$A = -\frac{1}{t|\bar{\gamma}|}\cos^2\theta f_{k\sigma} \tag{7.31}$$

and set about calculating these quantities. The system adopts the cubic-symmetric distribution orbitals when $B - A$ is negative. We need to use an effective density of states now to calculate where the transition occurs as a function of the chemical potential, and hence

the doping.

7.4 Stability

As usual, the stability of the Stoner criterion is provided by the next order term in the expansion. Thus, we have to find G_3 in the Landau expansion. This is given simply by the third derivative of the expansion at $m = 0$, and this is equal to

$$\frac{\partial^3 G}{\partial m^3} = \sum_{k\sigma} \left(\frac{\partial^3 E_{k\sigma}}{\partial m^3} f_{k\sigma} + 3 \frac{\partial E_{k\sigma}}{\partial m} \frac{\partial^2 E_{k\sigma}}{\partial m^2} \frac{\partial f_{k\sigma}}{\partial E_{k\sigma}} + \left(\frac{\partial E_{k\sigma}}{\partial m} \right)^3 \frac{\partial^2 f_{k\sigma}}{\partial E_{k\sigma}^2} \right).$$

We wish to calculate this to probe the behaviour of the symmetry broken phase. In a cubic environment, we cannot have a phase transition from cubic to tetragonal phases because of the existence of a third-order invariant. This is relevant here

We note that

$$\frac{\partial}{\partial m} \left(\frac{\partial^2 \Delta}{\partial m^2} \right) = -2 \frac{\partial \Delta}{\partial m} \frac{\partial^2 \Delta}{\partial m^2}, \tag{7.32}$$

and thus,

$$\frac{\partial^3 G}{\partial m^3} = -\frac{3}{\Delta} \frac{\partial \Delta}{\partial m} \frac{\partial^2 \Delta}{\partial m^2}, \tag{7.33}$$

and in turn, we have.

$$\frac{\partial \Delta}{\partial m} \frac{\partial^2 \Delta}{\partial m^2} = \frac{\partial \Delta}{\partial m} \left(U^2 - \left(\frac{\partial \Delta}{\partial m} \right)^2 \right). \tag{7.34}$$

Taking the limit $m \to 0$ of $\frac{\partial^3 G}{\partial m^3}$, we find G_3,

$$G_3 = U^3 \sin^3 \theta \Gamma^3 \left(3 \frac{\partial^2 f_{k\sigma}}{\partial E_{k\sigma}^2} - 3 \frac{\partial f_{k\sigma}}{\partial E_{k\sigma}} \frac{1}{t|\gamma|} + \frac{f_{k\sigma}}{(t|\gamma|)^2} \right) \tag{7.35}$$

If this quantity vanishes, for example $\theta = 0$, then the transition being first-order is no longer guaranteed. Interestingly, the cubic symmetric orbitals are precisely those with $\theta = 0$, and so calculations of the stability is irrelevant for regions where the symmetric orbitals are

predicted to occur. To determine the stability, and hence the other transitions in the system, we need to actually perform calculations of G_3. To this end, we introduce the concept of a joint density of states.

7.4.1 Joint Densities of States

The quantities that we require to calculate are singular. To remedy this, it is useful to work with densities of states to control the singular nature of the quantities. We start in reciprocal-space, using $\{k_1, k_2, k_3\}$ and want to end up using $\{\gamma_{\mathbf{k}}, \mid \tilde{\gamma}_{\mathbf{k}} \mid, \psi_{\mathbf{k}}\}$ instead.

After a sequence of transformations, we will find the original flat density goes to a quite singular density. Initially we transform to $\{c_1, c_2, c_3\}$ where

$$c_1 = \cos k_1 \quad c_2 = \cos k_2 \quad c_3 = \cos k_3 \tag{7.36}$$

for which

$$\rho(c_1, c_2, c_3) = \frac{1}{\pi^3} \prod_{\alpha=1}^{3} \frac{\theta[1 - c_\alpha^2]}{[1 - c_\alpha^2]^{\frac{1}{2}}} \tag{7.37}$$

and then to $\{\gamma, \tilde{\gamma}, \tilde{\gamma}^*\}$ by

$$\gamma = \frac{c_1 + c_2 + c_3}{3} \tag{7.38}$$

$$\tilde{\gamma} = \frac{\omega^{-1} c_1 + \omega c_2 + c_3}{3} \tag{7.39}$$

$$\tilde{\gamma}^* = \frac{\omega c_1 + \omega^{-1} c_2 + c_3}{3} \tag{7.40}$$

with jacobian

$$\frac{\partial[\gamma, \tilde{\gamma}, \tilde{\gamma}^*]}{\partial[c_1, c_2, c_3]} = \frac{1}{3\sqrt{3}} \tag{7.41}$$

and then finally to $\{\gamma, \mid \tilde{\gamma} \mid, \psi\}$ defined by

$$\tilde{\gamma} = \mid \tilde{\gamma} \mid e^{i\psi} \qquad \tilde{\gamma}^* = \mid \tilde{\gamma} \mid e^{-i\psi} \tag{7.42}$$

with jacobian

$$\frac{\partial[\tilde{\gamma},\tilde{\gamma}^*]}{\partial[\mid\tilde{\gamma}\mid,\psi]} = 2 \mid \tilde{\gamma} \mid \tag{7.43}$$

we arrive at

$$\rho(\gamma,\mid\tilde{\gamma}\mid,\psi) = \frac{6\sqrt{3}\mid\tilde{\gamma}\mid}{\pi^3}\prod_{\chi=-1}^{1}\frac{\theta\left[1-\left(\gamma+2\mid\tilde{\gamma}\mid\cos\left[\psi+\frac{2\pi}{3}\chi\right]\right)^2\right]}{\left[1-\left(\gamma+2\mid\tilde{\gamma}\mid\cos\left[\psi+\frac{2\pi}{3}\chi\right]\right)^2\right]^{\frac{1}{2}}} \tag{7.44}$$

$$= \frac{6\sqrt{3}\mid\tilde{\gamma}\mid}{\pi^3}\prod_{\tau=-1}^{1}\frac{\theta\left[(1+\tau\gamma)^3-3(1+\tau\gamma)\mid\tilde{\gamma}\mid^2+2\tau\mid\tilde{\gamma}\mid^3\cos 3\psi\right]}{\left[(1+\tau\gamma)^3-3(1+\tau\gamma)\mid\tilde{\gamma}\mid^2+2\tau\mid\tilde{\gamma}\mid^3\cos 3\psi\right]^{\frac{1}{2}}} \tag{7.45}$$

where $\chi \in \{-1,0,1\}$ but $\tau \in \{-1,1\}$ and the second form is useful for establishing the symmetry property that

$$\rho_n(\gamma,\mid\tilde{\gamma}\mid) \equiv \int_{-\pi}^{\pi} d\psi\rho(\gamma,\mid\tilde{\gamma}\mid,\psi)e^{in\psi} \tag{7.46}$$

is real and vanishes unless n is a multiple of 3, which is a manifestation of the cubic symmetry inherent in the problem. Note that $\rho_0(\gamma,\mid\tilde{\gamma}\mid)$ and $\rho_3(\gamma,\mid\tilde{\gamma}\mid)$ can be calculated once and for all and then that the ψ dependence becomes irrelevant. This is one of the great strengths of using joint-densities.

Note that our transition criteria satisfy

$$B - A = \frac{d}{d\mu}\int_0^{\infty} d\mid\tilde{\gamma}\mid\mid\tilde{\gamma}\mid\int_{-1}^{1}\frac{d\lambda}{2}\lambda\rho_0(\mu+\lambda\mid\tilde{\gamma}\mid,\mid\tilde{\gamma}\mid) \tag{7.47}$$

$$\begin{gathered} 3C - 3D + E = \\ \frac{d^2}{d\mu^2}\int_0^{\infty} d\mid\tilde{\gamma}\mid\int_{-1}^{1}\frac{d\lambda}{2}\frac{3\lambda^2-1}{2}\rho_3(\mu+\lambda\mid\tilde{\gamma}\mid,\mid\tilde{\gamma}\mid) \end{gathered} \tag{7.48}$$

and so these are the equations we will work with when calculating the transition criteria.

7.5 Comparison with Experimental Systems

We now move on to consider some of the experimentally observed facts that we will try and marry to the predictions of our model. The first system, the manganites, was the inspiration behind the modelling performed in this chapter, and was really the reason for the modelling. The second system we examine is a related, but completely different, compound. This system is the zinc-manganites. Chemically, the material is very different, but certain analogies survive. Most notably, we find the saturated ferromagnetism so crucial to our modelling. Since we really only require this of a transition metal oxide, we examine the possibilities for the proposed orbital ordering in this material. Note that our modelling depends crucially on the density of states only, providing all other assumptions are satisfied in a justified approximation.

7.5.1 Manganites

We observe the manganites have a perovskite crystal structure. The electronic structure is $\mathrm{La}^{3+}_{1-x}\mathrm{A}^{2+}_{x}(\mathrm{Mn}^{3+}\mathrm{Mn}^{4+})\mathrm{O}^{2-}_{3}$, where A is divalent, such as Sr and Ca. We are left with each manganese atom having a full t_{2g} sub-shell, and doping with Sr introduces holes into the system. In the parent compound, we have a single electron in e_g orbitals. Doping with Sr removes this sole electron in the e_g sector, and leaves it empty.

As we saw in section 3.2.2 $\mathrm{La}_{1-x}\mathrm{A}_x\mathrm{MnO}_3$ has a rich and varied phase diagram that renders our model inappropriate to describe much of the phase diagram. There is a high-temperature magnetic phase involving spin and orbital ordering, with strong local distortions of the lattice, and lattice distortions are ignored by our modelling. There are also a variety of insulating phases, which are also ignored by our modelling. We are looking for a region of the phase diagram that corresponds to a saturated ferromagnet, and this will leave only the orbital degree of freedom for us to describe. We are also looking for a metallic ferromagnetic phase, and with no structural distortion. This is the ferromagnetic metallic state without

structural distortion. This occurs around $x \approx 0.3$.

Our results for hole doped manganites are shown in figure 7.4.

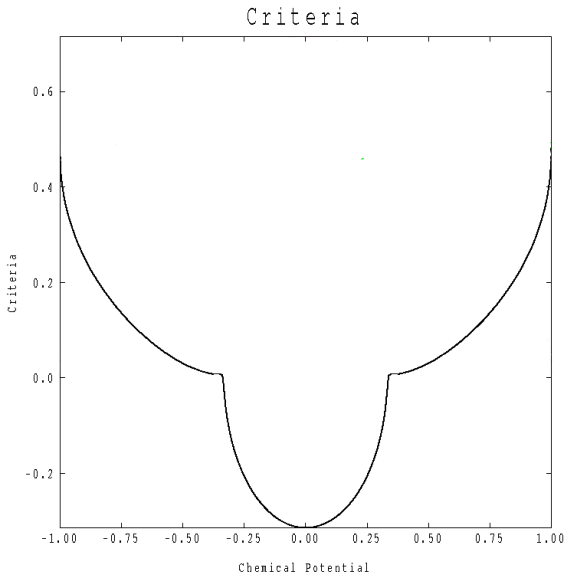

Figure 7.2: Stoner criterion for hole-doped manganites. The solid curve is the quantity $B-A$ and represents the Stoner criterion, and is plotted against the chemical potential. When it is negative, the system adopts the ordered state of symmetry unbroken orbitals. This occurs at $\mu = \pm 0.3$

If we ignore the region where the chemical potential is negative, the chemical potential is the same as the doping. That is in our modelling the material $LaMnO_3$ begins with a half-filled band. These plots were calculated using the cubic joint density of states. We note that the transition to cubic symmetric orbitals occurs around $x \approx 0.3$, which is the region of the phase diagram that is of most interest to us. Since this is a mean-field calculation, we should be wary and not get too excited. The material is definitely a strongly correlated material, and mean-field can only give us a weak-coupling prediction of the phase diagram. We will need another argument to support the possible existence of the cubic symmetric orbitals, which we will give in the next chapter. Even this will provide no guarantee of their existence, and only experiment is fit to judge our theory. Unfortunately, the experiments required to detect the cubic symmetric orbitals will be tricky since the orbitals are hexapolar

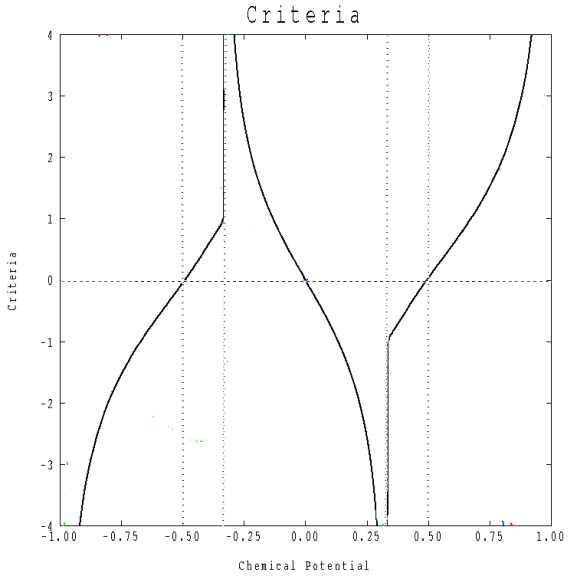

Figure 7.3: Stability of the Stoner Criterion for Hole-Doped Manganites. We fix $\theta = \frac{\pi}{2}$, and. Plotted is the quantity in $3C - 3D + E$ in 7.48 versus chemical potential or doping. This determines which of the symmetry broken orbitals will be populated when the transition is not second-order. When $3C - 3D + E$ is negative, we find we have the $3\hat{z}^2 - 1$ orbitals, and when it is positive we have the $\hat{x}^2 - \hat{y}^2$ orbitals.

in character, and the author is unaware of a probe that could detect them.

The other transitions are determined by the stability, and occur close to $\mu = \pm\frac{1}{2}$. We find that the $\hat{x}^2$-$\hat{y}^2$ orbital is favoured for $n < 0.5$ and the $2\hat{z}^2$-$\hat{x}^2$-$\hat{y}^2$ is favoured for $0.5 < n < 0.7$. The calculation of the stability is irrelevant in the region $0.7 < n < 1$, where the system is predicted to order with the cubic symmetry. For the parameter x, this transforms into cubic symmetry for $0 < x < 0.3$, the $2\hat{z}^2$-$\hat{x}^2$-$\hat{y}^2$ orbital for $0.3 < x < 0.5$ and the $\hat{x}^2$-$\hat{y}^2$ orbital for $0.5 < x < 1$.

7.5.2 Zinc Manganites

Although we had the LSMO manganites in mind when constructing the model, the theory makes no assumptions on the form of the density of states. Therefore, we should find the theory applicable to other systems with saturated ferromagnetic spin. One such system is a compound formed of a partial reaction of ZnO with MnO_2, mostly 2%MnO_2-98%ZnO [8].

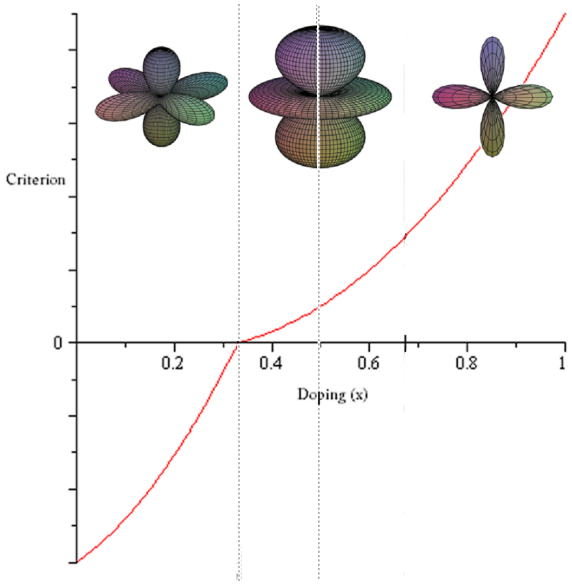

Figure 7.4: Mean-Field Orbital Phase Diagram Based on the Calculations as illustrated in figures 7.3 and 7.3

This system is a little more chemically complicated than the cubic manganites we considered previously. We still have the Mn^{3+} and Mn^{4+} with double exchange, as we require [9]. To model this system, we would have to calculate the effective density of states for this system which is a spinel, and perform analogous calculations. These have not been performed, but should be a straightforward extension of the theory.

7.6 Summary

We have performed a mean-field analysis on a model for cubic symmetric orbital ordering in manganites. We saw that the modelling predicts an orbitally ordered phase at precisely the point in the phase diagram for the manganites that we are interested in, around $x \approx 0.3$.

At the mean-field level we have investigated the analogue of the Stoner criterion for the itinerant orbital ordering of ferromagnetic e_g orbitals on the cubic lattice. We find there are three natural orbital orderings of $\hat{x}^2$-$\hat{y}^2$, $2\hat{z}^2$-$\hat{x}^2$-$\hat{y}^2$ orbitals and the cubic-symmetric orbitals. At low doping we expect the $\hat{x}^2$-$\hat{y}^2$ orbital, close to half-filling we expect the cubic-symmetric

orbitals and inbetween we expect the $2\hat{z}^2$-$\hat{x}^2$-$\hat{y}^2$ orbital. The most interesting possibility is the cubic-symmetric orbitals, because there is no associated structural phase transition and the ordering is hexapolar.

We are employing mean-field theory, which is a weak-coupling concept, and one should be sceptical about its relevance at strong-coupling. The analogue of the Stoner criterion, where itinerant orbital order is first predicted to occur, is quite complicated. Close to half-filling a second-order transition into an exotic state which maintains the cubic symmetry is predicted. Closer to the band edges a more traditional first-order transition into a symmetry-broken state is predicted, with two-dimensional orbitals preferred at low doping and the most one-dimensional orbitals being favoured in an intermediate region.

Technically, the fact that there exists a first-order transition means that the full calculation, where the magnetic moment itself is calculated ought to be performed but we have got the basic idea.

Chapter 8

Fluctuations and Impurities in e_g Orbital Problems

8.1 Introduction

In the previous chapter, we considered a generalised Hubbard model for an electrons delocalising in e_g orbitals. We obtained an energy for this problem in a mean-field picture. In this chapter, we challenge the validity of the mean-field picture by considering whether fluctuations in orbital character and impurities can provide a lower energy than the simple mean-field arguments of the previous chapter.

We will introduce the concept of an orbital Nagaoka problem with some simple examples. We will then work with a model of a hole delocalising in an orbitally ordered background on a perovskite lattice. This shows that the cubic symmetric orbitals are not favoured at half-filling, despite the predictions of the previous chapter. However, this is a single-impurity argument, and we would argue that the case of multiple impurities presents a very different picture.

8.2 The Orbital Nagaoka Problem

We now move on to the concept of an orbital Nagaoka problem, which is analogous to the Nagaoka problem for spins which we discussed in section 4.2.1. We consider a lattice half-filled with a particular configuration of orbitals, and then introduce a hole into the system and allow the hole to delocalise.

We do this to measure the stability of the phase. Unlike the Nagaoka problem for spins, the orbital Nagaoka problem is not solvable, and so we cannot determine exactly the lowest energy configuration of orbitals.

8.2.1 Examples

We now consider a simple illustration of the idea we will use. We will restrict attention to a filled system of p_x and p_y orbitals in a plane, and introduce a hole into the system, and allow the hole to delocalise. Let us take the example where only the p_x orbital is used. We will label this state as $|1>$, and pictorially is represented by

$$|1>= \begin{array}{ccc} p_x & p_x & p_x \\ p_x & h & p_x \\ p_x & p_x & p_x \end{array} \tag{8.1}$$

In this trivial example, the hole can only move left or right, and either of these final states is indistinguishable from the initial state due to translational invariance. Therefore,

$$\mathcal{H}|1>= -2t|1> \tag{8.2}$$

and thus, $\epsilon = -2t$.

We now move on to another example where we have a line of p_x orbital and the remaining orbitals are filled with p_y orbitals. We put the hole into the line of p_x orbitals, and let the

hole delocalise again. Now, our reference state $|1>$ is given by

$$|1>= \begin{matrix} p_y & p_y & p_y \\ p_x & h & p_x \\ p_y & p_y & p_y \end{matrix} \tag{8.3}$$

We label the initial state as $|1>$ and apply the Hamiltonian to get

$$\mathcal{H}|1>= -2t|1> -2t|2> \tag{8.4}$$

where $|2>$ describes the state where the hole has gone into one of the half-planes of p_y orbitals.

$$|2>= \begin{matrix} p_y & h & p_y \\ p_x & p_y & p_x \\ p_y & p_y & p_y \end{matrix} \tag{8.5}$$

This state has energy $\epsilon = 2 + 2\alpha$, where α is to be determined.

Applying the Hamiltonian to $|2>$ we get

$$\mathcal{H}|2>= -t|3> -t|1> \tag{8.6}$$

and in general, for $|n| \geq 2$, we get

$$\mathcal{H}|n>= -t|n+1> -t|n-1> . \tag{8.7}$$

and these offer the energies $\epsilon\alpha x^{n-1} = \alpha x^{n-2} + \alpha x^n$. We can solve these equations to obtain $\epsilon \approx -2.41$. This is a big improvement on the energy of -2 that was available from the uniform orbital solutions we first considered.

We can improve on this by allowing fluctuations into the picture. We begin by assuming

a state

$$|\theta >= \cos\theta\hat{x} + \sin\theta\hat{y} \tag{8.8}$$

and an orthogonal state

$$|\theta >= \cos\theta\hat{x} + \sin\theta\hat{y} \tag{8.9}$$

and we apply the Hamiltonian to this state, allowing fluctuations. We begin as usual with the state

$$|0 >= \begin{array}{ccc} \theta & \theta & \theta \\ \theta & h & \theta \\ \theta & \theta & \theta \end{array} \tag{8.10}$$

We now obtain

$$\begin{aligned} \mathcal{H}|0> &= -3t\left(\cos\theta(x+x^{-1}) + \sin\theta(y+y^{-1})\right)|0> \\ &- t\cos\theta x|1> -t\cos\theta x^{-1}|2> -t\sin\theta y|3> -t\sin\theta y^{-1}|4> \end{aligned} \tag{8.11}$$

where $x = \exp(i\hat{k}\hat{x})$ and $y = \exp(i\hat{k}\hat{y})$ and

$$|1 >= \begin{array}{ccc} \theta & \theta & \theta \\ \theta & h & \bar{\theta} \\ \theta & \theta & \theta \end{array} \tag{8.12}$$

$$|2 >= \begin{array}{ccc} \theta & \theta & \theta \\ \bar{\theta} & h & \theta \\ \theta & \theta & \theta \end{array} \tag{8.13}$$

$$|3>= \begin{matrix} \theta & \bar{\theta} & \theta \\ \theta & h & \theta \\ \theta & \theta & \theta \end{matrix} \tag{8.14}$$

$$|4>= \begin{matrix} \theta & \theta & \theta \\ \theta & h & \theta \\ \theta & \bar{\theta} & \theta \end{matrix} . \tag{8.15}$$

Applying the Hamiltonian to each of these new states we find

$$\mathcal{H}|1>= -t\cos\theta x^{-1}|0> -t\cos\theta x|2> \tag{8.16}$$

$$\mathcal{H}|2>= -t\cos\theta x|0> -t\cos\theta x^{-1}|1> \tag{8.17}$$

$$\mathcal{H}|3>= -t\sin\theta y^{-1}|0> -t\sin\theta y|4> \tag{8.18}$$

$$\mathcal{H}|4>= -t\sin\theta y|0> -t\sin\theta y^{-1}|3> \tag{8.19}$$

and so the Hamiltonian matrix for this system is

$$\mathcal{H} = -t\begin{bmatrix} -3t\left(\cos\theta(x+x^{-1})+\sin\theta(y+y^{-1})\right) & \cos\theta x & \cos\theta x^{-1} & \sin\theta y & \sin\theta y^{-1} \\ \cos\theta x^{-1} & 0 & \cos\theta x^{-1} & 0 & 0 \\ \cos\theta x & \cos\theta x & 0 & 0 & 0 \\ \sin\theta y^{-1} & 0 & 0 & 0 & \sin\theta y \\ \sin\theta y & 0 & 0 & \sin\theta y^{-1} & 0 \end{bmatrix} \tag{8.20}$$

8.3 Impurities and Fluctuations in e_g d Orbital Systems

We will consider the Hubbard-like model we have developed to be at half-filling, and we will consider the limit $U \to \infty$. We will then remove one particle in the manner of the Nagaoka problem, and consider the motion of the hole. The Hamiltonian in this limit is

$$-\frac{t}{2} \sum_{<jj'>\alpha} \left(1 - c^{\dagger}_{j'\bar{\alpha}} c_{j'\bar{\alpha}}\right) c^{\dagger}_{j'\alpha} c^{\dagger}_{j\alpha} \left(1 - c^{\dagger}_{j\bar{\alpha}} c_{j\bar{\alpha}}\right). \tag{8.21}$$

This excludes terms which involve doubly occupying a site. The Hamiltonian thus exchanges the hole with a nearest-neighbour particle, and resembles the motion of a single particle in an otherwise empty system.

8.4 Orbital Nagaoka Problem on a Lattice with Cubic Symmetry

We now consider the problem of the orbitals ordering in the basis cubic symmetric orbitals *exactly*. We will first work on the case that no fluctuations are permitted. We fill the system with orbitals of the form

$$|\theta> = \cos(\theta)\exp(-i\phi/2)|\omega> + \sin(\theta)\exp(i\phi/2)|\omega^2> . \tag{8.22}$$

Our space thus looks like

$$|0> = \begin{matrix} \theta & \theta & \theta \\ \theta & h & \theta \\ \theta & \theta & \theta \end{matrix} \tag{8.23}$$

and thus $\mathcal{H}|0> = -3|0>$, for *any* choice of θ and ϕ , since there are 6 directions the hole can hop. Thus, $\epsilon = -3$ for an arrangement of like orbitals .

We now work on the case that fluctuations are permitted in the system. We will introduce an orthogonal orbital to the one we have introduced by

$$|\bar{\theta} >= -\sin(\theta)\exp(-i\phi/2)|\omega > +\cos(\theta)\exp(i\phi/2)|\omega^2 > . \tag{8.24}$$

Now we focus on implementing a fixed background of our choosing onto the orbital Nagaoka problem we are considering. This may seem artificial, but the problem is not solvable, and we are forced into choosing background configurations of orbitals and showing the resulting energy is lower than we previously considered. We first look to a plane of $\hat{x}^2 - \hat{y}^2$ orbitals first, which we will denote by x for notational convenience.

We delocalise using (n_x, n_y) for position and

$$|x, y; 0 >= \frac{1}{\sqrt{N}} \sum_k x^{n_x} y^{n_y} |n_x, n_y > \tag{8.25}$$

for the Bloch transform. Now, we have

$$|0 >= \begin{matrix} x & x & x \\ x & h & x \\ x & x & x \end{matrix} \tag{8.26}$$

$$|1 >= \begin{matrix} x & x & x \\ x & h & z \\ x & x & x \end{matrix} \tag{8.27}$$

$$|2 >= \begin{matrix} x & x & x \\ z & h & x \\ x & x & x \end{matrix} \tag{8.28}$$

$$|3>= \begin{array}{ccc} x & z & x \\ x & h & x \\ x & x & x \end{array} \tag{8.29}$$

$$|4>= \begin{array}{ccc} x & x & x \\ x & h & x \\ x & z & x \end{array} \tag{8.30}$$

Applying the Hamiltonian to each of these states, we obtain

$$\mathcal{H}|0>= -\frac{3t}{4}\left(x+x^{-1}+y+y^{-1}\right)|0> -\frac{\sqrt{3}t}{4}\left(x|1>+x^{-1}|2>-x|3>-x^{-1}|4>\right) \tag{8.31}$$

$$\mathcal{H}|1>= -\frac{\sqrt{3}t}{4}x^{-1}|0> -\frac{t}{4}x^{-1}|2> \tag{8.32}$$

$$\mathcal{H}|2>= -\frac{\sqrt{3}t}{4}x|0> -\frac{t}{4}x|1> \tag{8.33}$$

$$\mathcal{H}|3>= -\frac{\sqrt{3}t}{4}y^{-1}|0> -\frac{t}{4}y^{-1}|4> \tag{8.34}$$

$$\mathcal{H}|4>= -\frac{\sqrt{3}t}{4}y|0> -\frac{t}{4}y|3> \tag{8.35}$$

The Hamiltonian matrix is thus

$$\mathcal{H}=-t\begin{bmatrix} \frac{3}{4}(x+x^{-1}+y+y^{-1}) & \frac{\sqrt{3}}{4}x & \frac{\sqrt{3}}{4}x^{-1} & -\frac{\sqrt{3}}{4}y & -\frac{\sqrt{3}}{4}y^{-1} \\ \frac{\sqrt{3}}{4}x^{-1} & 0 & \frac{1}{4}x^{-1} & 0 & 0 \\ \frac{\sqrt{3}}{4}x & \frac{1}{4}x & 0 & 0 & 0 \\ -\frac{\sqrt{3}}{4}y^{-1} & 0 & 0 & 0 & \frac{1}{4}y^{-1} \\ -\frac{\sqrt{3}}{4}y & 0 & 0 & \frac{1}{4}y & 0 \end{bmatrix} \tag{8.36}$$

and we wish to calculate the Green's function

$$G(\epsilon) = (\epsilon - \mathcal{H})^{-1}. \tag{8.37}$$

Using the fact the symmetry is unbroken, we have $x = y = 1$, and

$$G^{-1} = -t \begin{bmatrix} \epsilon + 3 & \frac{\sqrt{3}}{4} & \frac{\sqrt{3}}{4} & -\frac{\sqrt{3}}{4} & -\frac{\sqrt{3}}{4} \\ \frac{\sqrt{3}}{4} & \epsilon & \frac{1}{4} & 0 & 0 \\ \frac{\sqrt{3}}{4} & \frac{1}{4} & \epsilon & 0 & 0 \\ -\frac{\sqrt{3}}{4} & 0 & 0 & \epsilon & \frac{1}{4} \\ -\frac{\sqrt{3}}{4} & 0 & 0 & \frac{1}{4} & \epsilon \end{bmatrix} \tag{8.38}$$

We now look to a cubic lattice of $3\hat{z}^2 - 1$ orbitals in an analogous way.

$$|0> = \begin{matrix} z & z & z \\ z & h & z \\ z & z & z \end{matrix} \tag{8.39}$$

$$|1> = \begin{matrix} z & z & z \\ z & h & x \\ z & z & z \end{matrix} \tag{8.40}$$

$$|2> = \begin{matrix} z & z & z \\ x & h & z \\ z & z & z \end{matrix} \tag{8.41}$$

$$|3> = \begin{matrix} z & x & z \\ z & h & z \\ z & z & z \end{matrix} \tag{8.42}$$

$$|4>= \begin{matrix} z & z & z \\ z & h & z \\ z & x & z \end{matrix} \tag{8.43}$$

Again, delocalising over all sites, we have

$$|x,y,z;0>= \frac{1}{\sqrt{N}} \sum_n x^{n_x} y^{n_y} z^{n_z} |n_x, n_y, n_z; 0> \tag{8.44}$$

for the Bloch transform.

Again, applying the Hamiltonian to each of these states, we obtain

$$\mathcal{H}|0>= -t\left(z+z^{-1}+\frac{1}{4}\left(x+x^{-1}+y+y^{-1}\right)\right)|0> -\frac{\sqrt{3}t}{4}\left(x|1>+x^{-1}|2>-y|3>-y^{-1}|4>\right) \tag{8.45}$$

$$\mathcal{H}|1>= -\frac{\sqrt{3}t}{4}x^{-1}|0> -\frac{3t}{4}x^{-1}|2> -\frac{\sqrt{3}t}{4}\left(x|1>+x^{-1}|2>-y|3>-y^{-1}|4>\right) \tag{8.46}$$

$$\mathcal{H}|2>= -\frac{\sqrt{3}t}{4}x|0> -\frac{3t}{4}x|2> -\frac{\sqrt{3}t}{4}\left(x|1>+x^{-1}|2>-y|3>-y^{-1}|4>\right) \tag{8.47}$$

$$\mathcal{H}|3>= -\frac{\sqrt{3}t}{4}y^{-1}|0> -\frac{3t}{4}y^{-1}|4> -\frac{\sqrt{3}t}{4}\left(x|1>+x^{-1}|2>-y|3>-y^{-1}|4>\right) \tag{8.48}$$

$$\mathcal{H}|4>= -\frac{\sqrt{3}t}{4}y|0> -\frac{3t}{4}y|3> -\frac{\sqrt{3}t}{4}\left(x|1>+x^{-1}|2>-y|3>-y^{-1}|4>\right) \tag{8.49}$$

This time, our Hamiltonian matrix is

$$\mathcal{H}=-t\begin{bmatrix} \frac{3}{4}(x+x^{-1}+y+y^{-1}) & \frac{\sqrt{3}}{4}x & \frac{\sqrt{3}}{4}x^{-1} & -\frac{\sqrt{3}}{4}y & -\frac{\sqrt{3}}{4}y^{-1} \\ \frac{\sqrt{3}}{4}x^{-1} & 0 & \frac{1}{4}x^{-1} & 0 & 0 \\ \frac{\sqrt{3}}{4}x & \frac{1}{4}x & 0 & 0 & 0 \\ -\frac{\sqrt{3}}{4}y^{-1} & 0 & 0 & 0 & \frac{1}{4}y^{-1} \\ -\frac{\sqrt{3}}{4}y & 0 & 0 & \frac{1}{4}y & 0 \end{bmatrix} \tag{8.50}$$

Again, we want to find $G(\epsilon) = [\epsilon - \mathcal{H}]^{-1}$. However, this time we need to cut space to make a surface, and then we need to patch together these two subsystems.

When the hole lies in the plane, we force the rest of space to be uniform. We need to consider ten states now

$$\begin{bmatrix}
G_0 & G_1 & G_1 & -G_1 & -G_1 & 0 & 0 & 0 & 0 & 0 \\
G_1 & G_2 & G_3 & G_4 & G_4 & 0 & 0 & 0 & 0 & 0 \\
G_1 & G_3 & G_2 & G_4 & G_4 & 0 & 0 & 0 & 0 & 0 \\
-G_1 & G_4 & G_4 & G_2 & G_3 & 0 & 0 & 0 & 0 & 0 \\
-G_1 & G_4 & G_4 & G_3 & G_2 & 0 & 0 & 0 & 0 & 0 \\
0 & 0 & 0 & 0 & 0 & \tilde{G}_0 & 0 & 0 & 0 & 0 \\
0 & 0 & 0 & 0 & 0 & 0 & \tilde{G}_0 & \tilde{G}_1 & 0 & 0 \\
0 & 0 & 0 & 0 & 0 & 0 & \tilde{G}_1 & \tilde{G}_0 & 0 & 0 \\
0 & 0 & 0 & 0 & 0 & 0 & 0 & 0 & \tilde{G}_0 & \tilde{G}_1 \\
0 & 0 & 0 & 0 & 0 & 0 & 0 & 0 & \tilde{G}_1 & \tilde{G}_0
\end{bmatrix} \tag{8.51}$$

which are connected by

$$\left[\begin{array}{cccccccccc}
0 & 0 & 0 & 0 & 0 & -\sqrt{2} & 0 & 0 & 0 & 0 \\
0 & 0 & 0 & 0 & 0 & 0 & -\sqrt{2} & 0 & 0 & 0 \\
0 & 0 & 0 & 0 & 0 & 0 & 0 & -\sqrt{2} & 0 & 0 \\
0 & 0 & 0 & 0 & 0 & 0 & 0 & 0 & -\sqrt{2} & 0 \\
0 & 0 & 0 & 0 & 0 & 0 & 0 & 0 & 0 & -\sqrt{2} \\
-\sqrt{2} & 0 & 0 & 0 & 0 & 0 & 0 & 0 & 0 & 0 \\
0 & -\sqrt{2} & 0 & 0 & 0 & 0 & 0 & 0 & 0 & 0 \\
0 & 0 & -\sqrt{2} & 0 & 0 & 0 & 0 & 0 & 0 & 0 \\
0 & 0 & 0 & -\sqrt{2} & 0 & 0 & 0 & 0 & 0 & 0 \\
0 & 0 & 0 & 0 & -\sqrt{2} & 0 & 0 & 0 & 0 & 0
\end{array}\right] \tag{8.52}$$

8.5 Conclusions

In our study of a single hole in an otherwise singly-occupied strong-coupling system, we considered *inexactly* two situations. Firstly, the uniform orbital state with fluctuations, and secondly, the possibility of spatial localisation for the hole. *Both* styles of solution are seen to be competitive with each other energetically. Unfortunately, we *imposed* these possibilities and did not give the system a free choice. It is quite conceivable that a third, more sophisticated solution, is ultimately preferred by the system. To investigate this possibility, we examine the cubic-symmetric description of our model in more detail.

If we employ the cubic-symmetric basis for the orbitals, then the scale of hopping is $\frac{t}{2}$ and there are twelve hops available. We have six that connect like orbitals, with no phase change associated with a hop. We have another six hops that connect different cubic symmetric orbitals, and these hope picks up a phase corresponding to one of the cube-roots of unity,

and depends on the direction of the hopping.

Clearly, the energy is bounded by -6t, if all the hops were to be coherently accessed, but this is not possible in practice. Indeed, for a single square, the energy is -$\frac{3+\sqrt{17}}{4}t$=-1.78t. This is a lot worse energetically than the -2t that is thought to be available from this simple counting argument. However, this energy is a lot more than the single orbital energy of -1.5t using the appropriate planar orbital. We believe that this corresponds to a form of *frustration* which corresponds to issues when the hole circuits loops.

There are subtleties that plague this problem. Let us start from a random array of two cubic-symmetric orbitals. If we delocalise the hole using *orbital preserving* hops, then we achieve an energy of -3t with a state where each accessible orbital configuration is found with equal phase and equal probability. This state *is* a state with all sites having the same orbital, and that orbital is a uniform phase sum of the two cubic orbitals with amplitudes controlled by the initial numbers of the two orbitals. These states correspond to ϕ=0 but different values of θ for different initial fractions of cubic orbitals.

By using a uniform phase we promote hopping along the z-axis and we 'project' onto the appropriate orbital, in this case $2\hat{z}^2$-$\hat{x}^2$-$\hat{y}^2$. We could focus attention on $2\hat{x}^2$-$\hat{y}^2$-$\hat{z}^2$ orbitals if desired by picking up the appropriate cube-root of unity when hopping, to maintain the phase of $\hat{x}^2$ instead of $\hat{z}^2$. It is clear that we need to employ different phases in different directions, in order to align orbitals parallel to motion, and this is quite a sophisticated problem.

The most important observation is that this problem is very different from that of the Nagaoka problem for the isotropic Hubbard model. Both situations rely on loops, but for the isotropic Hubbard model, phase coherence around the loop providing either low-spin or high-spin is the key to the solution of the problem. For the orbital Nagaoka problem, the system would prefer *different* orbitals in passing round a loop in one direction from the other. In one case we want linear superpositions of multiple motions around the loop and in the

other we need a *local* choice of orbital to favour the *immediate* motion.

The classical picture of fixed orbitals with short-range orientation fluctuations ought to be an excellent approximation. We believe that our symmetry-broken solution is essentially the solution to the problem, but as with the Nagaoka problem, it is probably *not* physically relevant. The interaction between different holes very soon stabilises a fluctuating solution and the calculations suggest that the cubic-symmetric orbitals are a better starting point for cubic-symmetric motion.

Chapter 9

Magnetism in Pyrochlore Systems

9.1 Introduction

We now move on to examine the magnetic structure of a specific material, $Gd_2Ti_2O_7$. There exists some conflict between the prediction of neutron scatterers, and the evidence that Mossbauer provides. We seek to address the conflict here, following our paper [1], and provide our own interpretation of the experimental data. We show that our predicted state is consistent with both the neutron scattering data and the Mossbauer data, but completely different to the predictions of Bramwell et. al. [36].

The crystal structure of the material is pyrochlore, and this consists of a network of corner sharing tetrahedra (section 3.3.1). Heisenberg antiferromagnetism is highly frustrated on a tetrahedron, and so it is expected that other interactions will have to be taken into account to lift the degeneracy. One of the most studied extensions is adding next-nearest neighbour dipole interactions into a model [29]. As we will see, our modelling is inconsistent with the theoretical literature.

Pyrochlore antiferromagnetism has been much studied as it is one of the most frustrated geometries that can be found in real materials. There is expected to be a macroscopic degeneracy for the nearest-neighbour Heisenberg interaction which is expected to be lifted by much smaller interactions, which are often irrelevant in unfrustrated systems. $Gd_2Ti_2O_7$ and

$Gd_2Sn_2O_7$ are the best known experimental examples of a pyrochlore lattice with dominant nearest-neighbour Heisenberg interactions.

9.2 Experimental Input

$Gd_2Ti_2O_7$ has a pyrochlore crystal structure, and the electronic configuration is $Gd_2^{3+}Ti_2^{4+}O_7^{2-}$. This leaves Ti with a closed d-shell, and the active spin is on Gd.

Stewart et. al. performed neutron scattering experiments on a powdered sample of $Gd_2Ti_2O_7$ and concluded that the neutron scattering data can be indexed by a propagation vector $\left(\frac{1}{2}, \frac{1}{2}, \frac{1}{2}\right)$. From this, they proposed a state with two different moments around the tetrahedra. An illustration is show in figure 9.1. However, this state is in conflict with the Mossbauer data, which suggests a single moment.

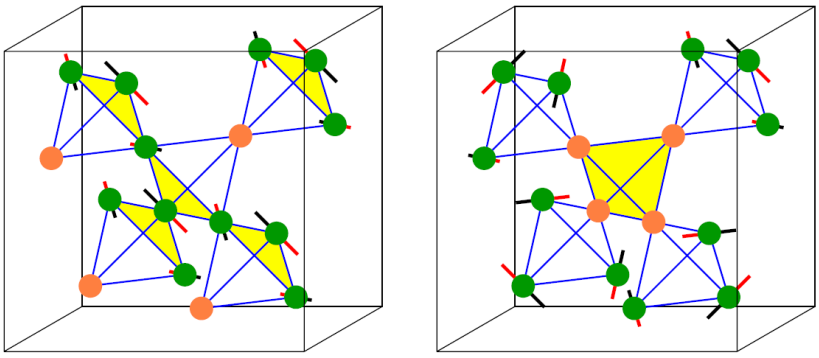

Figure 9.1: Magnetic Structure of $Gd_2Ti_2O_7$ according to [36]

The Mössbauer experiments suggest that the spins are all equal length, and that they are oriented perpendicular to the local crystallographic directions. We will employ these assumptions in our modeling. They also examine the possibility of two magnetic moments not both in the preferred planes, but *only* in the initial intermediate temperature phase. An additional degree of freedom always provides a better fit, and the improvement is not significant. The second magnetic moment is also much too large to agree with the states

proposed by the neutron scatterers. The low temperature phase does not appear to accept a phase with two different moments.

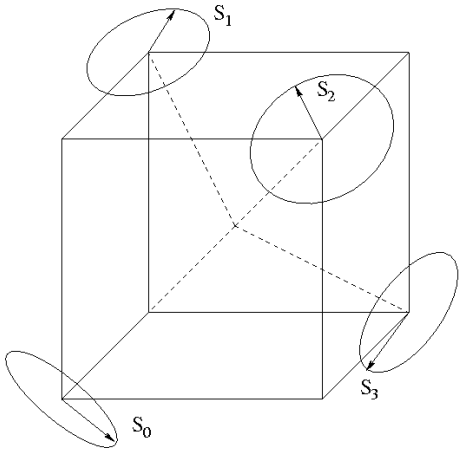

Figure 9.2: Planes of spin-anisotropy in tetrahedra

9.3 Theoretical Interpretation

We now marry the experimental inputs of the scattering data being indexed by $\left(\frac{1}{2}, \frac{1}{2}, \frac{1}{2}\right)$ and the evidence supplied by the Mossbauer experiments. We will then use this to aid our prediction of the magnetic structure of $Gd_2Ti_2O_7$, along with a few assumptions.

For a propagation vector of $\left(\frac{1}{2}, \frac{1}{2}, \frac{1}{2}\right)$, the magnetic unit cell becomes double the primitive tetrahedral unit cell in all directions, and so a hop on the grid illustrated in figure 9.3 picks up a phase of $\pm\sqrt{i}$. We may be tempted to interpret the spin labelled 3 as the opposite spin to the spin labelled 0, but since the manner in which phases picked up is arbitrary, it is not necessarily the same spin.

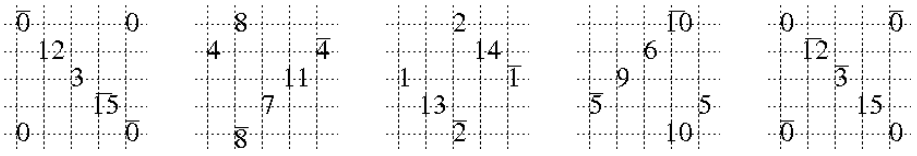

Figure 9.3: Implications of Neutron Scattering Data. A bar denotes a spin reflected with respect to the unbarred label. (Fig:9.6

The pyrochlore lattice has four atoms per primitive unit cell, and so the magnetic primitive unit cell will contain thirty-two atoms. This is far too many for the problem to be tractable. We will thus bear the neutron scattering data in mind, and move to interpreting the Mossbauer data. As we discussed earlier, the experiments suggest that at low temperatures, all moments are ordered with equal magnitude, and that they are ordered in planes perpendicular to the line pointing at the centre of a tetrahedron.

We now propose an assumption, which is that in each tetrahedron, the total spin is zero. This is only suggested by the experiments, and is not guaranteed. Assuming this, however, will render the problem tractable. We will thus obtain a very Heisenberg-like antiferromagnet on a tetrahedron. We can see the material is very unlike spin-ice (section 3.3.2), where the interactions are very unheisenberg-like.

9.3.1 The Heisenberg Interaction

The experiments suggest that $Gd_2Ti_2O_7$ is an excellent example of a Heisenberg antiferromagnet, and also suggest that the total spin in each tetrahedron is zero. We therefore seek to find the groundstate of the antiferromagnetic Heisenberg model on a tetrahedron. It is well known, however, that there is a high degree of frustration for this model on a tetrahedron. We will therefore obtain a manifold of ground states.

We need to find constraints on the spins which lie in the anisotropy planes such that the sum of our spins is zero. We employ the natural basis

$$\hat{\mathbf{S}}_0 = \left[\frac{2}{3}\right]^{\frac{1}{2}} [\hat{\mathbf{x}} \cos x_0 + \hat{\mathbf{y}} \cos y_0 + \hat{\mathbf{z}} \cos z_0] \tag{9.1}$$

$$\hat{\mathbf{S}}_1 = \left[\frac{2}{3}\right]^{\frac{1}{2}} [\hat{\mathbf{x}} \cos x_1 - \hat{\mathbf{y}} \cos y_1 - \hat{\mathbf{z}} \cos z_1] \tag{9.2}$$

$$\hat{\mathbf{S}}_2 = \left[\frac{2}{3}\right]^{\frac{1}{2}} [-\hat{\mathbf{x}} \cos x_2 + \hat{\mathbf{y}} \cos y_2 - \hat{\mathbf{z}} \cos z_2] \tag{9.3}$$

$$\hat{\mathbf{S}}_3 = \left[\frac{2}{3}\right]^{\frac{1}{2}} [-\hat{\mathbf{x}} \cos x_3 - \hat{\mathbf{y}} \cos y_3 + \hat{\mathbf{z}} \cos z_3] \tag{9.4}$$

and couple this with the constraint

$$x_\alpha = z_\alpha - \frac{2\pi}{3} y_\alpha = z_\alpha - \frac{2\pi}{3} z_\alpha = y_\alpha - \frac{2\pi}{3} \tag{9.5}$$

By construction, this ensures that the spins are in the anisotropy planes, and are also normalised. We can also decompose the spin coordinates as

$$S_0 = \left(\frac{2\hat{x} - \hat{y} - \hat{z}}{\sqrt{6}}\right) \cos x_0 + \left(\frac{\hat{y} - \hat{z}}{\sqrt{2}}\right) \sin x_0 \tag{9.6}$$

$$S_0 = \left(\frac{2\hat{y} - \hat{z} - \hat{x}}{\sqrt{6}}\right) \cos y_0 + \left(\frac{\hat{z} - \hat{x}}{\sqrt{2}}\right) \sin y_0 \tag{9.7}$$

$$S_0 = \left(\frac{2\hat{z} - \hat{x} - \hat{y}}{\sqrt{6}}\right) \cos z_0 + \left(\frac{\hat{x} - \hat{y}}{\sqrt{2}}\right) \sin z_0. \tag{9.8}$$

This relates the coordinate axes to the angles $x_\alpha, y_\alpha, z_\alpha$, and formulae for the other spins follow analogously.

Our task is now to find solutions to the constraint

$$S_0 + S_1 + S_2 + S_3 = 0. \tag{9.9}$$

The equivalent trigonometric constraints are

$$\cos x_0 + \cos x_1 - \cos x_2 - \cos x_3 = 0 \tag{9.10}$$

$$\cos y_0 - \cos y_1 + \cos y_2 - \cos y_3 = 0 \tag{9.11}$$

$$\cos z_0 - \cos z_1 - \cos z_2 + \cos z_3 = 0 \tag{9.12}$$

Firstly we break the symmetry and focus on z_α. Rewriting the first two equations provides

$$\begin{aligned} &\sin\left(\frac{z_0-z_3}{2}\right)\sin\left(\frac{z_0+z_3}{2}-\frac{2\pi}{3}\right) \\ &+\sin\left(\frac{z_1-z_2}{2}\right)\sin\left(\frac{z_1+z_2}{2}-\frac{2\pi}{3}\right) \quad = 0 \end{aligned} \tag{9.13}$$

$$\begin{aligned} &\sin\left(\frac{z_0-z_3}{2}\right)\sin\left(\frac{z_0+z_3}{2}+\frac{2\pi}{3}\right) \\ &-\sin\left(\frac{z_1-z_2}{2}\right)\sin\left(\frac{z_1+z_2}{2}+\frac{2\pi}{3}\right) \quad = 0 \end{aligned} \tag{9.14}$$

and then mixing them offers

$$\begin{aligned} &\sin\left(\frac{z_0-z_3}{2}\right)\sin\left(\frac{z_0+z_3}{2}\right) \\ &+\sqrt{3}\sin\left(\frac{z_1-z_2}{2}\right)\cos\left(\frac{z_1+z_2}{2}\right) \quad = 0 \end{aligned} \tag{9.15}$$

$$\begin{aligned} &\sqrt{3}\sin\left(\frac{z_0-z_3}{2}\right)\cos\left(\frac{z_0+z_3}{2}\right) \\ &+\sin\left(\frac{z_1-z_2}{2}\right)\sin\left(\frac{z_1+z_2}{2}\right) \quad = 0 \end{aligned} \tag{9.16}$$

including the third original equation as

$$\begin{aligned} &\cos\left(\frac{z_0-z_3}{2}\right)\cos\left(\frac{z_0+z_3}{2}\right) \\ &-\cos\left(\frac{z_1-z_2}{2}\right)\cos\left(\frac{z_1+z_2}{2}\right) \quad = 0. \end{aligned} \tag{9.17}$$

We can now eliminate z_1 and z_2 to provide

$$s_-^2\left(4s_+^2-3\right)\left(\left[9-8s_+^2\right]\left[1-s_-^2\right]+2s_+^2\right)=0 \tag{9.18}$$

in terms of

$$s_\pm=\sin\left(\frac{z_0\pm z_3}{2}\right) \tag{9.19}$$

The final solution is unphysical, so we generate two independent solutions. Firstly

$$\sin\left(\frac{z_0-z_3}{2}\right)=0 \quad \Rightarrow \quad \sin\left(\frac{z_1-z_2}{2}\right)=0 \tag{9.20}$$

and consequently (modulo 2π)

$$z_0=z_3 \quad z_1=z_2 \qquad \cos z_0=\cos z_1 \tag{9.21}$$

and the two solutions

$$z_0=z_1=z_2=z_3 \qquad z_0=-z_1=-z_2=z_3 \tag{9.22}$$

Secondly,

$$\sin^2\left(\frac{z_0+z_3}{2}\right)=\frac{3}{4} \quad \Rightarrow \quad \cos(z_0+z_3)=-\frac{1}{2} \tag{9.23}$$

and from Eq.9.15 and Eq.9.16

$$\sin\left(\frac{z_1-z_2}{2}\right)\sin\left(\frac{z_0+z_3}{2}-\frac{z_1+z_2}{2}\right)=0. \tag{9.24}$$

The solution z_1=z_2 provides a subset of the possible solutions, and a further possibility is

$$z_0+z_3=z_1+z_2. \tag{9.25}$$

This leads to two further solutions

$$z_0 + z_3 = \frac{4\pi}{3} = z_1 + z_2 \quad \Rightarrow \quad x_0 + x_3 = 0 = x_1 + x_2 \tag{9.26}$$

which reduces the original equations Eq.9.11 and Eq.9.12 to

$$\begin{aligned} &\cos\left(x_0 - \frac{2\pi}{3}\right) - \cos\left(x_1 - \frac{2\pi}{3}\right) \\ &+\cos\left(x_1 + \frac{2\pi}{3}\right) - \cos\left(x_0 + \frac{2\pi}{3}\right) \quad = 0 \end{aligned} \tag{9.27}$$

$$\begin{aligned} &\cos\left(x_0 + \frac{2\pi}{3}\right) - \cos\left(x_1 + \frac{2\pi}{3}\right) \\ &-\cos\left(x_1 - \frac{2\pi}{3}\right) + \cos\left(x_0 - \frac{2\pi}{3}\right) \quad = 0. \end{aligned} \tag{9.28}$$

This leads to the unique solution

$$x_0 = x_1 = -x_2 = -x_3 \tag{9.29}$$

which, together with

$$z_0 + z_3 = -\frac{4\pi}{3} = z_1 + z_2 \quad \Rightarrow \quad y_0 + y_3 = 0 = y_1 + y_2 \tag{9.30}$$

reduces the original equations 9.10 and 9.12 to

$$\begin{aligned} &\cos\left(y_0 + \frac{2\pi}{3}\right) + \cos\left(y_2 - \frac{2\pi}{3}\right) \\ &-\cos\left(y_2 + \frac{2\pi}{3}\right) - \cos\left(y_0 - \frac{2\pi}{3}\right) \quad = 0 \end{aligned} \tag{9.31}$$

$$\begin{aligned} &\cos\left(y_0 - \frac{2\pi}{3}\right) - \cos\left(y_2 + \frac{2\pi}{3}\right) \\ -&\cos\left(y_2 - \frac{2\pi}{3}\right) + \cos\left(y_0 + \frac{2\pi}{3}\right) \quad = 0 \end{aligned} \tag{9.32}$$

and the further unique solution

$$y_0 = -y_1 = y_2 = -y_3. \tag{9.33}$$

The situation is best illustrated in 9.6. The plane illustrated is the plane normal to the line pointing towards the centre of the tetrahedron.

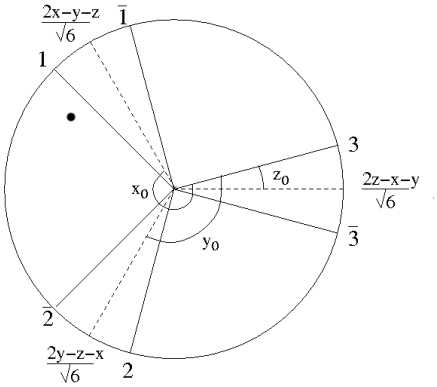

Figure 9.4: Polar plot of the physical situation. The plane illustrated is the anisotropy plane suggested by the Mossbauer experiments on the site S_0 as in figure 9.2. The axes on this figure are projection of the coordinate axes of the tetrahedral primitive unit cell onto the anisotropy plane, and the angles x_0, y_0 and z_0 from 9.1.

From this, we can see that restricting the spins to the anisotropy plane and the requirement of Heisenberg antiferromagnetism severely constrains the possible magnetic states. These possible states are annotated in figure 9.5.

We now have to enumerate the permitted states for the entire pyrochlore unit cell. This, however, is troublesome.

In spin-ice, the spins are oriented towards the centres of the tetrahedra, which is somewhat a simpler problem than the one we face. The spin-ice constraint means that the ground-states

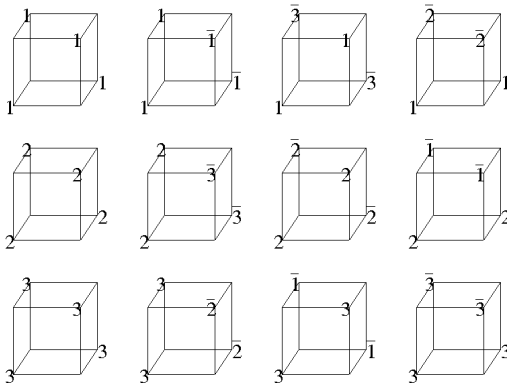

Figure 9.5: Permitted spin configurations for the Heisenberg Antiferromagnet on a Tetrahedron as labelled in Figure 9.4.

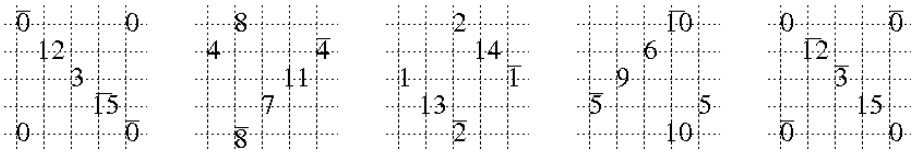

Figure 9.6: The six permitted angles for a global spin configuration according to modelling of the Heisenberg interaction.

may be generated by propagating a solution parallel to a Cartesian direction.

We being by ignoring the possibility of barred spins and focus only on spins labelled by $n \in \{1, 2, 3\}$. For the special case of z_0=0, there is indeed no distinction between barred and unbarred spins. Physically speaking, we would not expect the spins to employ arbitrary directions and the special cases of $z_0 \in \{0, \frac{2\pi}{3}, \frac{4\pi}{3}\}$ and $z_0 \in \{-\frac{\pi}{6}, \frac{\pi}{2}, \frac{\pi}{6}\}$ offer distinct extra symmetries with both involving only twelve global spin orientations. The first provides a restriction to three local orientations and the second finds commonality between distinct sublattice configurations leading to the orientations:

$$\{\frac{\pm\hat{\mathbf{y}} \pm \hat{\mathbf{z}}}{\sqrt{2}}, \frac{\pm\hat{\mathbf{z}} \pm \hat{\mathbf{x}}}{\sqrt{2}}, \frac{\pm\hat{\mathbf{x}} \pm \hat{\mathbf{y}}}{\sqrt{2}}\}. \tag{9.34}$$

This is, in our opinion, the best candidate for the magnetic structure of $Gd_2Ti_2O_7$.

By employing propagation along one of the Cartesian directions, we can use a similar

argument to the previous to investigate the degeneracy. We focus on a plane perpendicular to the z-direction which provides the restrictions that 1 and 2 may not be neighbours in the plane but pairs of 1 and 2 may propagate to the next plane using either 1 or 2 for the next pair. This provides a large but seemingly not exponential degeneracy, since as well as the new configurations from the choices of 1 and 2, there is also an associated loss from discounting states where 1 and 2 are neighbours in the next plane. The inclusion of the bar further complicates matters.

In our modeling, the restriction to having reversed spins is also a strong constraint. The easiest way to enforce it is to restrict attention to z_0=$\frac{\pi}{2}$ and then the two spins n and $\bar{n}$ are actually in *opposite* physical directions.

The previous problem of annotating permissible configurations in terms of the states n now provides an elementary solution. Firstly, pure solutions where each site has the same n. Secondly, alternating solutions where in a particular direction planes alternate between two distinct values of n. Thirdly, tetrahedral solutions with alternating tetrahedra alternating between two distinct values of n. Fourthly, period-four solutions where one plane in four has a distinct value of n.

A second set of solutions may be obtained from z_0=-$\frac{\pi}{6}$ where now the pairs $\{1,\bar{2}\}$ $\{2,\bar{3}\}$ and $\{3,\bar{1}\}$ correspond to reversed spins. Clearly by employing symmetry there are a mass of rotation and translationally associated analogues to the possible states. Investigations of these states demonstrate that in fact there are only two classes unrelated by symmetry, which we can choose to be the z_0=$\frac{\pi}{2}$ states. The first class of solution is coplanar, while the second fully three-dimensional.

In the triangular Heisenberg ferromagnet, we find solutions that cannot be rotated into each other, but do have reflection analogues. This is not the case with our two classes of spin configurations. While the antiferromagnetic Heisenberg model on a triangular lattice has the two chiral solutions that are not rotationally or translationally related, they can be

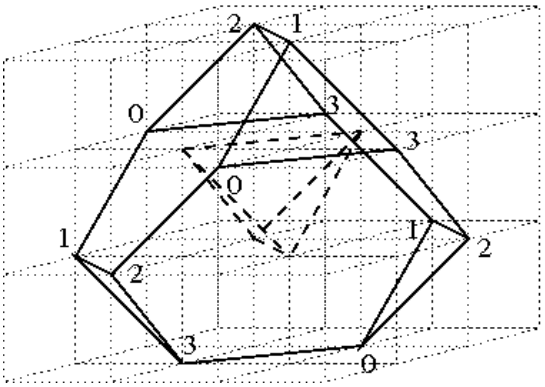

Figure 9.7: Cage of gadolinium atoms surrounding a tetrahedron of titanium atoms.

reflected onto each other. In our case, our two styles of solution have no obvious symmetry between them and so can be considered topologically distinct.

9.3.2 The Next-Nearest Neighbour Heisenberg Interactions

There are two natural interactions that could lift the degeneracy the antiferromagnetic Heisenberg model on a tetrahedron provides. The first we will discuss is in some sense the most natural. This is extending the interaction to next-nearest neighbours.

The actual additional Heisenberg interactions probably stem from pathways across titanium atoms, since the hopping matrix elements are so much larger. The cage of atoms depicted in figure 9.7 are all expected to develop Heisenberg interactions of various strengths. The bonds between members of the same sublattice should be largest. We employ two new matrix elements for the additional Heisenberg interactions across the hexagons depicted in figure 9.7, which we use λ for diametric and $\kappa\lambda$ for the remaining interactions. The structure factor is determined by the matrix

$$\Gamma_{\mathbf{k}} = \begin{bmatrix} \lambda\left(4xyz-1\right) & X+2\lambda\kappa x c_1 & Y+2\lambda\kappa y c_2 & Z+2\lambda\kappa z c_3 \\ X+2\lambda\kappa x c_1 & \lambda\left(4xYZ-1\right) & z+2\lambda\kappa Z c_3 & y+2\lambda\kappa Y c_2 \\ Y+2\lambda\kappa y c_2 & z+2\lambda\kappa Z c_3 & \lambda\left(4XyZ-1\right) & x+2\lambda\kappa X c_1 \\ Z+2\lambda\kappa z c_3 & y+2\lambda\kappa Y c_2 & x+2\lambda\kappa X c_1 & \lambda\left(4XYz-1\right) \end{bmatrix} \tag{9.35}$$

with,

$$x = \cos\frac{k_y - k_z}{2} \quad y = \cos\frac{k_z - k_x}{2} \quad z = \cos\frac{k_x - k_y}{2} \tag{9.36}$$

$$X = \cos\frac{k_y + k_z}{2} \quad Y = \cos\frac{k_z + k_x}{2} \quad Z = \cos\frac{k_x + k_y}{2} \tag{9.37}$$

$$c_1 = \cos k_x \quad c_2 = \cos k_y \quad c_3 = \cos k_z \tag{9.38}$$

as the associated parameterisation. In the absence of perturbations, this structure factor has two degenerate bands at $\Gamma = -1$ which control the spin degeneracy. We treat the additional perturbations as small and solve for the lifting of this degeneracy in the two degenerate bands. Employing the parameter ϵ to control the eigenvalues:

$$\Gamma = -1 - \lambda - 2\lambda\epsilon, \tag{9.39}$$

we find that the perturbed structure factor satisfies

$$(1-a_2)\epsilon^2 - 2\big(a_2[1+4\kappa] + 3a_2^2 - a_1[3a_1+a_3][1+\kappa]\big)\epsilon + 3a_2^2[4\kappa^2-1] - a_3[a_3+2a_1][1+\kappa]^2 + 9a_1^2a_2[1-\kappa^2] + 6a_1a_2a_3[1 \tag{9.40}$$

in terms of

$$a_1 = \frac{c_1 + c_2 + c_3}{3} \quad a_2 = \frac{c_2c_3 + c_3c_1 + c_1c_2}{3} \quad a_3 = c_1c_2c_3. \tag{9.41}$$

The ground-state is a function of κ, and involves a solution of the form

$$c_1 = c_2 = -\cos\theta \quad c_3 = 1. \tag{9.42}$$

This describes a spiral that starts out with $\theta = \frac{\pi}{3}$ when $\kappa = 0$ and ends up at the experimental $\theta = \frac{\pi}{2}$ with the unphysical value of $\kappa = 1$.

We conclude from this that the second-nearest-neighbour Heisenberg interactions are not sufficient to describe the physics, and that the zone-centre state has a very poor energy. We

have to discuss dipolar interactions to explain the experimentally observed phases.

9.3.3 The Dipolar Interaction

We now discuss the dipolar interaction, which has been discussed in the context of pyrochlore antiferromagnetism [29]. We note that the transition is observed around 0.7 K, and the dipolar interaction takes place at an energy scale around 1 K, and so it seems plausible that the dipolar interactions will be relevant to modelling the material, and could lift the degeneracy of the Heisenberg model.

Dipolar interactions take the generic form

$$\hat{H} = \frac{\mathbf{S}_\alpha.\mathbf{S}_\beta - 3\mathbf{S}_\alpha.\hat{\mathbf{r}}_{\alpha\beta}\hat{\mathbf{r}}_{\alpha\beta}.\mathbf{S}_\beta}{\mid \mathbf{r}_{\alpha\beta} \mid^3} \tag{9.43}$$

where $\mathbf{r}_{\alpha\beta} \equiv \mathbf{r}_\alpha - \mathbf{r}_\beta$ is a vector connecting the two interacting spins. This interaction is mathematically taxing because it is both long-range and it relates the spin orientation to the lattice directions which breaks spin isotropy.

We will extract the initial isotropic Heisenberg interactions which only renormalises the existing exchange-based interactions and focus only on the second term. This second term we will further restrict to nearest-neighbours

$$\hat{H} = -3\sum_{\alpha>\beta} \mathbf{S}_\alpha.\hat{\mathbf{r}}_{\alpha\beta}\hat{\mathbf{r}}_{\alpha\beta}.\mathbf{S}_\beta. \tag{9.44}$$

Solving this rescaled dipolar interaction on a single tetrahedron, we find five styles of solution at energies $\{-\frac{3}{2}(1+\sqrt{17}), -3, 3, \frac{3}{2}(\sqrt{17}-1), 12\}$. The ground-state has 86.4% of its moments parallel. It is consequently a high energy state if the nearest-neighbour Heisenberg interaction dominates. The next state is triply degenerate, and since it has zero , it is compatible with the nearest-neighbour Heisenberg interaction. The third state is doubly degenerate, and also has zero total-spin. The fourth state is not compatible as it has 13.6% of its moments

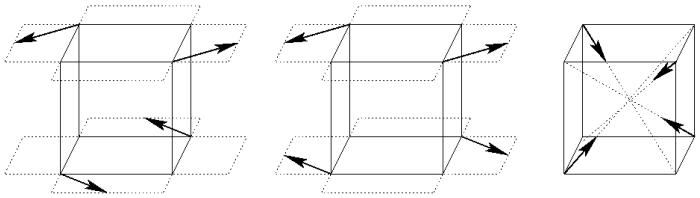

Figure 9.8: Total-spin zero eigenstates of the short-range dipolar model, in order of energy.

parallel. Finally the fifth state also has zero total-spin. The three compatible styles of states are depicted in figure 9.8 The crucial observation is that the two low energy states involve spins which are perpendicular to the natural crystallographic directions pointing towards the center of the tetrahedra, and thus the spins are in the planes indicated by the Mössbauer experiments.

The planar spin restrictions deduced from the Mössbauer experiments can be derived from the nearest-neighbour dipolar interactions subjected to dominant nearest-neighbour Heisenberg interactions. Enforcing equal length spins and including the Heisenberg constraints, we may rewrite the dipolar interactions, Eq.(9.44), as

$$\begin{aligned}\hat{H} = \frac{3}{4}\big[&(S_0^x + S_0^y + S_0^z)^2 + (S_1^x - S_1^y - S_1^z)^2 \\ &+(-S_2^x + S_2^y - S_2^z)^2 + (-S_3^x - S_3^y + S_3^z)^2\big] \\ +\frac{3}{8}\big[&(S_0^x + S_1^x - S_2^x - S_3^x)^2 \\ &+(S_0^y - S_1^y + S_2^y - S_3^y)^2 \\ &+(S_0^z - S_1^z - S_2^z + S_3^z)^2\big]\ . \end{aligned} \tag{9.45}$$

We can minimise by zeroing each of the seven quadratics, using reality of the spins. This is consistent and indeed uniquely specifies the three states shown in figure 9.13. In particular

we note that the first four quadratics may be represented by

$$[\mathbf{S}_0.(1,1,1))]^2 \qquad [\mathbf{S}_1.(1,-1,-1)]^2$$
$$[\mathbf{S}_2.(-1,1,-1)]^2 \qquad [\mathbf{S}_3.(-1,-1,1)]^2 \ . \tag{9.46}$$

Orienting the four spins perpendicular to their local crystallographic directions therefore partially minimises the local dipolar energy.

9.4 Bragg Spots

One crucial experimental observation relates to the relative intensities of the Bragg spots in the elastic neutron scattering experiments. The internal structure of our proposed states can be probed by measuring the relative intensities of the different magnetic Bragg spots. The itensities of the Bragg spots nearest the origin are directly related to the magnetic moments on each of the four underlying sublattices

$$\mathbf{B}_0 = \mathbf{S}_0 + \mathbf{S}_1 + \mathbf{S}_2 + \mathbf{S}_3 \qquad \mathbf{B}_1 = \mathbf{S}_4 + \mathbf{S}_5 + \mathbf{S}_6 + \mathbf{S}_7 \tag{9.47}$$

$$\mathbf{B}_2 = \mathbf{S}_8 + \mathbf{S}_9 + \mathbf{S}_{10} + \mathbf{S}_{11} \qquad \mathbf{B}_3 = \mathbf{S}_{12} + \mathbf{S}_{13} + \mathbf{S}_{14} + \mathbf{S}_{15}$$

and in all our states these quantities vanish, by requirement that $\mathbf{S}_0 + \mathbf{S}_1 + \mathbf{S}_2 + \mathbf{S}_3 = 0$.

The actual $\left(\frac{1}{2}, \frac{1}{2}, \frac{1}{2}\right)$ Bragg spot, and its symmetrically equivalent neighbours form alternating Kagome planes and a sparse triangular lattice. The phase within such a plane it kept uniform and the phase alternates between neighbouring *equivalent* geometries. Interestingly, our antiferromagnetic ansatz directly *controls* this character. The Kagome planes may be decomposed into two inversion related sets of triangles, as depicted in Fig.9.9. One set corresponds to a set of triangular faces of tetrahedra which are completed above the plane and the other form a set of corresponding tetrahedra which are completed below the plane.

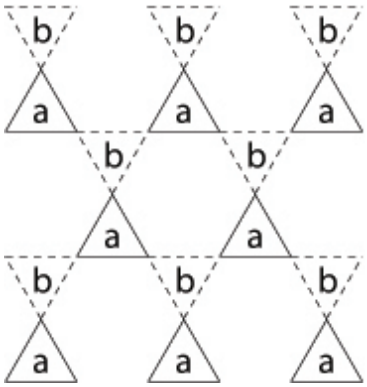

Figure 9.9: Kagome plane decomposed into the two inversion related triangles. The **a** denote atoms that complete tetrahedra above and the **b** denote atoms that complete tetrahedra below.

These atoms form the aforementioned neighbouring sparse triangular planes.

The constraint that each tetrahedron has zero total spin that we impose then enforces the total spin in a Kagome plane to be antiparallel to both of the neighbouring triangular planes. The relationship that neighbouring triangular planes should be antiparallel then enforces that the total spin in each Kagome plane must vanish and consequently that the associated Bragg spots must vanish.

Physically, the argument only depends on the nearest-neighbour Heisenberg interactions in that each tetrahedron should have vanishing total spin. The Kagome argument of Fig.9.9 then provides that the total spin of each neighbouring plane along the (1,1,1) direction and it analogues be antiparallel. Since the relevant Bragg spots add every second plane with an alternating sign, the appearance of such a Bragg spot is inconsistent with the nearest-neighbour Heisenberg interaction. We have imposed the additional constraint that our solutions have the observed magnetic periodicity and this additionally requires that the total-spin of each plane vanishes.

The Bragg spot at $\left(\frac{1}{2},\frac{1}{2},\frac{1}{2}\right)$ is likely to be experimentally important, and work is being performed to relax the constraint that the spins should lie in the anisotropy planes so strictly, but at least be as close as can be to them so that the Bragg spot at $\left(\frac{1}{2},\frac{1}{2},\frac{1}{2}\right)$ is present in

our modelling.

9.5 Conclusions

Taking the above into account, we can make a prediction of the magnetic structure of $Gd_2Ti_2O_7$. The actual spin arrangment is quite difficult to depict, and so we draw one-half of the magnetic cell for coplanar spins in figure 9.10, and for non-coplanar spins in figure 9.11

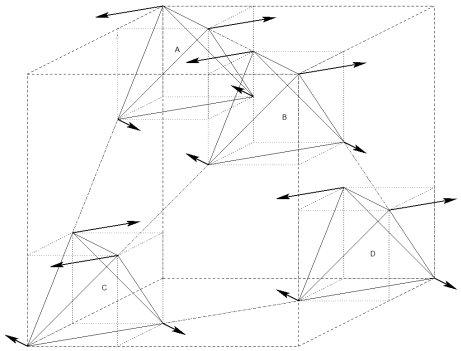

Figure 9.10: Our prediction of the magnetic structure of $Gd_2Ti_2O_7$ for Coplanar Spins. The remainder of the lattice is difficult to depict. The basic principle is that there is periodicity of reflected spins. Continuing the patten in the positive x-direction, if we rotate the cell about the z-axis, we find the tetrahedron labelled B will be the tetrhedon labelled A for a different cell. Similarly, the D tetrahedron will be a C tetrahedron for a different cell, and not the same one as the one the B tetrahedron is mapped into. If we then reverse the spins after the rotation, we will have the magnetic structure of the translated cell. This works similarly for the other cartesian directions.

We may be tempted to be satisfied with the interpretation that the material is goverened by strong nearest-neighbour antiferromagnetic Heisenberg interactions with weaker nearest-neighbour dipolar interactions. This would be premature, however. The state predicted by these two interactions is *not* the experimentally observed state. We therefore have to provide some argument for this.

The dipolar interaction takes place on an energy scale similar to the observed transition temperature, and so it is likely that it is relevant to the modelling of $Gd_2Ti_2O_7$. However,

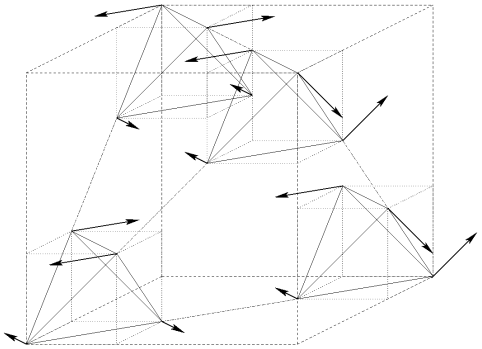

Figure 9.11: Our prediction of the magnetic structure of $Gd_2Ti_2O_7$ for Non-Coplanar Spins. The translations are as in 9.10

it does not lift the degeneracy of the Heisenberg antiferromagnetism. Our calculations are inconsistent with predictions of other theoretical studies performed by Palmer and Chalker [29].

We have found a set of solutions based on some well-grounded assumptions, and the local dipolar energy is much worse than the $\mathbf{q} = \mathbf{0}$ solution that is expected from the calculations of Palmer and Chalker. The motivation behind their calculation was the lifting of a degeneracy that remained when the dipolar interaction was included, essentially exactly in the classical limit at zero temperature. In our calculations we ought to have found a solution that was degenerate with the $\mathbf{q} = \mathbf{0}$ solution.

The states with spins of different average lengths require fluctuations to explain the reduction in lengths, either thermal or quantum in nature. At low temperature, the entropy measurements indicate that thermal fluctuations are irrelevant and so we are left solely with quantum fluctuations. This is a possible explanation, because quantum fluctuations gain energy by making spins locally antiparallel in directions perpendicular to the classical order. They do not require any entropy, as they amount to a particular phase for the fluctuation and not a random one.

There are various possible resolutions to the inconsistencies. Firstly, we have restricted our calculations to states which are perpendicular to the crystal directions and this eliminates

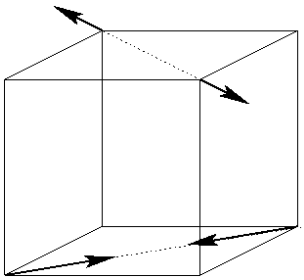

Figure 9.12: Possible spin configuration ignored so far.

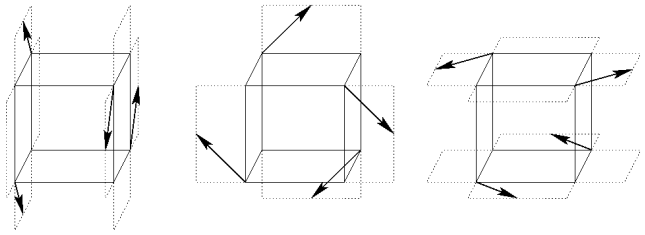

Figure 9.13: Local dipolar ground-states when total-spin of tetrahedron vanishes.

two additional zero total-spin states from our optimisation. One is the state with spins pointing to the centre of the cube and the other is the state depicted in figure 9.12. These states, however, are of higher energy than the ground-state. Use of these additional states, therefore, cannot lift us to the energy of the $\mathbf{q} = \mathbf{0}$ solution. We can exactly solve the problem of dominant nearest-neighbour Heisenberg and local dipolar interactions. Thus, we are restricted to the states depicted in figure 9.13. These states, which are in the perpendicular subspace, constitute three of the possible configurations in figure 9.8.

For the case $z_0 = 0$ they are the three configurations with $\{n, n, \bar{n}, \bar{n}\}$, and we can only construct $\mathbf{q}$=$\mathbf{0}$ solutions from these configurations Secondly, we have only considered the local dipolar interaction and the longer-range contributions could overturn our argument. Although the dipolar interaction is long-range, the divergence is irrelevant and we do not anticipate issues here. Thirdly there might be a loop-hole in the previous theoretical arguments. The previous calculations for the Heisenberg and dipolar interactions combined calculated the effective structure factor for the classical magnetic problem, but they did not proceed on to provide an actual magnetic solution.

It was presumed that an appropriate magnetic solution would exist. Unfortunately, this is not guaranteed. For classical magnetism there are additional constraints in that the magnitude of the spin of each atom on each sublattice must independently be normalised. For Heisenberg-like exchange models there is always an elementary spiral that will provide a solution. In this dipolar problem, however, one needs to make a multiple-q state involving all four appropriate q's, and unfortunately we only live in three dimensions. It would appear that solving the dipolar problem is harder than first imagined.

Chapter 10

A Conjectured Improvement to Mean-Field Theory for Strongly Correlated Systems

10.1 Introduction

We now move on to discuss the concept of a non-linear fermionic transformation. We do this in the hope that it will make our mean-field approximation to hamiltonians containing quartic terms where strong correlations are present which provide constraints to fermions occupying the same lattice site. The methods will apply to Hamiltonians containing different styles of fermion. For example, the Anderson lattice contains the strongly correlated f-electrons, and the conduction electrons. Further, there ought to be some connection between the two subspaces of fermions. This is achieved by hybridisation in the Anderson lattice.

We consider the Anderson lattice, and apply the non-linear transformation that we will construct to it. Then, we will project out one of the fermionic species. This is equivalent to the infinite U limit of the Anderson lattice, but it will allow us to handle this limit in a much more controllable manner than, for example, the slave boson method and dynamic mean-field theory.

We aim to find an effective Hubbard model by constructing a transformation of the

fermionic operators in the Anderson lattice Hamiltonian. The Anderson lattice Hamiltonian is given by

$$\mathcal{H} = -t \sum_{\langle jj' \rangle \sigma} c^{\dagger}_{j\sigma} c_{j'\sigma} + V \sum_{j\sigma} (f^{\dagger}_{j\sigma} c_{j\sigma} + \text{h.c}) + E \sum_{j\sigma} f^{\dagger}_{j\sigma} f_{j\sigma} + U \sum_{j} f^{\dagger}_{j\uparrow} f_{j\uparrow} f^{\dagger}_{j\downarrow} f_{j\downarrow}. \tag{10.1}$$

We wish to work with the limit in which U goes to infinity in the Anderson lattice. This means in practice that we have to project out all doubly occupied sites, so that two f-electrons cannot be present on the same site.

We have 16 basis states that we will need to work with. Our plan is to change the c and f basis into a new basis, which we will call d and g. We will then perform mean-field theory on this new Hamiltonian. However, we will argue that having two g fermions present will correspond to having two f electrons present. In mean-field theory, it is inevitable that if one type of particle makes itself present, then we will eventually have two types of the same particle present on the same site. Therefore, if we have one g-fermion present, then eventually we will have another on the same site, and going back to the original basis, this means we will have two f-electrons on the same site. This is precisely the thing we wish to forbid. Hence, we will have to project out all the g degrees of freedom in our transformed Hamiltonian if we wish to use a mean-field analysis of the model under the required limit.

After performing this projection, we will have an effective Hubbard model consisting of these new d fermions. It is this Hamiltonian on which we will perform mean field theory.

10.2 The Non-Linear Basis

We now move to construct the new basis of states in terms of d and g fermions. We require that the vacuum in the f and c basis should be mapped onto the vacuum in the d and g basis, and so

$$|0\rangle_{dg} = |0\rangle_{fc}. \tag{10.2}$$

These vacua are equivalent and we shall drop the labels that distinguish them. For the single particle states, we require f and c to be composed of a mix of d and g electrons, as mean-field theory creates a mixture of electron species. We are thus led to

$$c_\sigma^\dagger|0\rangle = \left(\sin\theta_1 d_\sigma^\dagger + \cos\theta_1 g_\sigma^\dagger\right)|0\rangle \tag{10.3}$$

$$f_\sigma^\dagger|0\rangle = \left(\cos\theta_1 d_\sigma^\dagger - \sin\theta_1 g_\sigma^\dagger\right)|0\rangle \tag{10.4}$$

The two-particle states are the states that we should take more care with. We wish to prevent double occupation of an f electron state. We wish to map singlets to singlets and triplets to triplets. Clearly the $f_\sigma^\dagger f_\sigma^\dagger|0\rangle$ state is of the most importance, since we wish to project out the g fermions from the new basis, so it seems most sensible to choose

$$f_\sigma^\dagger f_{\bar{\sigma}}^\dagger|0\rangle = g_\sigma^\dagger g_{\bar{\sigma}}^\dagger|0\rangle. \tag{10.5}$$

and the analogous state for the conduction electrons is

$$c_\sigma^\dagger c_\sigma^\dagger|0\rangle = \left[\frac{\cos\phi}{\sqrt{2}}\left(d_\sigma^\dagger g_{\bar{\sigma}}^\dagger + g_\sigma^\dagger d_\sigma^\dagger\right) + \sin\phi d_\sigma^\dagger d_{\bar{\sigma}}^\dagger\right]|0\rangle. \tag{10.6}$$

The remaining singlet is then given by

$$\frac{1}{\sqrt{2}}\left(f_\sigma^\dagger c_{\bar{\sigma}}^\dagger + c_\sigma^\dagger f_{\bar{\sigma}}^\dagger\right)|0\rangle = \left[-\frac{\sin\phi}{\sqrt{2}}\left(d_\sigma^\dagger g_{\bar{\sigma}}^\dagger + g_\sigma^\dagger d_{\bar{\sigma}}^\dagger\right) + \cos\phi d_\sigma^\dagger d_{\bar{\sigma}}^\dagger\right]|0\rangle. \tag{10.7}$$

$$f_\sigma^\dagger c_\sigma^\dagger = d_\sigma^\dagger g_\sigma^\dagger. \tag{10.8}$$

$$\frac{1}{\sqrt{2}}\left(f_\sigma^\dagger c_{\bar{\sigma}}^\dagger - c_\sigma^\dagger f_{\bar{\sigma}}^\dagger\right) = \frac{1}{\sqrt{2}}\left(d_\sigma^\dagger g_{\bar{\sigma}}^\dagger - g_\sigma^\dagger d_{\bar{\sigma}}^\dagger\right) \tag{10.9}$$

We now work backwards, and work with the four particle states. This is simples, as there

is only one choice

$$f_\sigma^\dagger f_{\bar{\sigma}}^\dagger c_\sigma^\dagger c_{\bar{\sigma}}^\dagger |0\rangle = d_\sigma^\dagger d_{\bar{\sigma}}^\dagger g_\sigma^\dagger g_{\bar{\sigma}}^\dagger |0\rangle \tag{10.10}$$

Finally, we work with the three-particle states in terms of the four-particle states in an analogous way to working with the one-particle states in terms of the vacuum. That is, we call the four-particle state $|F>$, and consider $d_\sigma|F>$ and $g_\sigma|F>$ as operators that create a hole. We then mix these holes as we did for the single-particle states, but we use a different mixing angle.

$$f_\sigma^\dagger f_{\bar{\sigma}}^\dagger c_{\bar{\sigma}}^\dagger = \left(\cos\theta_2 f_\sigma^\dagger f_{\bar{\sigma}}^\dagger c_\sigma^\dagger c_{\bar{\sigma}}^\dagger + f_\sigma^\dagger f_{\bar{\sigma}}^\dagger c_\sigma^\dagger c_{\bar{\sigma}}^\dagger\right)|0\rangle \tag{10.11}$$

$$f_{\bar{\sigma}}^\dagger c_\sigma^\dagger c_{\bar{\sigma}}^\dagger = \left(\sin\theta_2 d_\sigma^\dagger d_{\bar{\sigma}}^\dagger g_{\bar{\sigma}}^\dagger + \cos\theta_2 d_{\bar{\sigma}}^\dagger g_\sigma^\dagger g_{\bar{\sigma}}^\dagger\right)|0\rangle \tag{10.12}$$

We will calculate the action of $f_\sigma^\dagger$ and $c_\sigma^\dagger$ on each of the d and g basis vectors, and hence the f and c operators in the d and g basis. The basis states are summarised in tables 10.1 and 10.2.

In this section and the following, we will calculate the action of $f_\sigma^\dagger$ and $c_\sigma^\dagger$ on each of the new basis vectors, and hence the operators themselves in the new basis.

We also need the inverted basis to calculate what the operators should transform to in the Anderson lattice Hamiltonian.

We could calculate the basis vectors d and g in the f and c basis, and indeed we have done. However, using this raw form of the operator is both complicated and not useful. Indeed, the Anderson lattice is far more complicated in this basis. Since our aim is instead to prevent double occupation of an f-site, we must project away the g electrons, and so we will project away any g-electon creation operators from the basis defined above.

State in f and c Basis	State in d and g Basis
$\|0\rangle$	$\|0\rangle$
$d_\sigma^\dagger\|0\rangle$	$\left(\cos\theta_1 d_\sigma^\dagger + \sin\theta_1 g_\sigma^\dagger\right)\|0\rangle$
$g_\sigma^\dagger\|0\rangle$	$\left(-\sin\theta_1 d_\sigma^\dagger + \cos\theta_1 g_\sigma^\dagger\right)\|0\rangle$
$d_\sigma^\dagger d_{\bar\sigma}^\dagger\|0\rangle$	$\left(\frac{\cos\phi}{\sqrt{2}}(f_\sigma^\dagger c_{\bar\sigma}^\dagger + c_\sigma^\dagger f_{\bar\sigma}^\dagger + \sin\phi c_\sigma^\dagger c_{\bar\sigma}^\dagger\right)\|0\rangle$
$g_\sigma^\dagger g_{\bar\sigma}^\dagger\|0\rangle$	$f_\sigma^\dagger f_{\bar\sigma}^\dagger\|0\rangle$
$d_\sigma^\dagger g_{\bar\sigma}^\dagger\|0\rangle$	$f_\sigma^\dagger c_{\bar\sigma}^\dagger\|0\rangle$
$\frac{1}{\sqrt{2}}\left(d_\sigma^\dagger g_{\bar\sigma}^\dagger + g_\sigma^\dagger d_{\bar\sigma}^\dagger\right)\|0\rangle$	$\left(-\frac{\sin\phi}{2}(f_\sigma^\dagger c_{\bar\sigma}^\dagger + c_\sigma^\dagger f_{\bar\sigma}^\dagger + \cos\phi c_\sigma^\dagger c_{\bar\sigma}^\dagger\right)\|0\rangle$
$\frac{1}{\sqrt{2}}\left(d_\sigma^\dagger g_{\bar\sigma}^\dagger - g_\sigma^\dagger d_{\bar\sigma}^\dagger\right)\|0\rangle$	$\frac{1}{\sqrt{2}}\left(f_\sigma^\dagger c_{\bar\sigma}^\dagger - c_\sigma^\dagger f_{\bar\sigma}^\dagger\right)\|0\rangle$
$d_\sigma^\dagger d_{\bar\sigma}^\dagger g_\sigma^\dagger g_{\bar\sigma}^\dagger\|0\rangle$	$f_\sigma^\dagger f_{\bar\sigma}^\dagger c_\sigma^\dagger c_{\bar\sigma}^\dagger\|0\rangle$
$d_{\bar\sigma}^\dagger g_\sigma^\dagger g_{\bar\sigma}^\dagger\|0\rangle$	$\left(\cos\theta_2 f_\sigma^\dagger f_{\bar\sigma}^\dagger c_\sigma^\dagger c_{\bar\sigma}^\dagger + f_\sigma^\dagger f_{\bar\sigma}^\dagger c_\sigma^\dagger c_{\bar\sigma}^\dagger\right)\|0\rangle$
$d_\sigma^\dagger d_{\bar\sigma}^\dagger g_{\bar\sigma}^\dagger\|0\rangle$	$\left(f_\sigma^\dagger f_{\bar\sigma}^\dagger c_\sigma^\dagger c_{\bar\sigma}^\dagger + f_\sigma^\dagger f_{\bar\sigma}^\dagger c_\sigma^\dagger c_{\bar\sigma}^\dagger\right)\|0\rangle$

Table 10.1: f basis states in d and g Basis

10.3 Two-Particle Projected Basis

In constructing this Hamiltonian, it is unnecessary, and indeed unhelpful to work with the full range of states. If we included all states in the transformed basis, the periodic Anderson model will be far more complicated than when we started. We will restrict our attention to only the two particle states containing no g electrons. This will allow us to control the projection of double occupancy. We will denote this projection operator by P_g.

After taking the restrictions we desire into account, we are left with only four states:

$$|0\rangle = |0\rangle \tag{10.13}$$

$$d_\sigma^\dagger|0\rangle = \left(\cos\theta_1 f_\sigma^\dagger + \sin\theta_1 c_\sigma^\dagger\right)|0\rangle \tag{10.14}$$

$$d_\sigma^\dagger d_{\bar\sigma}^\dagger|0\rangle = \left(\frac{\cos\phi}{\sqrt{2}}(f_\sigma^\dagger c_{\bar\sigma}^\dagger + c_\sigma^\dagger f_{\bar\sigma}^\dagger) + \sin\phi c_\sigma^\dagger c_{\bar\sigma}^\dagger\right)|0\rangle \tag{10.15}$$

These are included in the non-linearly transformed basis, but since we are now projecting out states involving the g-electrons. The basis of f and c thus is very different, and is not

State in d and g Basis	State in f and c Basis
$\|0\rangle$	$\|0\rangle$
$f_\sigma^\dagger \|0\rangle$	$\left(\cos\theta_1 d_\sigma^\dagger - \sin\theta_1 g_\sigma^\dagger\right)\|0\rangle$
$c_\sigma^\dagger \|0\rangle$	$\left(\sin\theta_1 d_\sigma^\dagger + \cos\theta_1 g_\sigma^\dagger\right)\|0\rangle$
$f_\sigma^\dagger f_{\bar\sigma}^\dagger \|0\rangle$	$g_\sigma^\dagger g_{\bar\sigma}^\dagger \|0\rangle$
$c_\sigma^\dagger c_{\bar\sigma}^\dagger \|0\rangle$	$\left(\frac{\cos\phi}{\sqrt{2}}(d_\sigma^\dagger g_{\bar\sigma}^\dagger + g_\sigma^\dagger d_{\bar\sigma}^\dagger - \sin\phi d_\sigma^\dagger d_{\bar\sigma}^\dagger\right)\|0\rangle$
$f_\sigma^\dagger c_\sigma^\dagger \|0\rangle$	$d_\sigma^\dagger g_\sigma^\dagger \|0\rangle$
$\frac{1}{\sqrt{2}}\left(d_\sigma^\dagger g_{\bar\sigma}^\dagger + g_\sigma^\dagger d_{\bar\sigma}^\dagger\right)\|0\rangle$	$\left(\frac{\sin\phi}{\sqrt{2}}(d_\sigma^\dagger g_{\bar\sigma}^\dagger + g_\sigma^\dagger d_{\bar\sigma}^\dagger + \cos\phi d_\sigma^\dagger d_{\bar\sigma}^\dagger\right)\|0\rangle$
$\frac{1}{\sqrt{2}}\left(d_\sigma^\dagger g_{\bar\sigma}^\dagger - g_\sigma^\dagger d_{\bar\sigma}^\dagger\right)\|0\rangle$	$\frac{1}{\sqrt{2}}\left(f_\sigma^\dagger c_{\bar\sigma}^\dagger - c_\sigma^\dagger f_{\bar\sigma}^\dagger\right)\|0\rangle$
$f_\sigma^\dagger f_{\bar\sigma}^\dagger c_\sigma^\dagger c_{\bar\sigma}^\dagger \|0\rangle$	$d_\sigma^\dagger d_{\bar\sigma}^\dagger g_\sigma^\dagger g_{\bar\sigma}^\dagger \|0\rangle$
$f_{\bar\sigma}^\dagger c_\sigma^\dagger c_{\bar\sigma}^\dagger \|0\rangle$	$\left(\cos\theta_2 d_\sigma^\dagger d_{\bar\sigma}^\dagger g_{\bar\sigma}^\dagger - \sin\theta_2 d_{\bar\sigma}^\dagger g_\sigma^\dagger g_{\bar\sigma}^\dagger\right)\|0\rangle$
$f_\sigma^\dagger f_{\bar\sigma}^\dagger c_{\bar\sigma}^\dagger \|0\rangle$	$\left(\sin\theta_2 d_\sigma^\dagger d_{\bar\sigma}^\dagger g_{\bar\sigma}^\dagger + \cos\theta_2 d_{\bar\sigma}^\dagger g_\sigma^\dagger g_{\bar\sigma}^\dagger\right)\|0\rangle$

Table 10.2: f basis states in d and g Basis

an inverse of the d and g basis. This basis takes the form

$$P_g|0\rangle = |0\rangle \tag{10.16}$$

$$P_g f_\sigma^\dagger|0\rangle = \cos\theta d_\sigma^\dagger|0\rangle \tag{10.17}$$

$$P_g c_\sigma^\dagger|0\rangle = \sin\theta d_\sigma^\dagger|0\rangle \tag{10.18}$$

$$P_g c_\sigma^\dagger c_{\bar\sigma}^\dagger|0\rangle = \sin\phi d_\sigma^\dagger d_\sigma^\dagger|0\rangle \tag{10.19}$$

$$P_g(\frac{1}{\sqrt{2}}\left(f_\sigma^\dagger c_{\bar\sigma}^\dagger + c_\sigma^\dagger f_{\bar\sigma}^\dagger\right)|0\rangle = \cos\phi d_\sigma^\dagger d_\sigma^\dagger|0\rangle \tag{10.20}$$

This reflects the fact that we have performed a projection, and so it is impossible for the invertibility to remain intact.

10.4 Effective Hubbard Description of the Anderson Lattice

We have the d and g operators in a two-particle projected basis, as calculated in the previous chapter. We will now insert them into the Anderson lattice Hamiltonian to generate a

Hubbard description of the Anderson lattice. Inserting these operators into the Anderson lattice, we find

$$\mathcal{H} = -t' \sum_{<jj'>\sigma} \left(1 - \alpha d^\dagger_{j\sigma} d_{j\sigma}\right) d^\dagger_{j\sigma} d_{j'\sigma} \left(1 - \alpha d^\dagger_{j'\sigma} d_{j'\sigma}\right) + \epsilon' \sum_{j\sigma} d^\dagger_{j\sigma} d_{j\sigma} + U' \sum_j d^\dagger_{j\uparrow} d_{j\uparrow} d^\dagger_{j\downarrow} d_{j\downarrow} \tag{10.21}$$

The parameters depends on the angles θ and ϕ, and are related to the parameters of the Anderson lattice by

$$t' = t \sin^2\theta \tag{10.22}$$

$$\epsilon' = \epsilon \cos^2\theta + 2V \cos\theta \sin\theta \tag{10.23}$$

$$U' = \epsilon \left(\frac{\cos^2\phi}{\sqrt{2}} - \cos^2\theta\right) + 2V \left(\frac{\cos\phi \sin\phi}{2} - \cos\theta \sin\theta\right) \tag{10.24}$$

We now have an effective Hubbard model description of the Anderson Lattice model. Unfortunately, this is still an intractable model, and so we must once again resort to mean-field approximations. There are some differences between this Hubbard model, and the customary Hubbard model.

10.5 Mean-Field Theory of the Effective Hubbard Description

We now perform a mean-field analysis of the effective hubbard model derived above. We will first perform a mean-field analysis with a paramagnetic background, and compare it to the mean-field analysis we performed on the Anderson lattice. The paramagnetic background allows us to decompose the correlations by spin.

We now have two sets of terms that we must find expectation values for. We have now

terms in t' as well as U'. Let

$$\alpha = 1 - \left(\frac{\cos\phi \cos\theta}{\sqrt{2}\sin\theta} + \sin\phi \right) \tag{10.25}$$

We have

$$< \left(1 - \alpha d^{\dagger}_{j\bar{\sigma}} d_{j\bar{\sigma}}\right) d^{\dagger}_{j\sigma} d_{j'\sigma} \left(1 - \alpha d^{\dagger}_{j'\bar{\sigma}} d_{j'\bar{\sigma}}\right) = n_1((1-\alpha n_0)^2 - \alpha^2 n_1^2). \tag{10.26}$$

We assume inversion symmetry, and so we have

$$n_1 =< d^{\dagger}_{j\sigma} d^{\dagger}_{j'\sigma} >=< d^{\dagger}_{j'\sigma} d^{\dagger}_{j\sigma} > \tag{10.27}$$

For the expectation value of the term in U', for now we simply decorrelate the spins to obtain

$$< d^{\dagger}_{j\sigma} d_{j\sigma} d^{\dagger}_{j\bar{\sigma}} d_{j\bar{\sigma}} >=< d^{\dagger}_{j\sigma} d_{j\sigma} >< d^{\dagger}_{j\bar{\sigma}} d_{j\bar{\sigma}} > \tag{10.28}$$

Our mean-field Hamiltonian then takes the form

$$\begin{aligned} \mathcal{H}_{MF} &= -t^{'} \sum_{<jj'>\sigma} \left(2(1-\alpha n_0)^2 + 2n_1\alpha^2\right) d^{\dagger}_{j\sigma} d_{j'\sigma} \\ &+ \sum_{j\sigma} (\epsilon^{'} + U^{'} n_0 - 2n_1\alpha(1-\alpha n_0)) d^{\dagger}_{j\sigma} d_{j\sigma} \end{aligned} \tag{10.29}$$

We can diagonalise this with the usual Bloch transform, and our diagonalised mean-field Hamiltonian is then

$$\begin{aligned} \mathcal{H}_{MF} &= \sum_{k\sigma} (-t^{'}(2(1-\alpha n_0)^2 + 2n_1\alpha^2)\gamma_k - 2n_1\alpha(1-\alpha n_0) \\ &- 2n_1\alpha(1-\alpha n_0) + \epsilon^{'} + U^{'}) d^{\dagger}_{k\sigma} d_{k\sigma} \end{aligned} \tag{10.30}$$

We can then simply optimise over θ and ϕ to solve this Hamiltonian. This can be done only numerically, and unfortunately has not been completed for the submission of this thesis. The Stoner criterion is analogue to the simple case of the Hubbard model we computed in section 5.4. However, to obtain results, we do need to optimise over θ and ϕ first.

We illustrate some problems we are aware of in the next section, make some predictions based on work that has been completed at least in part, and suggest some improvements to the work carried out in this chapter.

10.6 Further Work

Aside from the optimisations we have to make over θ and ϕ for the paramagnetic mean-field theory, we can also decompose the correlation function to include superconducting correlations.

We anticipate superconductivity in the Anderson lattice model when $t < V$. This will relate to superconductivity in high-temperature superconductors where the hybridisation between copper and oxygen is strong, but direct oxygen-oxygen hopping is weak. Obviously, we would have to perform these calculations to be able to comment in any amount of detail.

Performing the above non-linear transformation is fine at a mathematical level, but we anticipate physical problems. This is related to Nozieres exhaustion, where we find if every conduction electron forms a Kondo singlet with the local electrons, the conduction electrons will no longer have any members left to pair with localised moments [27].

To remedy this, we suggest combining the non-linear transformation with a non-orthogonal transformation, introduced by Long [24]. The idea here is that a general non-interacting solution to the Anderson lattice takes the form

$$\prod_{\mathbf{k}\in K\sigma} \left[\alpha_{\mathbf{k}} f^{\dagger}_{\mathbf{k}\sigma} + \beta_{\mathbf{k}} c^{\dagger}_{\mathbf{k}\sigma}\right] \mid 0\rangle \tag{10.31}$$

where we will treat $\alpha_{\mathbf{k}}$ and $\beta_{\mathbf{k}}$ as *variables* which need to be variationally chosen. Usually this initial state is chosen to be the solution to a non-interacting ALH, but this is not general enough for our purpose, although such a system does play a crucial role. This state is then Gutzwiller projected with an operator which we represent by P_G.

We define new operators by

$$g^\dagger_{\mathbf{k}\sigma} \equiv \frac{\beta_{\mathbf{k}}}{\alpha_{\mathbf{k}}} c^\dagger_{\mathbf{k}\sigma} \qquad\qquad d^\dagger_{\mathbf{k}\sigma} \equiv f^\dagger_{\mathbf{k}\sigma} + g^\dagger_{\mathbf{k}\sigma} \tag{10.32}$$

where the g-electrons are *non-orthogonal* linear combinations of the c-electrons, in terms of which the Gutzwiller projected state is

$$P_G \prod_{\mathbf{k}\in K\sigma} d^\dagger_{\mathbf{k}\sigma} \mid 0\rangle \tag{10.33}$$

Since the projection operator acts in real-space, we consider the expansion in real-space and observe that for each site in every contribution the only combinations that we can find are

$$\mid 0\rangle \qquad d^\dagger_{i\uparrow} \mid 0\rangle \qquad d^\dagger_{i\downarrow} \mid 0\rangle \qquad d^\dagger_{i\uparrow} d^\dagger_{i\downarrow} \mid 0\rangle \tag{10.34}$$

and once projected these map down to

$$\mid 0\rangle \qquad \left[f^\dagger_{i\uparrow} + g^\dagger_{i\uparrow}\right] \mid 0\rangle \qquad \left[f^\dagger_{i\downarrow} + g^\dagger_{i\downarrow}\right] \mid 0\rangle \tag{10.35}$$

$$\left[f^\dagger_{i\uparrow} g^\dagger_{i\downarrow} + g^\dagger_{i\uparrow} f^\dagger_{i\downarrow} + g^\dagger_{i\uparrow} g^\dagger_{i\downarrow}\right] \mid 0\rangle \tag{10.36}$$

where only the final state is affected.

We define an operator which satisfies

$$d^\dagger_{i\sigma} \mid 0\rangle \equiv \left[f^\dagger_{i\sigma} + g^\dagger_{i\sigma}\right] \mid 0\rangle \tag{10.37}$$

$$d^{\dagger}_{i\sigma}d^{\dagger}_{i\bar{\sigma}} \mid 0\rangle \equiv \gamma \left[f^{\dagger}_{i\sigma}g^{\dagger}_{i\bar{\sigma}} + g^{\dagger}_{i\sigma}f^{\dagger}_{i\bar{\sigma}} + g^{\dagger}_{i\sigma}g^{\dagger}_{i\bar{\sigma}} \right] \mid 0\rangle \tag{10.38}$$

and then when γ=1 the pure state

$$\prod_{\mathbf{k}\in K\sigma} d^{\dagger}_{\mathbf{k}\sigma} \mid 0\rangle \tag{10.39}$$

corresponds to the previous Gutzwiller projected state.

The non-orthogonality is the crucial tool. If we choose to employ states of the form

$$g^{\dagger}_{i\sigma} \equiv \sum_{\mathbf{k}\in\tilde{K}} \gamma_{\mathbf{k}} g^{\dagger}_{\mathbf{k}\sigma} \tag{10.40}$$

then by construction, if we include enough electrons, we are forced into achieving the non-interacting free electron ground-state to the conduction electron motion and the conduction electrons and localised electrons are decorrelated.

After deriving an analogue of the Anderson lattice for this basis, we then intend to perform an analogue of the non-linear fermionic transformation that we carried out previously in this chapter. Then we wish to find the Stoner criterion for this resulting model, but what the Stoner criterion is for a system with non-orthogonal mean-fields is certainly not clear.

10.7 Summary

We have introduced the concept of a non-linear transformation in terms of the creation and annihilation operators of the Anderson lattice. The full transformation is of little use to us since it will make the Anderson lattice more difficult to solve. We need to project the f component of states in the d and g basis, since this is the only way to ensure that double-f occupancy is never realised in a mean-field approximation.

After the mean-field approximation, we are left with a dependence on two parameters θ and ϕ, in much the same way we had after performing a mean-field analysis for the problem of orbital ordering in e_g. The dependence on the parameter is much more complicated than

in this model, however. We cannot perform the optimisation to find the values of θ and ϕ the system would like as in the case of the e_g orbital ordering problem.

Eventually we would like to be able to model superconductivity in heavy fermion materials. Currently, the superconducting analogue of the mean-field calculation is being carried out, and we hope to show that superconductivity is favoured at some fillings when we have t ¡ V in the original Anderson lattice model. This would mimic the situation for high-temperature superconductors, where the direct oxygen-oxygen hopping is minimal, and the supercurrent is carried by strongly correlated electrons on the copper sites hybridising with the conduction electrons on the oxygen sites.

Modelling heavy-fermion superconductors, however, will be a greater challenge. The Nozieres paradox suggests that pairing each conduction electron to a strongly-correlated electron will be energetically expensive. We assume then that a conduction electron pairs with *many* strongly correlated electrons. Mathematically, we can achieve this by introducing a non-orthogonal fermionic transformation that will complement the non-linear transformation we have developed in this chapter. However, since the resulting wavefunction will not decouple over sites, the concept of the Stoner criterion will become difficult to contend with.

Part III

End Matter

Chapter 11

Conclusions

In this thesis, we have chiefly been concerned with modelling orbital ordering in transition metal oxides at the level of mean-field theory. We do this by employing a generalisation of the Stoner criterion for ferromagnetism in Landau's phenomological theory of phase transitions. We see that the predictions of this approximation to various models are clear, but are liable to mislead.

The first thing we apply the mean-field theory to is a problem of orbital ordering in t_{2g} problems. We hoped to find an example of an itinerant Jahn-Teller distorted system in Sr_2FeMoO_6. However, if we described anything about the system at all, we described the insulating state of the system. There are also other candidates for this line of modelling in magnetite, and {Ca,Sr}RuO_3. We have a clear plan of work to carry out on magnetite, whereas {Ca,Sr}RuO_3 is less clear. We will need to think hard about modelling the hopping due to the strong distortions present. However, there is the possibility of describing an itinerant Jahn-Teller distorted system in the material.

We then consider orbital ordering in e_g systems. We have the colossal magnetoresistive manganites in mind for this task. We construct e_g orbitals with cubic symmetry, and model them as anisotropic Heisenberg spins in a Hubbard model. We see that for the standard e_g orbitals, the transition to an orbitally ordered state is first order, like most orbital transitions. However, with the cubic symmetric orbitals, the transition is second order.

In our model of orbital ordering in e_g problems, we see that while the modelling at the Stoner level predicts orbital ordering of the cubic symmetric orbitals, we can construct an analogue of the Nagaoka problem. While we cannot solve this exactly, we can unambiguously show that there is a lower energy solution than the mean-field prdictions.

This leads to a desire to improve mean-field theory, especially for a problem we originally had in mind at the start of the work on this thesis. We wish to improve on mean-field theory for the Anderson lattice, which is thought to be an excellent model of heavy-fermion behaviour. We see that mean-field theory would almost always predict this model to exhibit ferromagnetism. Also, double occupation of a strongly correlated f-site becomes inevitable.

To this end, we introduce the concept of a non-linear fermionic transformation. Unfortunately, there is still much to work to do on the theory. For example, we find the mean-field theory depends on two angles, θ and ϕ. These control the relative mixtures of f and c electrons in the quasiparticle that we are constructing. We require the energy to be minimised as a function of these parameters. This requires a numerical approach, and time elapsed before we were able to complete it.

We anticipate physical problems with the above procedure, and suggest further improvements in the form of non-orthogonal basis states. The Stoner criterion which is a key tool in this thesis is anticipated to become complicated with these non-orthogonal states. Indeed, it is not clear that we will be able to recover an analogue of the Stoner criterion. This will take a great deal more work.

Inbetween these two themes of the thesis, we have an interlude discussing antiferromagnetism on a pyrochlore lattice, which has a great deal of geometric frustration. This is due to the pyrochlore lattice consisting of a network of tetrahedra, which again are in some sense a network of triangles, and Heisenberg antiferromagnetism is perhaps the most elementary example of geometric frustration there is. We follow an argument based on two sets of experiments performed on $Gd_2Ti_2O_7$. The first, and in our opinion the most important is the

neutron scattering experiments performed by Bramwell et al. However, we disagree with their predictions. There are Mossbauer experiments performed by that suggest the multiple moment scheme suggested by Bramwell et al. is unlikely, and that the spins are constrained to planes that are perpendicular to the direction point towards the centre of the tetrahedron.

Appendix A

Mean-Field Solutions of the Anderson Lattice

A.1 Mean-Field Phases of the Anderson Lattice

We now discuss some of the phases present in the phase-diagram of the mean-field Anderson Lattice. These are solutions to equations (5.38) and (5.39). We begin with the large U limit, shown in $A.1$. Here we see the consequences of little hybridisation, at least at the level of mean-field theory. A small moment develops in the f-electrons. Interestingly, the conduction electrons adopt the opposite moment, and so. We see this trend continue in figures $A.2$, $A.3$ and $A.4$. In figure $A.5$, we see the hybridisation leads to demagnetisation at half-filling. Figure $A.6$ shows a trend which is complete in the limit $V \to \infty$, as shown in figure $A.7$. Here, we find the hybrisation is so strong that there is no longer any difference between the f-electrons and the conduction electrons.

For heavy fermion materials, the relevant figure is A.1. Heavy fermion materials have no magnetic moment at all in the heavy-fermion state, and so mean-field theory as it stands is inappropriate for their modelling. We hope to improve this situation with the program of work outlined in chapter 10.

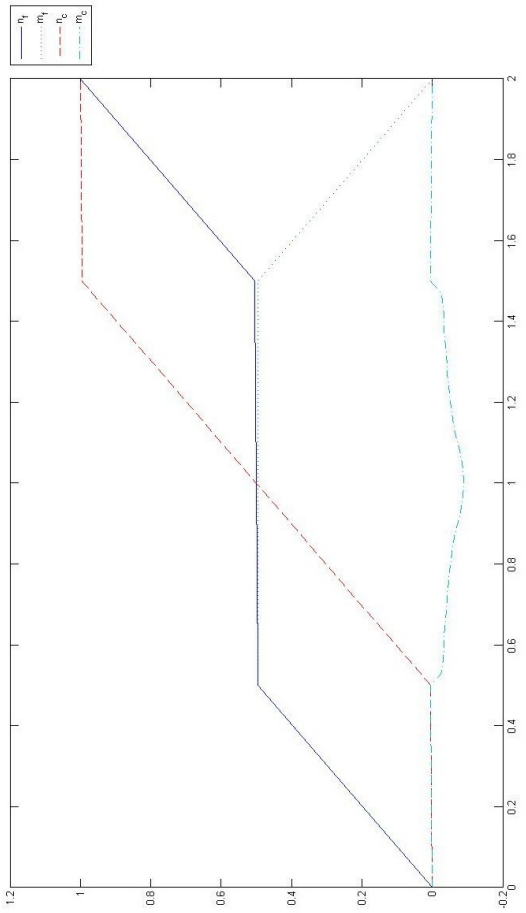

Figure A.1: All figures are plotted with chemical potential on the x-axis. The solid curve is the f-electron occupancy per spin per site, the solid dashed curve is the conduction electron number per spin per site. The dotted curve is the magnetic moment of the f-electrons, and the solid curve with dots is the magnetic moment of the conduction electrons, which is generally opposite to that of the f-electrons. The general trend is that f electrons are placed first with uniform spin, then conduction electrons are filled with little regard to their spin. The hybridisation leads to magnetisation of the conduuction electrons. Eventually, two f-electrons are placed on a site, which we would not expect to happen in reality.

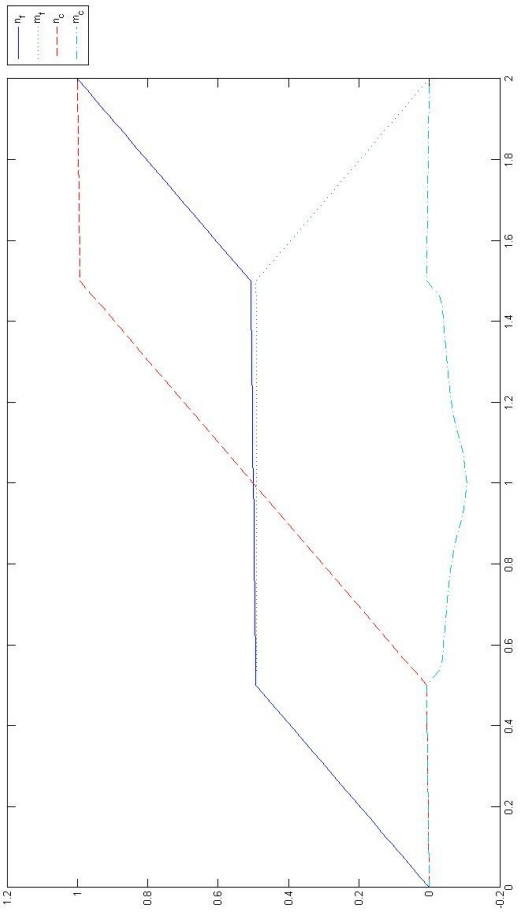

Figure A.2:

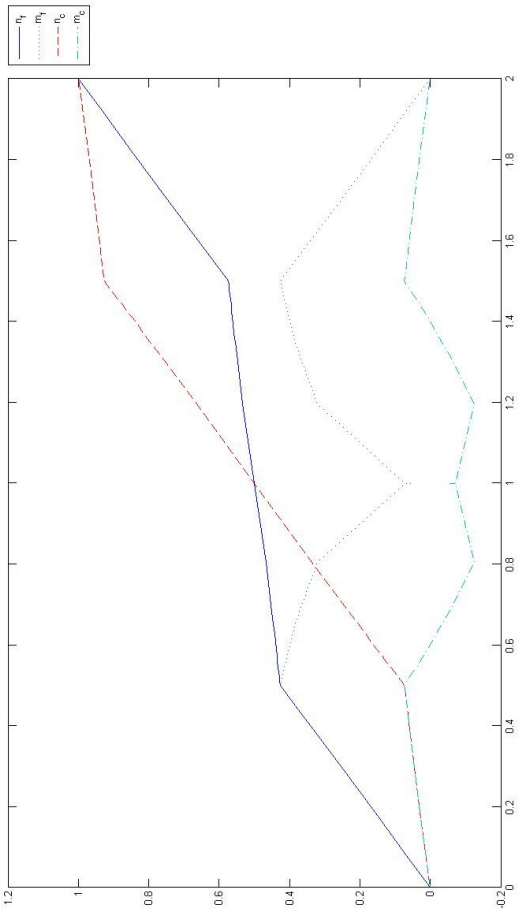

Figure A.3:

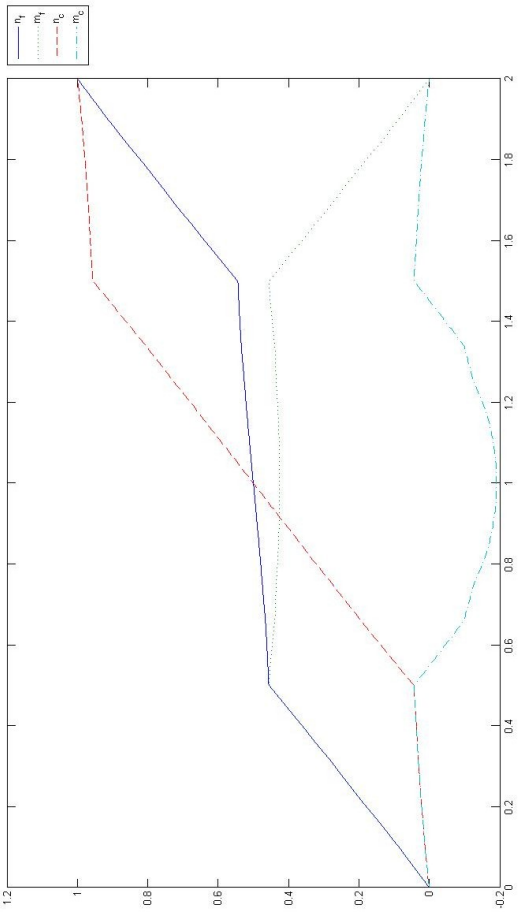

Figure A.4: $V = U$

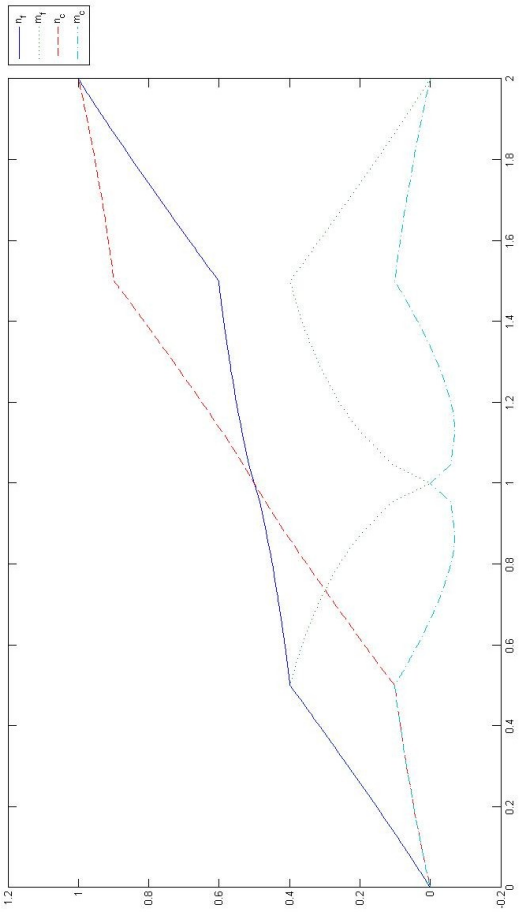

Figure A.5: $V = 2U$

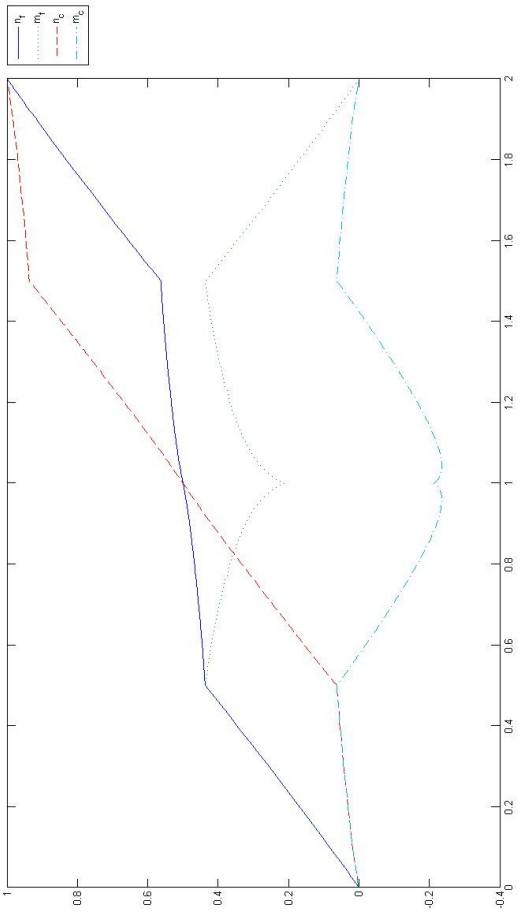

Figure A.6: The limit in which V is much bigger than U

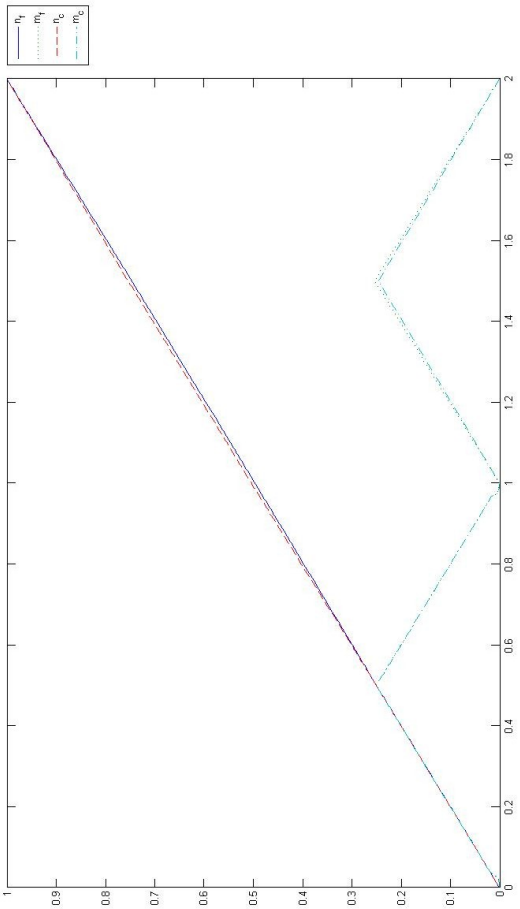

Figure A.7: Limit $V \to \infty$

Bibliography

[1] M. I. Brammall M.W. Long A.K. Briffa. *Phys. Rev. B,* Accepted Dec. 2010, 2010.

[2] P. W. Anderson. Absence of diffusion in certain random lattices. *Phys. Rev.*, 109(5):1492–1505, Mar 1958.

[3] P. W. Anderson. Localized magnetic states in metals. *Phys. Rev.*, 124(1):41–53, Oct 1961.

[4] J. G. Bednorz and K. A. Mller. Possible high t_c superconductivity in the ba-la-cu-o system. *Zeitschrift fr Physik B Condensed Matter*, 64:189–193, 1986. 10.1007/BF01303701.

[5] H. Bethe. *Ann. Physick*, 5(133), 1929.

[6] Steven T. Bramwell and Michel J. P. Gingras. Spin Ice State in Frustrated Magnetic Pyrochlore Materials. *Science*, 294(5546):1495–1501, 2001.

[7] Elbio Dagotto. *Nanoscale Phase Separation and Colossal Magnetoresistance*. Springer.

[8] F. Rubio-Marcos et. al. *J Solid State Chem.*, 182(1211-1216), 2009.

[9] M.A. Garcia et. al. *Phys. Rev. Let.*, 94(217206), 2005.

[10] A Fert and I A Campbell. Electrical resistivity of ferromagnetic nickel and iron based alloys. *Journal of Physics F: Metal Physics*, 6(5):849, 1976.

[11] Gaston Floquet. *Ann. cole Norm. Sup.*, 12:4788, 1883.

[12] P. Grünberg, R. Schreiber, and Y. Pang. Layered Magnetic Structures: Evidence for Antiferromagnetic Coupling of Fe Layers across Cr Interlayers. *Physical Review Letters*, 57(19):2442–2445, November 1986.

[13] J Hubbard. Electron Correlations in Narrow Energy Bands. *Proceedings of the Royal Society of London Series A Mathematical and Physical Sciences 19341990*, 276(1365):238–257, 1963.

[14] J. Hubbard. Electron Correlations in Narrow Energy Bands. II. The Degenerate Band Case. *ProcRSocLonSerA*, 277(1369):237–259, 1964.

[15] J. Hubbard. Electron Correlations in Narrow Energy Bands. III. An Improved Solution. *Proceedings of the Royal Society of London Series A Mathematical and Physical Sciences*, 281(1386):401–419, 1964.

[16] J. Hubbard. Electron Correlations in Narrow Energy Bands. IV. The Atomic Representation. *Proceedings of the Royal Society of London Series A Mathematical and Physical Sciences 19341990*, 285(1403):542–560, 1965.

[17] J. Hubbard. Electron Correlations in Narrow Energy Bands. V. A Perturbation Expansion About the Atomic Limit. *Proceedings of the Royal Society of London Series A Mathematical and Physical Sciences 19341990*, 296(1444):82–99, 1967.

[18] J. Hubbard. Electron Correlations in Narrow Energy Bands. VI. The Connexion with Many-Body Perturbation Theory. *Proceedings of the Royal Society of London Series A Mathematical and Physical Sciences 19341990*, 296(1444):100–112, 1967.

[19] E. Jahn, H. Teller. *Proc. Royal Soc. London*, 121(220), 1936.

[20] Robert Joynt and Louis Taillefer. The superconducting phases of upt_3. *Rev. Mod. Phys.*, 74(1):235–294, Mar 2002.

[21] Kanamori. *Prog. Theor. Phys.*, 30:275, 1963.

[22] Jun Kondo. Resistance minimum in dilute magnetic alloys. *Progress of Theoretical Physics*, 32(1):37–49, 1964.

[23] K.I. Kugel and D. I. Khomskii. *Sov. Phys. Usp.*, 25:231, 1982.

[24] M.W. Long. *Private Communication*.

[25] R. S. Mulliken. *J. Chem. Phys.*, 23:1833–1840, 1955.

[26] Yosuke Nagaoka. Ferromagnetism in a narrow, almost half-filled s band. *Phys. Rev.*, 147(1):392–405, Jul 1966.

[27] P. Nozieres. *Ann. Phys. (Paris)*, 10(19), 1985.

[28] W. Bao P. Schiffer, A. P. Ramirez and S.-W. Cheong. *Phys. Rev. Lett.*, 75(3336), 1995.

[29] S. E. Palmer and J. T. Chalker. Order induced by dipolar interactions in a geometrically frustrated antiferromagnet. *Phys. Rev. B*, 62(1):488–492, Jul 2000.

[30] P. G. Radaelli, D. E. Cox, L. Capogna, S.-W. Cheong, and M. Marezio. Wigner-crystal and bi-stripe models for the magnetic and crystallographic superstructures of $la_{0.333}ca_{0.667}mno_3$. *Phys. Rev. B*, 59(22):14440–14450, Jun 1999.

[31] Myron B. Salamon and Marcelo Jaime. The physics of manganites: Structure and transport. *Rev. Mod. Phys.*, 73(3):583–628, Aug 2001.

[32] J. R. Schrieffer and P. A. Wolff. Relation between the anderson and kondo hamiltonians. *Phys. Rev.*, 149(2):491–492, Sep 1966.

[33] F. Steglich, J. Aarts, C. D. Bredl, W. Lieke, D. Meschede, W. Franz, and H. Schäfer. Superconductivity in the presence of strong pauli paramagnetism: Cecu_2si_2. *Phys. Rev. Lett.*, 43(25):1892–1896, Dec 1979.

[34] G. R. Stewart. Heavy-fermion systems. *Rev. Mod. Phys.*, 56(4):755–787, Oct 1984.

[35] G. R. Stewart, Z. Fisk, J. O. Willis, and J. L. Smith. Possibility of coexistence of bulk superconductivity and spin fluctuations in upt_3. *Phys. Rev. Lett.*, 52(8):679–682, Feb 1984.

[36] J R Stewart, G Ehlers, A S Wills, S T Bramwell, and J S Gardner. Phase transitions, partial disorder and multi- k structures in gd 2 ti 2 o 7. *Journal of Physics: Condensed Matter*, 16(28):L321, 2004.

[37] Edmund C. Stoner. Collective Electron Ferromagnetism. *Proceedings of the Royal Society of London. Series A, Mathematical and Physical Sciences (1934-1990)*, 165(922):372–414, April 1938.

[38] Jahn, H. Teller, E. *Phys. Rev*, 49(874), 1937.

[39] W. Thomson. *Proc. R. Soc. Lond.*, 8:546550, 1856.

[40] J VANSANTEN. Electrical conductivity of ferromagnetic compounds of manganese with perovskite structure. *Physica*, 16(7-8):599–600, August 1950.

[41] G. K. Woodgate. *Elementary Atomic Structure*. Oxford University Press, USA.

[42] Y. Yafet, C. M. Varma, and B. Jones. Ground state of an ion fluctuating between two magnetic valence states. *Phys. Rev. B*, 32(1):360–370, Jul 1985.

[43] Clarence Zener. Interaction between the d-Shells in the Transition Metals. II. Ferromagnetic Compounds of Manganese with Perovskite Structure. *Physical Review*, 82(3):403–405, May 1951.

[44] W Zhong, W Liu, C T Au, and Y W Du. Tunnelling magnetoresistance of double perovskite sr 2 femoo 6 enhanced by grain boundary adjustment. *Nanotechnology*, 17(1):250, 2006.